Study of collective motions in nuclear systems within microscopic transport models

Bogdan Nicolae Frecuș

Coordinator: Prof. Dr. Virgil Băran

Physics Faculty,
University of Bucharest,
Romania 2012

Abstract

In this thesis we explore new features of various collective dipole modes in exotic nuclear systems. Our main interest will be concerned with the pygmy dipole resonance (PDR), a collective mode intensively studied experimentally, and theoretically, in the last decade. We shall propose two different approaches for the study of the PDR, and a presentation of the main ingredients of our methods of investigation will be provided. Firstly, we generalize to neutron-rich nuclei a model first introduced by Brink to study microscopically the giant dipole resonance (GDR). Thus, within the harmonic oscillator shell model we identify the dipole normal modes in neutron rich nuclei. One of these modes corresponds to the motion of the neutron skin against the core. The model allows to calculate the energy-weighted sum rule exhausted by each normal dipole mode. An upper limit for the energy-weighted sum rule exhausted by PDR is obtained. A comparison with the experimental data allows us to evaluate the neutron skin contribution to the collective dynamics of the pygmy motion. Motivated by the main conclusions arising from this schematic model, we extend our investigation of the PDR within a self-consistent microscopic transport model. Within the framework of Fermi liquid theory, by solving the self-consistent coupled Landau-Vlasov kinetic equations for neutrons and protons, we explore the structure of different dipole vibrations in neutron rich nuclei. Using different parametrizations of the symmetry energy with the density, we inquire on the role of the symmetry energy upon the various dipole motions. An isoscalar-like collective mode with an energy well bellow the giant dipole resonance is identified, with features expected for the PDR. The energy centroid of this so called pygmy mode is rather independent to the symmetry energy parametrization employed. However, its strength is sensitive to the behaviour of the symmetry energy below saturation, which affects the number of neutrons belonging to the skin. The systematic investigation of the mass dependence of the PDR is also performed. We obtain that the parametrization $42 \cdot A^{-1/3}$ closely reproduces the position of the energy centroid of this elusive collective mode.

Rezumat

În această teză sînt explorate noi aspecte ale diferitelor moduri dipolare în sistemele nucleare exotice. În principal, vom viza rezonanța dipolară de tip pygmy (PDR), un mod colectiv intens studiat în ultima decadă, atît experimental cît și teoretic. Pentru studiul PDR, vom propune două abordări diferite și ingredientele principale ale metodelor folosite vor fi prezentate. În primul rînd, vom generaliza pentru sistemele nucleare bogate în neutroni, un model introdus inițial de Brink pentru studiul microscopic al rezonanței gigant dipolare (GDR). Astfel, în cadrul acestui model, vom identifica modurile dipolare normale în nucleele bogate în neutroni. Unul dintre aceste moduri corespunde mișcării *skin*-ului neutronic în opoziție de fază cu *core*-ul nucleului. De asemenea, modelul permite calcularea regulii de sumă epuizate de către fiecare mod dipolar. O limită superioară este obținută pentru regula de sumă epuizată de către PDR. Comparația cu datele experimentale ne permite să evaluăm contribuția *skin*-ului neutronic la dinamica colectivă a mișcării de tip pygmy. Motivați de principalele concluzii emergente acestui model schematic, vom extinde studiul PDR în cadrul unui model de transport microscopic self-consistent. În cadrul teoriei lichidelor Fermi, prin rezolvarea ecuațiilor cinetice cuplate de tip Landau-Vlasov pentru neutroni și protoni, vom explora structura diferitelor moduri dipolare de vibrație în nucleele bogate în neutroni. Utilizînd diferite parametrizări ale energiei de simetrie în raport cu densitatea, vom studia dependența oscilațiilor dipolare de energia de simetrie. Este obținut un mod colectiv pygmy de tip isoscalar, cu o energie mult sub cea a rezonanței dipolare gigant. Centroidul energiei corespunzător modului pygmy este mai degrabă independent de parametrizarea energiei de simetrie utilizată. Cu toate acestea, tăria modului e sensibilă la comportamentul energiei de simetrie sub densitatea de saturație, care afectează numărului de neutroni aparținînd *skin*-ului. De asemenea, este studiată dependența de masă a centroizilor rezonanței dipolare pygmy, fiind obținută parametrizarea $42 \cdot A^{-1/3}$.

Acknowledgments

I would like to express my gratitude to my supervisor Prof. Dr. Virgil Băran, for the guidance I have received in the field of theoretical and nuclear physics. Without his support and help, I would not have been written this thesis. For this, I am profoundly indebted to him.

I would also like to thank Prof. Dr. Mihai Gîrțu and Dr. Fănică Cimpoeșu for the guidance and support I have received from them in the past years, as a student and collaborator. I also wish to express my sincere gratitude to Prof. Dr. Hans Ågren, Dr. Žilvinas Rinkevičius and all the people from the theoretical chemistry department at KTH, for their lectures, guidance and support I have been receiving during my visits in Stockholm.

Many thanks to my colleagues in the theoretical physics group, Alexandra and Valentina Tudorache, Luiza Munteanu, Remus Păun and Mihai Cuciuc, for the pleasant time we shared at the department.

Finally, I would like to acknowledge the financial support obtained through the strategic grant POSDRU/88/1.5/S/56668.

Contents

Chapter 1

Introduction

1.1 Collective motions in nuclear systems

The emergence of collective features and their structure in terms of the individual motions of the constituents, is one of the important challenges in many-body physics. Atomic nuclei are finite fermionic systems for which several collective motions were discovered experimentally and described in the framework of various theoretical models. This includes the monopole, quadrupole, and octupole motions, both isoscalar (when protons and neutrons are oscillating in phase), and isovector (when protons and neutrons are oscillating out of phase). One of the most robust collective motions is the giant dipole resonance (GDR), which, at the macroscopic level can be viewed as an oscillation of the neutrons against the protons. This collective motion which is present in all nuclei, has an energy centroid position that varies as $80 \cdot A^{-1/3}$ MeV for medium-heavy nuclei. Moreover, the GDR can be used as a probe to explore the properties of nuclei in extreme conditions of deformation and temperature [1]. With the advent of modern experimental methods, atomic nuclei which are far from the valley of stability have been studied. Apart from the intrinsic interest related to the evolution of the collective dynamics far from stability, such investigations were also motivated by astrophysical reasons. Indeed, one way to extract information about neutron stars is to investigate the nuclear skin properties [2, 3]. A neutron-rich skin located on the nuclear surface is a hallmark of exotic heavy nuclei. These nuclei are characterized by specific structural properties, including the weak bonding between the peripheral and core nucleons, inducing diffuse distributions of neutron densities towards surface, and the formation of neutronic skin or nuclear halo [4, 5, 6, 7]. Due to these properties, the structure of collective multipolar response in nuclei with high N/Z ratio, (with N, Z being the number of neutrons and protons respectively), is modified, and new specific excitation modes arise. In light nuclei, the dipole strength in the low lying region is caused by the non-resonant single particle excitations of weakly bound neutrons, whereas in medium or heavy nuclei a concentration of dipolar response below the GDR centroid was identified experimentally in several cases. Such a resonance was named pygmy dipole resonance (PDR) and was interpreted as resulting from the out of phase oscillation of neutron skin against the isospin-saturated core.

In the case of neutron rich tin isotopes (^{130}Sn and ^{132}Sn), Adrich *et al.* [8] have observed a pronounced energy centroid at around 10 MeV corresponding to a resonant-like shape distribution. In the case of stable tin nuclei, Özel *et al.* [9] reported a concentration

of dipole excitations near and below the particle emission threshold, providing a benchmark test for microscopic calculations whose scope is the PDR description in neutron rich tin isotopes. The strongest dipole transitions for ^{112}Sn were located between 5 and 8 MeV, and a sizeable fraction of the energy-weighted sum rule (EWSR) exhausted by these modes has been reported [9]. Klimkiewicz *et al.* [10] observed a correlation between the pygmy dipole strength and the isospin neutron-proton asymmetry in exotic nuclei. Moreover, the size of the neutron skin is influenced by the properties of the symmetry energy below saturation density (i.e. $\rho_0 = 0.16$ fm^{-3}) [11, 12, 13, 2]. Consequently, a connection between the size of the neutron skin and the exhausted EWSR of the pygmy mode can be expected. From a comparison of the available data from stable and unstable isotopes, a correlation between the pygmy dipole strength and neutron to proton asymmetry was also reported [10]. This behaviour was connected to the symmetry energy properties below saturation. Since the size of the neutron skin is influenced by the symmetry energy, a correlation between the PDR and the skin thickness can also be expected [13, 2, 11]. Nevertheless, we also remark that other theoretical investigations suggest a weak connection between the PDR and the skin thickness [14].

In spite of the fact that the properties of the PDR have been extensively studied, the available information is still incomplete, and several questions regarding its nature still remain unanswered. In a recent study, Paar [15] has advanced a series of open questions, regarding the nature of the pygmy dipole resonance. The first question is related to the collective nature of the pygmy mode. While the collective features of the GDR are well established, there are contradictory results regarding the collective nature of the low-lying dipole states which correspond to the PDR [16]. Indeed, some microscopic studies predict a large fragmentation of dipole strength and the absence of the collective states in the low lying region of ^{132}Sn [17]. The second is related to the exact location of the energy centroid corresponding to the PDR, which for light nuclei is located below the neutron threshold, while for heavier, more neutron-rich nuclei, the peak is higher than the neutron separation energy. The third question deals with the possible connections that can be made between the nature of the PDR in stable nuclei and those away from the valley of stability. Lastly, the macroscopic picture of neutron and proton vibrations for this resonance, as well as the role of the symmetry energy in the PDR are questioned. Along the next two subsections we shall briefly review the main experimental results as well as the most important theoretical approaches to the pygmy response existing in the literature.

1.2 Experimental evidences for the pygmy dipole resonance

Attempts to evidence the possible presence of a low lying dipole strength in various nuclei have been performed by various experimental groups, using different techniques. Ottini-Hustache *et al.* [18], using a ^{86}Kr beam at 60 MeV/nucleon on ^{40}Ca and ^{48}Ca target isotopes, in scattering processes, observed a non-negligible electric dipole ($E1$) strength in the low excitation energy region between 6 and 12 MeV. They do not observed any $E1$ strength difference between the two systems. Another experimental group [19, 20, 21], within a (γ, γ') high resolution photon scattering experiment, investigated the dipole and

quadrupole responses of the same calcium isotopes up to 10 MeV energies. At energies between 6 and 10 MeV, a possible evidence for a bound $E1$ response, caused by the neutron excess has been signaled, from the comparison of the two isotopes. However, for the calcium isotope, ^{48}Ca, a concentration of low lying dipole strength which exhaust 0.3% (about 20 times smaller than in the previous findings [18]) of the $E1$ EWSR has been observed. The difference in the EWSR exhausted by the pygmy mode between the reported values of the previous studies, calls for a more detailed picture which can be achieved throughout both experimental as well as theoretical investigations. We remark that these studies are the first focusing on the isotopic chain under the same experimental conditions, allowing for a systematic study about the effects of the N/Z ratio on the PDR.

Regarding the search for the pygmy resonance in medium-nuclei, Wieland et al. [22, 23] reported for the first time the evidence for PDR in the neutron-rich nickel isotope, ^{68}Ni, within the virtual photon scattering technique. A low lying dipole strength, with the energy centroid at around 11 MeV, located well below the GDR region has been reported. The EWSR acquired by the pygmy mode is reported to range between 5% and 9%, implying the need for more accurate experiments, as well as theoretical studies, to establish the $E1$ strength with smaller uncertainty. Based on these results, the correlations between the neutron skin size, the percentage of the EWSR exhausted by the PDR, and the properties of the symmetry energy below saturation were also investigated in the framework of various theoretical models.

Within a Coulomb dissociation technique following an in-flight fission of a ^{238}U beam, at energies around 500 MeV/nucleon for the secondary Sn beams, Adrich *et al.* [8] investigated the pygmy and giant resonances for the unstable, ^{130}Sn and for the double magic ^{132}Sn tin isotopes. A value of $\sim$ 10 MeV is reported for the PDR energy centroid, while a value of $\sim$ 16 MeV is reported for the GDR one, with little differences in the two isotopes studied. Moreover, Adrich *et al.* [8] stress that although a sizeable response concentrated well below the GDR region is observed, the extent to which a collective motion is formed for those oscillations is yet under debate. Furthermore, within a (γ, γ') photon scattering experiment conducted by Savran *et al.* [24], a resonance-like concentration for the semi-magic xenon isotope, ^{136}Xe is observed, well below neutron separation energy, while, within a polarized proton inelastic scattering at very forward angles approach, Tamii *et al.* [25] recently investigated the complete electric dipole response in ^{208}Pb.

1.3 Theoretical approaches to the pygmy dipole resonance

In addition to the experimental information regarding the PDR, several theoretical approaches have been employed over the years. These approaches can be classified mainly into four distinct categories: (i) phenomenological approaches based on hydrodynamics or fluid dynamics equations, (ii) non-relativistic microscopic approaches using random phase approximation (RPA) with various effective interactions, (iii) relativistic quasiparticle RPA, and (iv) transport approaches based on Landau-Vlasov equation.

Within a hydrodynamical model, employing three component fluids, Mohan *et al.* [26], predicted the existence of two independent modes of giant dipole type, instead of a single mode, as in the two-fluid model of Steinwedel and Jensen [27]. For ^{208}Pb these

modes are situated at 13 MeV and at 4.4 MeV respectively. It is observed that the higher energy mode is quite close to the GDR centroid observed experimentally and it was identified with the GDR state. The lower energy mode corresponds to a motion in which the protons and blocked neutrons move together, while the excess neutrons move in the opposite direction. This picture corresponds to the PDR mode. For the GDR, a mass dependence proportional to $A^{-1/3}$ is predicted. It is concluded that most of the strength remains in the high energy mode.

More recently, within a S-J hydrodynamical model, Suzuki *et al.* [28], concluded that the excess nucleons in neutron rich nuclei or proton rich nuclei, will play a distinctive role due to the loose coupling to the core. They considered a two-fluid system formed by the core and excess fluids. Again, a PDR mode is predicted. The resonance energy and the dipole strength for the PDR increase with the increasing number of excess neutrons. For the extremely rich neutron-rich nucleus ^{61}Ca it is found that the PDR excitation energy attains $\sim$ 8 MeV and the EWSR fraction is around $\sim$ 16%. In this case, the nucleus ^{46}Ca was chosen as the core, since the binding energy per particle is the biggest among the calcium isotopes. It is worth mentioning also the quantum fluid approaches within a hydrodynamical formulation reported by Bastrukov *et al.* [29], where, it is argued that the PDR emerges as a soft dipole motion of elastic shell oscillations of irrotational flow, confined in the finite depth surface layer. The analytical equation for the frequency of this dipole vibration leads to an estimate of the PDR energy centroid $31 \cdot A^{-1/3}$ on the mass. In this model, a decomposition into two spherical domains appears: the undisturbed inner region corresponds to the static core, while the external layer undergoes elastic shear vibrations. Moreover, it is mentioned that the emergence of the elastic force responsible for the PDR, is related to the resistivity to disruption of peripheral circular periodic orbits of uninterrupted Fermi-motion of independent particles in the nuclear mean-field.

Microscopic approaches within the random phase approximation (RPA) formalism, have been employed using various effective interactions [30, 31, 32]. Within such an approach, Tsoneva and Lenske [30] investigated the dipole excitation in various tin isotopes in the low lying region. A sizeable dipole strength below the neutron emission threshold was obtained for the neutron rich isotopes from ^{112}Sn to ^{132}Sn, while, for the proton rich isotopes, ^{100}Sn $\rightarrow$ ^{104}Sn, a proton PDR has been obtained. Co' *et al.* [31], investigated several neutron-rich isotopes, within a phenomenological RPA approach without pairing effects. In the oxygen isotopes cases, instead of the emergence of a new excitation pygmy-like mode, a fragmentation of the giant mode has been observed. For the neutron-rich ^{48}Ca isotope, an energy centroid located in the low lying region, at around 8.5 MeV, has been attributed to a PDR. Moreover, from the zirconium and tin isotopes studied, the calculations clearly predicted that the emergence of the distinct pygmy-like collective motion is a common feature of medium and heavy nuclei. In another study performed by Yoshida [32], the deformed even-even neutron-rich magnesium isotopes (^{36}Mg $\rightarrow$ ^{40}Mg) have been investigated within a quasi-particle RPA approach, using a Skyrme SkM* energy density functional (EDF), as well as the local mixed-type pairing EDF. It has been found that the PDR has both an isoscalar as well as an isovector character, while a considerable coupling between the isovector dipole, isoscalar octupole and compressional dipole modes occurs in the low lying region, due to the mixing of different angular momenta in deformed systems. Quite recently, Roca-Maza *et al.* [33] investigated the even-even neutron rich nuclei ^{68}Ni, ^{132}Sn and ^{208}Pb, within the fully self-consistent

mean-field Skyrme-Hartree-Fock plus RPA approach. Three different Skyrme interactions (namely, SGII, SLy5 and SKI3) were employed, to investigate the correlations between the isoscalar and isovector responses in the low-lying region on the slope parameter of the symmetry energy, L. Consequently, increasing the values of the slope parameter, the centroid of the strength function in the low-lying region, for both isoscalar and isovector dipole responses, are shifted towards larger energies for all the nuclei previously mentioned. Moreover, the PDR for these nuclei manifest a mixed character, with a strong isoscalar and also a non-negligible isovector components. While a clear collective nature of the isoscalar component is found, there are no evidences to support the same collective nature of the isovector response.

Using the density functional theory (DFT) formalism, Chambers *et al.* [34] performed calculations for even-even calcium isotopes between ^{40}Ca and ^{48}Ca. An additional resonance below 10 MeV in neutron rich isotopes, corresponding to an oscillation of the surface neutrons against the inert core was obtained. The energy centroid corresponding to the PDR, is reported as 9.1 MeV for ^{42}Ca, while for ^{48}Ca it decreases to 7.6 MeV. The exhausted EWSR is reported to be around $\sim 2\%$ for ^{48}Ca isotope.

Besides the non-relativistic methods previously presented, the low-lying dipole states in neutron rich isotopes have been investigated using relativistic quasi-particle RPA approaches [35, 36, 37, 38, 39, 40]. The collectivity of the low-lying dipole strength was investigated in the relativistic RPA by Vretenar *et al.* [35]. The development of the isovector collective response was investigated in the chain of oxygen, calcium, nickel and tin isotopes. A clear splitting between the GDR and PDR modes was evidenced with the increase of the excess number of neutrons. In the same time, the strength distribution becomes more fragmented and spreads to low energy regions. In light nuclei, the low-energy response is the result of single particle excitations of loosely bound neutrons, while for medium-heavy nuclei a coherent superposition of many neutron particle-hole configurations was interpreted as a collective PDR corresponding to a vibration of the excess neutrons against the symmetric inner core, exhausting few percents of the EWSR. A detailed analysis of the corresponding transition densities and velocity distributions reveals the detailed dynamics of this mode, including the competition between the isoscalar and isovector components [36]. Very recently, in 2012, in the framework of relativistic energy density functional, employing a fully self-consistent RPA, Vretenar *et al.* [40] investigated the evolution of pygmy dipole states for ^{68}Ni, ^{132}Sn, and ^{208}Pb, as a function of the value of symmetry energy at saturation as well as a function of the symmetry energy slope. Several conclusions from this exhaustive study emerge: (i) the occurrence of the PDR as a collective state is enhanced with the increase of the symmetry energy and slope values, (ii) in all cases, few percentages of the isovector EWSR are exhausted by the PDR, and, in general, the fraction exhausted by the PDR increases with the slope parameter. Contrary to the results reported by Roca-Maza [33], for the isovector response, the centroid for the low-lying strength shifts towards lower values, with the increase of a_4 (the value of symmetry energy at saturation) and L (the slope parameter of the symmetry energy - see also Chapter 3). Moreover, for a given interaction, the centroid of the low-lying strength shifts towards lower values when one moves from lighter (e.g. nickel) towards heavier nuclei (e.g. lead) (see also Fig. 1 from Ref. [40]).

After 2009, the problem of the collective nature of the low-lying isovector excitations was tackled also from a transport approach perspective [41, 42, 43]. In a semi-

phenomenological approach, Abrosimov and Davydovs'ka [41], studied the linearized kinetic Vlasov equation for a nucleus assumed to be composed from a core and a low density spherical external layer. They applied this formalism to calculate the strength function for ^{208}Pb and obtained that the maximum response lies at an energy of 7.8 MeV and exhausted 7.5% of the dipole EWSR, assuming that all the excess neutrons are located in the external layer. Assuming less neutrons belong to the external layer, the energy centroid shifts to 8.6 nMeV, while the exhausted EWSR is reduced with 1%. Using the bulk part of the Barcelona-Catania-Paris functional [44], and in the absence of Coulomb interactions among protons, within a semi-classical Thomas-Fermi-Vlasov approach, Urban [43] investigated the electric dipole and isoscalar torus response in neutron rich isotopes. It was concluded, from the peak positions, velocity fields, and transition densities that the PDR has an important isoscalar torus component. However, his conclusion contradicts the results of Bastrukov *et al.* [29] obtained within a hydrodynamical approach, relying on the elasticity of the nuclear medium due to quantum effects.

Based on the experimental observations and the different, and sometimes contradictory conclusions regarding the theoretical investigations of the PDR, we also investigated the PDR both within a microscopic schematic model and within a transport model based on the Vlasov equation, in connection with the properties of the symmetry energy below saturation density.

Following the introduction from the first Chapter, in Chapters 2 and 4, we develop the original subject matter of the thesis. In the second Chapter, within a harmonic oscillator shell model (HOSM) extended to neutron-rich nuclei, we show that the collective coordinates associated to protons, core and excess neutrons are separable, and, upon a dipolar excitation, the vibration of the excess neutrons against the isospin saturated core emerges, which can be ascribed to the PDR. Consequently, we obtain an upper limit for the EWSR exhausted by this pygmy mode. We discuss the predictions of the model for different systems from the nuclear chart.

In Chapter 4, based on the understanding of the structure of the dipole normal modes in exotic nuclei, provided by the schematic model, we explore, in a description based on Landau Fermi liquid theory, the structure of the dipole vibrations, by solving the two coupled Landau-Vlasov kinetic equations describing the neutrons and protons dynamics. Our self-consistent treatment, including the Coulomb interaction, and employing three different parametrizations with the density of the isovector mean field, allows the disentangling of the symmetry energy role on the dipolar response of neutron-rich nuclei. We shall focus on two important observables concerning the collective response, namely the energy centroid and the corresponding EWSR exhausted by the pygmy mode. Moreover, the dependence on the mass number, A, of the low-lying dipole response is also addressed. Taking into account that the main ingredients in our approach are the transport equations and the symmetry energy, in Chapter 3, we expose the main concepts related to the nuclear equation of state and the properties of the symmetry energy as well as the position of the kinetic equations of Vlasov-type in the context of time-dependent studies of nuclear systems.

Chapter 2

Pygmy dipole resonance in a schematic model

In this Chapter we explore some features of the dipole dynamics in nuclear systems within a harmonic oscillator shell model. We firstly present the work of Brink [45], who has shown that within this model, the coordinate corresponding to the dipole photon absorption operator is entirely separable. We then generalize this approach for neutron rich nuclei, and identify the dipole normal modes defined by this Hamiltonian.

With the help of the Thomas-Reiche-Kuhn (TRK) sum rule, which for the sake of completeness will also be discussed, an upper limit for the energy weighted sum rule (EWSR) exhausted by the pygmy mode will be obtained. The dependence of the fraction of the EWSR associated by this mode will be analyzed for various calcium, nickel, tin and lead isotopes.

2.1 Giant dipole resonance in a Harmonic Oscillator Shell Model

The giant dipole resonance can be phenomenologically represented as a collective mode within two different models, the first being proposed by Goldhaber and Teller [46] in 1948 and the second by Steinwedel and Jensen [27] in 1950. Within the first model the whole protons and neutrons spheres vibrate one against the other without distortion. In the second model, the collective mode manifests as an out of phase change of local relative densities of protons and neutrons wile the total nuclear density remains unchanged. While in the first model the surface of the nuclear system changes, in the second model it remains fixed (see also Fig. 2.1). In 1957 Brink [45] provided the first microscopic justification of the G-T dynamics, within a shell model description. He showed that it is possible to perform a separation in four independent (commuting) parts a system of $A = N + Z$ nucleons moving in a harmonic oscillator well with the Hamiltonian:

$$H_{sm} = \sum_{i=1}^{A} \frac{\mathbf{p}_i^2}{2m} + \frac{K}{2} \sum_{i=1}^{A} \mathbf{r}_i^2 \ . \tag{2.1}$$

The Hamiltonian, H_{sm}, can be split in the following form:

$$H_{sm} = H_{n \text{ int}} + H_{p \text{ int}} + H_{\text{CM}} + H_D \ . \tag{2.2}$$

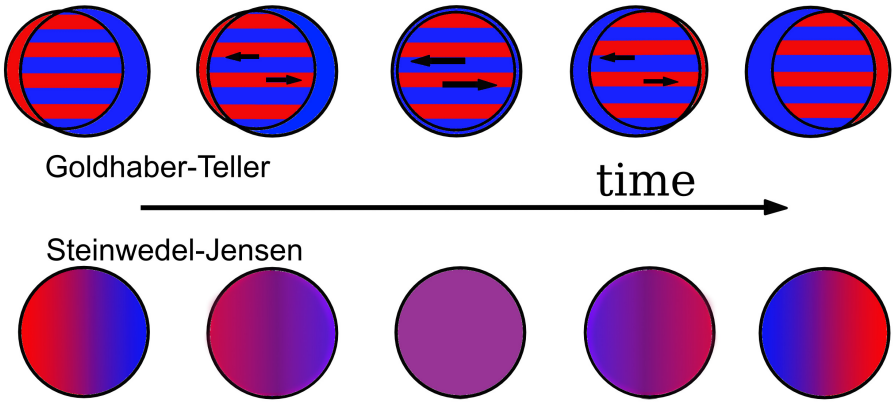

Figure 2.1: Graphical representation of the half-period of the giant dipole resonance in the G-T (top - notice that the protons and neutrons systems should be considered as undistorted spheres, upper/lower arrows indicate the magnitude of the neutrons/protons velocities) and S-J (bottom - notice that when the mode is excited, even though the total nuclear density remains unchanged, the local proton and neutron densities change) pictures, with the neutrons being depicted in blue, while protons in red.

The first two terms of the sum above depend only on the proton-proton and neutron-neutron relative coordinates, and characterize the internal motions of each of the two subsystems:

$$H_{n\ \mathrm{int}} = \frac{1}{2}\sum_{i,j=1}^{N}\frac{(\mathbf{p}_i-\mathbf{p}_j)^2}{2m} + \frac{1}{2N}\,\frac{K}{2}\sum_{i,j=1}^{N}(\mathbf{r}_i-\mathbf{r}_j)^2\ , \tag{2.3}$$

and

$$H_{p\ \mathrm{int}} = \frac{1}{2}\sum_{i,j=1}^{Z}\frac{(\mathbf{p}_i-\mathbf{p}_j)^2}{2m} + \frac{1}{2Z}\,\frac{K}{2}\sum_{i,j=1}^{Z}(\mathbf{r}_i-\mathbf{r}_j)^2\ . \tag{2.4}$$

The center of mass Hamiltonian, H_{CM}, characterises an oscillatory motion of the center of mass of the nucleus:

$$H_{\mathrm{CM}} = \frac{1}{2\,m\,A}\,\mathbf{P}^2_{\mathrm{CM}} + \frac{K\,A}{2}\,\mathbf{R}^2_{\mathrm{CM}}\ , \tag{2.5}$$

which appears due to breaking of the translational symmetry by the spherical harmonic oscillator potential. Finally, H_D, describes the protons against the neutrons Goldhaber-Teller type vibration [46], and is associated from a microscopic point of view to the GDR:

$$H_D = \frac{A}{2\,m\,N\,Z}\,\mathbf{P}^2 + \frac{K\,N\,Z}{2\,A}\,\mathbf{X}^2\ . \tag{2.6}$$

In Eq. (2.5), the center of mass position vector, $\mathbf{R}_{\mathrm{CM}}$:

$$\mathbf{R}_{\mathrm{CM}} = \frac{1}{A}\big(Z\,\mathbf{R}_p + N\,\mathbf{R}_n\big)\ , \tag{2.7}$$

with its conjugate momenta:

$$\mathbf{P}_{\mathrm{CM}} = \mathbf{P}_p + \mathbf{P}_n\ , \tag{2.8}$$

appears. In these expressions, the position vectors of the protons and neutrons enter:

$$\mathbf{R}_p = \frac{1}{Z}\sum_{i=1}^{Z}\mathbf{r}_i \qquad ; \qquad \mathbf{R}_n = \frac{1}{N}\sum_{i=1}^{N}\mathbf{r}_i \ . \tag{2.9}$$

Their conjugate momenta are:

$$\mathbf{P}_p = \sum_{i=1}^{Z}\mathbf{p}_i \qquad ; \qquad \mathbf{P}_n = \sum_{i=1}^{N}\mathbf{p}_i \ . \tag{2.10}$$

In terms of the same quantities, the neutron-proton relative coordinate, $\mathbf{X}$, has the following expression:

$$\mathbf{X} = \mathbf{R}_p - \mathbf{R}_n \ , \tag{2.11}$$

while, its conjugate momenta is:

$$\mathbf{P} = \frac{NZ}{A}\Big(\frac{1}{Z}\,\mathbf{P}_p - \frac{1}{N}\,\mathbf{P}_n\Big) \ . \tag{2.12}$$

In the above equations, the oscillator constant, $K = m\,\omega_0^2$, is chosen to reproduce the observed nuclear mean square radius [47]. Since, for a nucleon in the shell defined by the quantum number N_i, one has

$$\big\langle r^2\big\rangle_i = \frac{\hbar}{m\omega_0}\Big(N_i + \frac{3}{2}\Big) \ , \tag{2.13}$$

and the mean square radius is

$$\big\langle R^2\big\rangle = \frac{1}{A}\sum_{i=1}^{A}\big\langle r^2\big\rangle_i = \frac{3}{5}\,A\,R_0^2 \ , \tag{2.14}$$

we obtain:

$$\hbar\,\omega_0 \approx \frac{5}{4}\left(\frac{3}{2}\right)^{1/3}\frac{\hbar^2}{m{r_0}^2}\,A^{-1/3} \approx 40\cdot A^{-1/3}\ \text{MeV} \ . \tag{2.15}$$

For the nuclear radius R_0 we considered $R_0 = r_0\ A^{-1/3}$, with $r_0 = 1.2$ fm.

It is worth mentioning that the collective conjugate variables satisfy the usual commutation relations, e.g.:

$$\big[\,\mathbf{X}_\alpha\,,\,\mathbf{P}_\beta\big] = i\,\hbar\,\delta_{\alpha\beta} \ . \tag{2.16}$$

where α, β are the indices for the Cartesian components.

As a result of the mentioned decomposition of the Hamiltonian the eigenstate of the nucleus is represented as a product of four wave-functions which are the eigenstates of each of the above Hamiltonians:

$$\Psi = \psi_{n,\text{int}}\ \chi_{p,\text{int}}\ \alpha(\mathbf{R}_{\text{CM}})\ \beta(\mathbf{X}) \ . \tag{2.17}$$

Since the only part of the state product which depends on $\mathbf{X}$ is the eigenfunction $\beta(\mathbf{X})$, for an electric dipole absorption, with the dipole operator:

$$\mathbf{D} = \frac{NZ}{A}\ \mathbf{X} \ , \tag{2.18}$$

a Goldhaber-Teller collective motion is induced. The GDR wave-function will change from the ground state $\beta^0(\mathbf{X})$, to one phonon state $\beta^1(\mathbf{X})$:

$$\Psi^1 = \psi_{n,\text{int}}\ \chi_{p,\text{int}}\ \alpha(\mathbf{R}_{\text{CM}})\ \beta^1(\mathbf{X}) \ . \tag{2.19}$$

2.2 From sum rules to the total dipole cross section

The behavior of the nuclear system to a dipole excitation, or, more generally, to an excitation determined by an operator, G, is characterized by the response function. The interaction between the system and an external field which oscillates in time with the frequency ω, is given by the Hamiltonian, $H_{\rm int}$ [48]:

$$H_{\rm int} = \lambda\big(G^{+}\,{\rm e}^{-i\omega t} + G\,{\rm e}^{i\omega t}\big)\,{\rm e}^{\,\eta\,t}\ , \tag{2.20}$$

where λ controls the strength of the coupling. The exponential ${\rm e}^{\,\eta\,t}$, with $\eta > 0$ sufficiently small, ensures that at $t \to -\infty$ the system is in its ground state, $|0\rangle$, and is described by the unperturbed Hamiltonian, H. Consequently, the time dependence of the perturbed system is given by the Schrödinger equation:

$$(H + H_{\rm int})|\psi(t)\rangle = i\,\frac{\partial}{\partial t}\,|\psi(t)\rangle\ , \tag{2.21}$$

where $|\psi(t)\rangle$ represents the N-body wave-function, and thus, the average value of an arbitrary operator, F, can be expressed:

$$\langle\psi(t)|F|\psi(t)\rangle - \langle 0|F|0\rangle = F_{+}\,e^{-i\omega t}\,{\rm e}^{\eta t} + F_{-}{\rm e}^{i\omega t}\,{\rm e}^{\eta t}\ . \tag{2.22}$$

The unperturbed Hamiltonian, H, has a set of eigenstates $|n\rangle$ defined from the equation:

$$H\,|n\rangle = E_n\,|n\rangle\ , \tag{2.23}$$

where E_n are the corresponding eigenvalues.

Assuming that the interaction is sufficiently weak, the system response to the external field is determined by the linear response function:

$$\chi(F,G,\omega) = \lim_{\lambda\to 0}\frac{F_{+}}{\lambda}\ . \tag{2.24}$$

Considering F to be hermitian and equal to G, and using first order perturbation theory, the response function can be written [48]:

$$\chi(F,\omega) = 2\sum_{n}\omega_{n0}\,\frac{\big|\langle n|F|0\rangle\big|^{2}}{(\omega+i\eta)^{2}-\omega_{n0}^{2}}\ , \tag{2.25}$$

where $\omega_{n0} = E_n - E_0$ is the excitation energy. The properties of the response function can be related to the excitation strength function [49]:

$$S(E) = \sum_{n\neq 0}\big|\langle n|F|0\rangle\big|^{2}\,\delta\big(E-(E_n-E_0)\big)\ , \tag{2.26}$$

which is a measure of the amplitude probability of the system to reach one of the excited states, under the effect of the perturbation, and contains all the information about the response of the nucleus. For example, in the limit of high frequencies or very low frequencies $\chi(F,\omega)$ can be expanded as a function of ω as follows:

$$\lim_{\omega\to\infty}\chi(F,\omega) = \frac{2}{\omega^{2}}\left(m_1 + \frac{1}{\omega^{2}}\,m_3 + \cdots\right)\ , \tag{2.27}$$

and

$$\lim_{\omega\to 0}\chi(F,\omega) = -\,2\left(m_{-1} + \omega^2\, m_{-3} + \cdots\right)\,, \tag{2.28}$$

where m_k represents the k^{th} moment of the strength function:

$$m_k = \int_0^\infty E^k\, S(E)\;\mathrm{d}E = \sum_{n\neq 0}\left|\langle n|F|0\rangle\right|^2\,(E_n - E_0)^k\;. \tag{2.29}$$

With the assumption that the perturbation operator F satisfies $\langle 0|F|0\rangle = 0$, the moments of the strength function, m_k, can be expressed as mean values *only* on the ground state, which express the physical content of the sum rules:

$$m_k = \langle\, 0\,|F\,(H - E_0)^k\,F\,|\,0\,\rangle\;. \tag{2.30}$$

One can proof Eq. (2.30) by expressing the squared modulus of the matrix elements $\langle n|\,F\,|0\rangle$ in Eq. (2.29):

$$m_k = \sum_{n\neq 0}\left|\langle n|F|0\rangle\right|^2\,(E_n - E_0)^k = \sum_{n\neq 0}\langle n|F|0\rangle\,\langle n|F|0\rangle^*\,(E_n - E_0)^k\;. \tag{2.31}$$

Using the hermiticity of the perturbation operator F, and Eq. (2.23) one gets:

$$m_k = \sum_{n\neq 0}\langle 0|F|n\rangle\,\langle n|F|0\rangle\,(E_n - E_0)^k = \langle 0|\,F(H - E_0)^k \sum_{n\neq 0}|n\rangle\langle n|F|0\rangle\;. \tag{2.32}$$

Since the eigenstates form a complete system (i.e. $\sum|n\rangle\langle n| = I$), one easily arrives to Eq. (2.30). Moreover, one can express these moments, m_k, in terms of expectation values on ground state of commutators or anticommutators of the Hamiltonian, H, with the perturbation operator, F. For example:

$$m_0 = \frac{1}{2}\big\langle 0\big|\,\{F,F\}\,\big|0\big\rangle\;, \tag{2.33}$$

$$m_1 = \frac{1}{2}\big\langle 0\big|\,[F,[H,F]]\,\big|0\big\rangle\;, \tag{2.34}$$

$$m_2 = \frac{1}{2}\big\langle 0\big|\,\big\{[F,H],[H,F]\big\}\,\big|0\big\rangle\;, \tag{2.35}$$

$$m_3 = \frac{1}{2}\big\langle 0\big|\,\big[[F,H],[H,[H,F]]\big]\,\big|0\big\rangle\;\ldots \tag{2.36}$$

The proof of Eq. (2.33) is straightforward, for Eq. (2.34) one has:

$$\begin{aligned} m_1 = \langle 0|F(H-E_0)F|0\rangle = \langle 0|F(HF - FE_0)|0\rangle &= \langle 0|F(HF-FH)|0\rangle \\ &= \langle 0|F[H,F]|0\rangle\;. \end{aligned} \tag{2.37}$$

In the same manner, one can also write:

$$\begin{aligned} m_1 = \langle 0|F(H-E_0)F|0\rangle = \langle 0|(FH - E_0F)F|0\rangle &= \langle 0|(FH-HF)F|0\rangle \\ &= \langle 0|[F,H]F|0\rangle\;. \end{aligned} \tag{2.38}$$

Summing up Eqs. (2.37) and (2.38), one gets:

$$\begin{aligned} m_1 &= \frac{1}{2}\big(\langle 0|F[H,F]|0\rangle + \langle 0|[F,H]F|0\rangle\big) \\ &= \frac{1}{2}\big(\langle 0|F[H,F]|0\rangle - \langle 0|[H,F]F|0\rangle\big) \\ &= \frac{1}{2}\left\langle 0\right|\big[F,[H,F]\big]\left|0\right\rangle . \end{aligned} \tag{2.39}$$

Using similar procedures one can also proof the remaining expressions for the moments of the strength function, m_k.

We shall now return to the perturbation of the nuclear system, upon the action of a dipolar excitation, which can determine the transition from the ground state to one GDR phonon state. The cross section for the excitation of the system to the final state $|f\rangle$, by absorbing a photon of energy E, is given by [50]:

$$\sigma_f(E) = \frac{4\,\pi^2 e^2}{\hbar\, c}\,(E_f - E_0)\,\left|\langle f|D|0\rangle\right|^2\,\delta(E - E_f + E_0)\,, \tag{2.40}$$

where E_f and E_0 are the energies of the system in the final and ground state respectively. The dipolar cross section for the absorption of a photon of energy E, is obtained by summing over all final states, where we remark the appearance of the strength function:

$$\begin{aligned} \sigma(E) = \sum_f \sigma_f(E) &= \frac{4\,\pi^2 e^2}{\hbar c}\sum_f (E_f - E_0)\,\left|\langle f|D|0\rangle\right|^2\,\delta(E - E_f + E_0) \\ &= \frac{4\,\pi^2 e^2}{\hbar\, c}\;E\;S(E)\,. \end{aligned} \tag{2.41}$$

The total dipole absorption cross section is obtained from Eq. (2.41) integrating over photon energies, E:

$$\sigma_D = \int_0^\infty \sigma(E)\;\mathrm{d}E = \frac{4\,\pi^2 e^2}{\hbar\, c}\sum_f (E_f - E_0)\,\left|\langle f|D|0\rangle\right|^2\,, \tag{2.42}$$

being proportional to the first moment of the strength function. Therefore, with the help of Thomas-Reiche-Kuhn sum rule, which provides the moment, m_1, in terms of expectation values of double commutator of the dipole operator with the Hamiltonian, on ground state, we have:

$$\begin{aligned} \sigma_D = \frac{4\,\pi^2 e^2}{\hbar\, c}\;m_1 &= \frac{4\pi^2 e^2}{\hbar c}\,\frac{1}{2}\,\left\langle 0\right|\big[D,[H_{sm},D]\big]\left|0\right\rangle \\ &= \frac{2\,\pi^2 e^2}{\hbar\, c}\,\left\langle 0\right|\big[D,[H_D,D]\big]\left|0\right\rangle\,, \end{aligned} \tag{2.43}$$

since the only part of the HOSM Hamiltonian, H_{sm}, which does not commute with the dipole operator is H_D, more specifically, only its kinetic energy part. It is straightforward that:

$$[H_D, D] = \frac{A}{2mNZ}\,\frac{NZ}{A}\,[\mathbf{P}^2,\mathbf{X}] = \frac{1}{2m}\big(\mathbf{P}\,[\mathbf{P},\mathbf{X}] + [\mathbf{P},\mathbf{X}]\,\mathbf{P}\big) = -\,\frac{i\hbar}{m}\,\mathbf{P}\,, \tag{2.44}$$

and so:

$$\left\langle 0\right| \left[D,\left[H_D,D\right]\right] \left|0\right\rangle = \left\langle 0\right| \Big[\frac{NZ}{A}\,\mathbf{X}\,,-\frac{i\hbar}{m}\,\mathbf{P}\Big] \left|0\right\rangle = \left\langle 0\right| \frac{\hbar^2}{m}\,\frac{NZ}{A} \left|0\right\rangle = \frac{\hbar^2}{m}\,\frac{NZ}{A}\langle 0|0\rangle$$
$$= \frac{\hbar^2}{m}\,\frac{NZ}{A}\,. \qquad (2.45)$$

Consequently, the total dipole absorption cross section, which represents the energy-weighted sum rule for the dipole operator becomes:

$$\sigma_D = \frac{2\pi^2 e^2}{\hbar c}\,\frac{\hbar^2}{m}\,\frac{NZ}{A} = 60\,\frac{NZ}{A}\ \text{mb MeV}\,. \qquad (2.46)$$

It was experimentally observed, that in medium- and heavy-nuclei, the GDR exhausts practically almost 100% of the sum rule, indicating that the GDR corresponds to a state $D|0\rangle$, resulting from the action of the dipole operator on the ground state.

2.3 Pygmy dipole resonance in a Harmonic Oscillator Shell Model

In this section we shall extend the work of Brink [45], briefly described previously, to the case of neutron-rich nuclei. In this case, we consider the system as being described in terms of three subsystems: (i) all protons, Z, (ii) a number of bound neutrons, N_c, and (iii) the less bound excess neutrons, N_e. Hence, the total number of neutrons is split between the core and excess neutrons, so that $N = N_c + N_e$ is satisfied, while, the first two subsystem define the core, $A_c = Z + N_c$. Our aim is to perform an analogous decomposition of the HOSM Hamiltonian (see Eq. (2.1)) into several commuting Hamiltonians, one of them associated to the pygmy motion i.e. the out of phase oscillations of the excess neutrons against the core. In order to achieve this, we shall replace the collective coordinates associated to the center of mass of protons, core and excess neutrons:

$$\mathbf{R}_p = \frac{1}{Z}\sum_{i=1}^{Z}\mathbf{r}_i\ ; \qquad \mathbf{R}_{n_c} = \frac{1}{N_c}\sum_{i=1}^{N_c}\mathbf{r}_i\ , \qquad \mathbf{R}_{n_e} = \frac{1}{N_e}\sum_{i=1}^{N_e}\mathbf{r}_i\ , \qquad (2.47)$$

and their conjugate momenta:

$$\mathbf{P}_p = \sum_{i=1}^{Z}\mathbf{p}_i\ ; \qquad \mathbf{P}_{n_c} = \sum_{i=1}^{N_c}\mathbf{p}_i\ , \qquad \mathbf{P}_{n_e} = \sum_{i=1}^{N_e}\mathbf{p}_i\ , \qquad (2.48)$$

with a different set of collective variables, including the pygmy degree of freedom. Consequently, we first introduce the center of mass position vector:

$$\mathbf{R}_{\rm CM} = \frac{1}{A}\left(Z\,\mathbf{R}_p + N_c\,\mathbf{R}_{n_c} + N_e\,\mathbf{R}_{n_e}\right)\,, \qquad (2.49)$$

with its conjugate momenta:

$$\mathbf{P}_{cm} = \mathbf{P}_p + \mathbf{P}_{n_c} + \mathbf{P}_{n_e}\,. \qquad (2.50)$$

Then, we define the distance between the center of mass of the protons and core neutrons:

$$\mathbf{X}_c = \mathbf{R}_p - \mathbf{R}_{n_c} \ , \tag{2.51}$$

with its conjugate momenta:

$$\mathbf{P}_c = \frac{N_c Z}{A_c} \left(\frac{\mathbf{P}_p}{Z} + \frac{\mathbf{P}_{n_c}}{N_c} \right) \ . \tag{2.52}$$

Eventually, the last set of variables will account for the distance between the center of mass of the core and the excess neutrons:

$$\mathbf{Y} = \frac{Z}{A_c} \, \mathbf{R}_p + \frac{N_c}{A_c} \, \mathbf{R}_{n_c} - \mathbf{R}_{n_e} \ , \tag{2.53}$$

and the corresponding conjugate momenta:

$$\mathbf{P}_y = \frac{N_e A_c}{A} \left(\frac{\mathbf{P}_p + \mathbf{P}_{n_c}}{A_c} + \frac{\mathbf{P}_{n_e}}{N_e} \right) \ . \tag{2.54}$$

With these new variables defined, we should return to the HOSM Hamiltonian (Eq. (2.1)) and expand the sums over position vectors and momenta with the help of the following expansion:

$$\begin{aligned} \sum_{i=1}^{A} \mathbf{x}_i \sum_{j=1}^{A} \mathbf{x}_j &= \sum_{i,j=1}^{A} (\mathbf{x}_i - \mathbf{x}_j + \mathbf{x}_j)(\mathbf{x}_j - \mathbf{x}_i + \mathbf{x}_i) \\ &= \sum_{i,j=1}^{A} (\mathbf{x}_i - \mathbf{x}_j)(\mathbf{x}_j - \mathbf{x}_i) + \sum_{i,j=1}^{A} \mathbf{x}_i^2 + \sum_{i,j=1}^{A} \mathbf{x}_j^2 - \sum_{i,j=1}^{A} \mathbf{x}_i \mathbf{x}_j \ ; \end{aligned} \tag{2.55a}$$

$$2A \sum_{i=1}^{A} \mathbf{x}_i^2 = 2 \sum_{i=1}^{A} \mathbf{x}_i \sum_{j=1}^{A} \mathbf{x}_j + \sum_{i,j=1}^{A} (\mathbf{x}_i - \mathbf{x}_j)^2 \tag{2.55b}$$

where $\mathbf{x}_i \in \{\mathbf{r}_i, \mathbf{p}_i\}$. Consequently, considering also Eqs. (2.47) and (2.48), we get for position vectors:

$$\sum_{i=1}^{B} \mathbf{r}_i^2 = B \, \mathbf{R}_b^2 + \frac{1}{2B} \sum_{i,j=1}^{B} (\mathbf{r}_i - \mathbf{r}_j)^2 \ , \tag{2.56}$$

and for conjugate momenta:

$$\sum_{i=1}^{B} \mathbf{p}_i^2 = \frac{1}{B} \, \mathbf{P}_b^2 + \frac{1}{2} \sum_{i,j=1}^{B} (\mathbf{p}_i - \mathbf{p}_j)^2 \ , \tag{2.57}$$

where $b \in \{p, n_c, n_e\}$ and $B \in \{Z, N_c, N_e\}$.

Using Eq. (2.56) the potential energy part of the HOSM Hamiltonian, H_{sm}, becomes:

$$\sum_{i=1}^{A} \mathbf{r}_i^2 = Z \, \mathbf{R}_p^2 + N_c \, \mathbf{R}_{n_c}^2 + N_e \, \mathbf{R}_{n_e}^2 + \text{ internal terms} \ . \tag{2.58}$$

We replace the position vectors associated to the center of mass of protons, core and excess neutrons with the previously defined collective variables $\mathbf{R}_{cm}, \mathbf{X}_c$ and $\mathbf{Y}$, using the relations:

$$\begin{aligned} \mathbf{R}_p &= \mathbf{R}_{cm} + \frac{N_e}{A}\,\mathbf{Y} + \frac{N_c}{A_c}\,\mathbf{X}_c\ , \\ \mathbf{R}_{n_c} &= \mathbf{R}_{cm} + \frac{N_e}{A}\,\mathbf{Y} - \frac{Z}{A_c}\,\mathbf{X}_c\ , \\ \mathbf{R}_{n_e} &= \mathbf{R}_{cm} - \frac{A_c}{A}\,\mathbf{Y}\ . \end{aligned} \tag{2.59}$$

Then, Eq. (2.58) becomes:

$$\sum_{i=1}^{A} \mathbf{r}_i^2 = A\,\mathbf{R}_{cm}^2 + \frac{N_e A_c}{A}\,\mathbf{Y}^2 + \frac{N_c Z}{A_c}\,\mathbf{X}_c^2 + \text{internal terms}\ , \tag{2.60}$$

Analogously, using Eq. (2.57), the kinetic energy part of the HOSM Hamiltonian can be written:

$$\sum_{i=1}^{A} \mathbf{p}_i^2 = \frac{1}{Z}\,\mathbf{P}_p^2 + \frac{1}{N_c}\,\mathbf{P}_{n_c}^2 + \frac{1}{N_e}\,\mathbf{P}_{n_e}^2 + \text{internal terms}\ . \tag{2.61}$$

Now, we replace the conjugate momenta of all protons, core and excess neutrons, in terms of the collective momenta, by employing the relations:

$$\begin{aligned} \mathbf{P}_p &= \frac{Z}{A}\,\mathbf{P}_{cm} + \frac{Z}{A_c}\,\mathbf{P}_y + \mathbf{P}_c\ , \\ \mathbf{P}_{n_c} &= \frac{N_c}{A}\,\mathbf{P}_{cm} + \frac{N_c}{A_c}\,\mathbf{P}_y - \mathbf{P}_c\ , \\ \mathbf{P}_{n_e} &= \frac{N_e}{A}\,\mathbf{P}_{cm} - \mathbf{P}_y\ . \end{aligned} \tag{2.62}$$

One gets for Eq. (2.61) :

$$\sum_{i=1}^{A} \mathbf{p}_i^2 = \frac{1}{A}\,\mathbf{P}_{cm}^2 + \frac{A}{A_c N_e}\,\mathbf{P}_y^2 + \frac{A_c}{Z N_c}\,\mathbf{P}_c^2 + \text{internal terms}\ . \tag{2.63}$$

Summing up Eq. (2.60) and Eq. (2.63) into Eq. (2.1) we reach the following decomposition, in terms of six commuting Hamiltonians [51, 52]:

$$\begin{aligned} H_{sm} &= H_{p,\text{int}} + H_{n_c,\text{int}} + H_{n_e,\text{int}} + H_{\text{CM}} + H_c + H_y = \\ &= H_{p,\text{int}} + H_{n_c,\text{int}} + H_{n_e,\text{int}} + \frac{1}{2Am}\,\mathbf{P}_{cm}^2 + \frac{KA}{2}\,\mathbf{R}_{cm}^2 \\ &\quad + \frac{A_c}{2ZN_c m}\,\mathbf{P}_c^2 + \frac{KN_cZ}{2A_c}\,\mathbf{X}_c^2 + \frac{A}{2A_cN_e m}\,\mathbf{P}_y^2 + \frac{KN_eA_c}{2A}\,\mathbf{Y}^2\ . \end{aligned} \tag{2.64}$$

As previously stated, the first three terms describe the internal motion of nucleons in each ensemble, and depend only on the relative coordinates and momenta of the nucleons belonging to each subsystem (protons, neutrons core and neutrons in excess):

$$H_{p,\text{int}} = \frac{1}{2}\sum_{i,j=1}^{Z} \frac{(\mathbf{p}_i - \mathbf{p}_j)^2}{2m} + \frac{1}{2\,Z}\,\frac{K}{2}\sum_{i,j=1}^{Z} (\mathbf{r}_i - \mathbf{r}_j)^2\ , \tag{2.65}$$

$$H_{n_c,\text{int}} = \frac{1}{2}\sum_{i,j=1}^{N_c}\frac{(\mathbf{p}_i-\mathbf{p}_j)^2}{2m} + \frac{1}{2\,N_c}\,\frac{K}{2}\sum_{i,j=1}^{N_c}(\mathbf{r}_i-\mathbf{r}_j)^2\ , \tag{2.66}$$

and

$$H_{n_e,\text{int}} = \frac{1}{2}\sum_{i,j=1}^{N_e}\frac{(\mathbf{p}_i-\mathbf{p}_j)^2}{2m} + \frac{1}{2N_e}\frac{K}{2}\sum_{i,j=1}^{N_e}(\mathbf{r}_i-\mathbf{r}_j)^2\ . \tag{2.67}$$

The center of mass Hamiltonian:

$$H_{\text{CM}} = \frac{1}{2\,A\,m}\,\mathbf{P}_{cm}^2 + \frac{KA}{2}\,\mathbf{R}_{cm}^2\ , \tag{2.68}$$

characterizes the center of mass motion of the nuclear system.

The core Hamiltonian:

$$H_c = \frac{A_c}{2\,Z\,N_c\,m}\,\mathbf{P}_c^2 + \frac{K\,N_c\,Z}{2\,A_c}\,\mathbf{X}_c^2\ , \tag{2.69}$$

describes the isovector Goldhaber-Teller vibration of protons against the core neutrons. The pygmy Hamiltonian:

$$H_y = \frac{A}{2\,A_c\,N_e\,m}\,\mathbf{P}_y^2 + \frac{K\,N_e\,A_c}{2\,A}\,\mathbf{Y}^2\ , \tag{2.70}$$

instead, is characteristic to the Goldhaber-Teller mode of the excess neutrons against the core, and represents the so-called pygmy mode. It is worth mentioning that both H_c and H_y will contribute to the dipole response, since the total dipole operator can be expressed as a sum of the core and pygmy dipole operators:

$$\begin{aligned}\mathbf{D} = \frac{NZ}{A}\,\mathbf{X} = \frac{NZ}{A}\big(\mathbf{R}_p-\mathbf{R}_n\big) = \frac{NZ}{A}\left(\frac{N_e}{N}\,\mathbf{Y} + \frac{AN_c}{A_cN}\,\mathbf{X}_c\right) = \frac{Z\,N_e}{A}\,\mathbf{Y} + \frac{Z\,N_c}{A_c}\,\mathbf{X}_c \\ = \mathbf{D}_y + \mathbf{D}_c\ .\end{aligned} \tag{2.71}$$

The total dipole absorption cross section corresponding to the excitation of the pygmy mode, can be estimated:

$$\begin{aligned}\sigma_y = \int_0^\infty \sigma_y(E)\,\mathrm{d}E &= \frac{4\,\pi^2e^2}{\hbar\,c}\sum_f (E_f-E_0)\,\big|\langle f|D_y|0\rangle\big|^2 \\ &= \frac{4\,\pi^2e^2}{\hbar\,c}\,m_{1_y} = \frac{4\,\pi^2e^2}{\hbar\,c}\,\frac{1}{2}\,\langle 0|[D_y,[H_{sm},D_y]]|0\rangle \\ &= \frac{2\,\pi^2e^2}{\hbar\,c}\,\big\langle 0\big|\big[D_y,[H_y,D_y]\big]\big|0\big\rangle\ .\end{aligned} \tag{2.72}$$

Evaluating the commutator one has:

$$\begin{aligned}[H_y,D_y] = \frac{A}{2mA_cN_e}\,\frac{N_eZ}{A}\,[\mathbf{P}_y^2,\mathbf{Y}] &= \frac{Z}{2mA_c}\big(\mathbf{P}_y[\mathbf{P}_y,\mathbf{Y}] + [\mathbf{P}_y,\mathbf{Y}]\mathbf{P}_y\big) \\ &= -\frac{i\hbar Z}{mA_c}\,\mathbf{P}_y\ .\end{aligned} \tag{2.73}$$

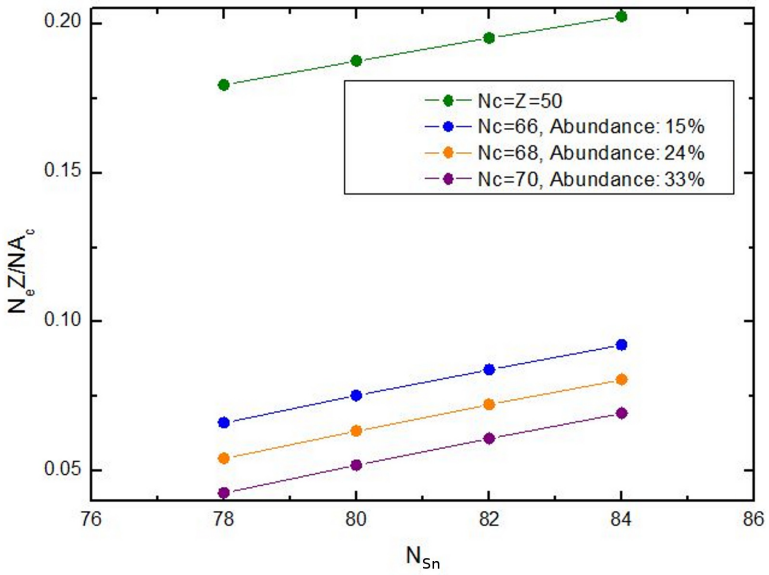

Figure 2.2: Graphical representation for the fraction, $f_y = (N_e Z)/(NA_c)$, of the EWSR exhausted by the pygmy mode for tin isotopes ^{128}Sn, ^{130}Sn, ^{132}Sn and ^{134}Sn, at various number of neutrons in the core.

Then:

$$\begin{aligned}\langle 0|[D_y,[H_y,D_y]]|0\rangle &= \langle 0|\Big[\frac{N_eZ}{A}\,\mathbf{Y},-\frac{i\hbar Z}{mA_c}\,\mathbf{P}_y\Big]|0\rangle \\ &= \langle 0|\frac{\hbar^2}{m}\,\frac{N_eZ^2}{AA_c}|0\rangle = \frac{\hbar^2}{m}\,\frac{N_eZ^2}{AA_c}\langle 0|0\rangle = \frac{\hbar^2}{m}\,\frac{N_eZ^2}{AA_c}\,. \end{aligned} \tag{2.74}$$

Eventually, the EWSR exhausted by the pygmy mode is obtained:

$$\sigma_y = \frac{2\pi^2e^2}{\hbar c}\,\frac{\hbar^2}{m}\,\frac{N_eZ^2}{AA_c} = \frac{N_eZ}{NA_c}\,\sigma_D\,. \tag{2.75}$$

This shows that a specific fraction, $f_y = \dfrac{N_eZ}{NA_c}$, depending on the number of excess neutrons from the total absorption cross section is exhausted by the PDR. We mention that this result is consistent with the molecular sum rule introduced by Alhassid and coworkers [53]. Moreover, within the sum-rule model approach, proposed by Kurasawa and Suzuki [54] an identical expression was obtained for the EWSR exhausted by the PDR.

If we consider the case of tin isotope ^{132}Sn, with the number of excess neutrons taken to be the difference between the total number of neutrons and protons, $N_e = N - Z = 32$, a particular fraction, $f_y = 19.5\%$, exhausted by the pygmy mode is obtained (see also Fig. 2.2). This value is larger than the experimentally estimated value, which is roughly 4% [8]. A possible explanation for the difference between the HOSM prediction and the experimental value, is that only a part of all the excess neutrons contribute to the pygmy mode, the rest being bound to the core. Actually, a core containing 50 neutrons and 50 protons is expected to be quite unstable, so, an additional number of excess neutrons

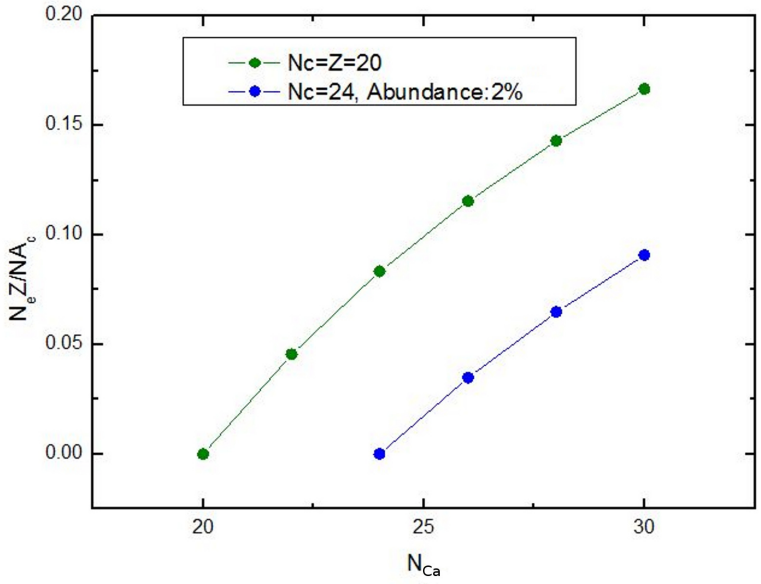

Figure 2.3: Graphical representation for the fraction, $f_y = (N_e Z)/(N A_c)$, of the EWSR exhausted by the pygmy mode for calcium isotopes ^{40}Ca, ^{42}Ca, ^{44}Ca, ^{46}Ca, ^{48}Ca a and ^{50}Ca, at various number of neutrons in the core.

will be bound to the core, making it more stable. To obtain a fraction of the EWSR close to the experimental value of 4%, we have to assume that only an effective number of $N_y = 10$ neutrons will participate in the pygmy mode, while the rest of 22 are blocked in the core. A similar conclusion was traced by Adrich *et al.* [8].

We extend now our analysis to other neutron rich calcium, nickel and lead isotopes. In the case of calcium isotope, ^{48}Ca, Ottini-Hustache *et al.* [18] have reported a fraction of about 5% of the electric dipole ($E1$) EWSR exhausted by the pygmy mode, whereas Hartmann *et al.* [19] found a value of 0.3%. In the symmetric isotope, $N = Z = 20$, ^{40}Ca, no PDR strength was found [19]. This is consistent with the results proposed by HOSM, since the excess number of neutrons in this case is 0. In the case of ^{48}Ca, the EWSR exhausted by the pygmy mode, as predicted by HOSM (see Fig. 2.3), varies from $\sim 14\%$ (when considering $N = Z = 20$ and $N_y = N_e = 8$) to $\sim 6\%$ (when the number of skin neutrons is reduced to $N_y = 4$).

For the nickel isotope ^{68}Ni, with the number of excess neutrons taken to be the difference between the total number of neutrons and protons, $N_e = N - Z = 12$, the corresponding EWSR exhausted by the pygmy mode would be $f_y = 15\%$. Wieland *et al.* reported in their experimental study [22] an EWSR between $5\% \rightarrow 9\%$, the largest value corresponding to the case where the level density was assumed to be a simple extrapolation from stable nuclei. If a more stable core is considered, $N_c = 32$ (so $N_y = 8$), the predicted EWSR exhausted by the PDR decreases to $f_y \approx 9\%$ (see Fig. 2.4), much closer to the experimental result. Moreover, for the nickel isotope ^{68}Ni, within a quasi-particle relativistic random phase approximation approach, Cao and Ma [55] reported a percentage of 10% of the EWSR exhausted in the low-lying region.

If we now consider lead isotopes, in particular ^{208}Pb, Ryezayeva *et al.* [56] have reported a fraction, $f_y = 2\%$ of the total $E1$ strength in the low-lying energy region. For

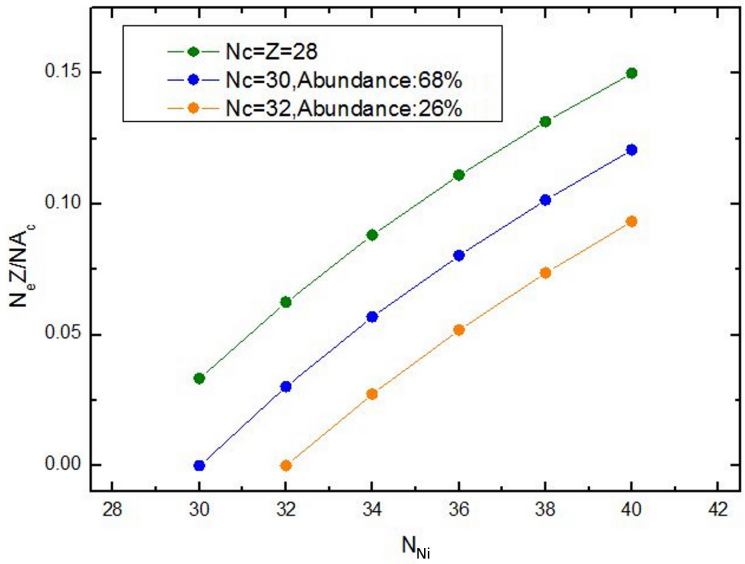

Figure 2.4: Graphical representation for the fraction, $f_y = (N_e Z)/(NA_c)$, of the EWSR exhausted by the pygmy mode for nickel isotopes ^{58}Ni, ^{60}Ni, ^{62}Ni, ^{64}Ni, ^{66}Ni, and ^{68}Ni, at various number of neutrons in the core.

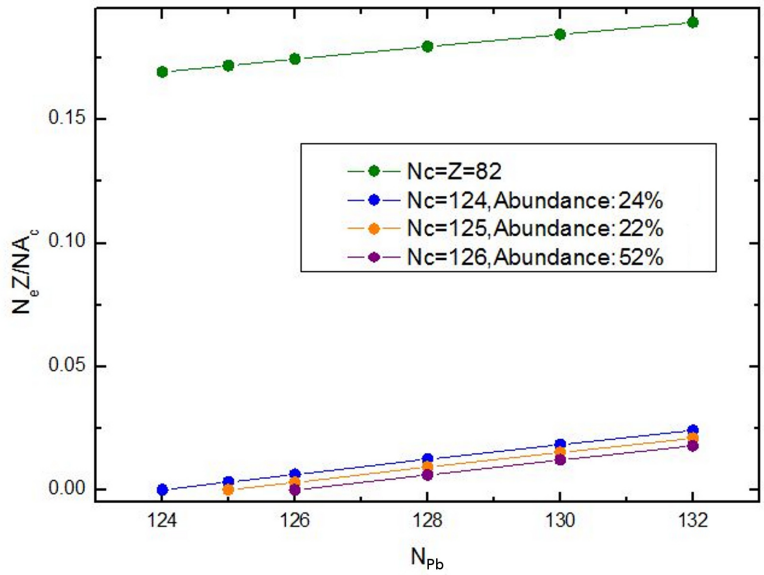

Figure 2.5: Graphical representation for the fraction, $f_y = (N_e Z)/(NA_c)$, of the EWSR exhausted by the pygmy mode for lead isotopes ^{206}Pb, ^{207}Pb, ^{208}Pb, ^{210}Pb, ^{212}Pb and ^{214}Pb, at various number of neutrons in the core.

the same isotope, within HOSM, the predicted fraction is around $f_y \approx 17.5\%$, when all the excess neutrons are involved in the pygmy oscillations (i.e. $N_y = N_e = 44$)(see Fig. 2.5). Considering now a more stable core, comprising $N_c = 124$ neutrons and $Z = 82$ protons, the EWSR exhausted by the pygmy mode gets closer to $f_y \approx 1\%$, with only 2 neutrons belonging to the skin (i.e. $N_y = 2$).

Considering the above examples, it is clear that the EWSR exhausted by the pygmy mode overestimates the experimental data, if all the excess neutrons are considered to take part in the pygmy oscillations against the symmetric $N_c = Z$ core. A better agreement with the experimental results is achieved if one consider a more stable core, which, in general, requires an $N_c > Z$ neutrons. In this case a smaller number of neutrons involved in the pygmy motion, $N_y < N_e$, leads to a smaller fraction of the EWSR exhausted. Therefore, it is important to test in more elaborated and self-consistent approaches, this possibility.

Indeed, a more accurate picture of the dipole response in finite nuclear matter corresponds to an admixture of Goldhaber-Teller and Steinwedel-Jensen vibrations. Consequently, the HOSM model, although powerful in providing a microscopic Hamiltonian picture of the pygmy and giant dipole responses, is yet unable to describe such an admixture.

In this respect, we shall consider a microscopic, self-consistent transport approach within the Landau theory of Fermi liquids aimed to investigate various dipole collective features of nuclear systems. In particular, we shall study the interplay between pygmy and isovector core vibration, and we will test the hypothesis suggested by the HOSM concerning the number of neutrons associated to the pygmy motion. In this model, the proton and neutron one-body distribution functions, $f_{p,n}(\mathbf{r}, \mathbf{p}, t)$, are obtained by solving two coupled Landau-Vlasov kinetic equations. This model was successfully employed to study various features of the GDR in hot nuclei [57], the pre-equilibrium excitation of the dipole mode in fusion entrance channel [58, 57], as well as in the description of the transition from isovector zero sound to first sound in symmetric nuclear matter [59, 60]. Since the main ingredients of this method are the mean-field and the kinetic equations, we shall devote the next Chapter for their description.

Chapter 3

Transport approach to nuclear dynamics

Traditional *ab initio* methods, in particular Hartree-Fock theory and its descendants, are based on the finding of the many-body wave-function of the system. Once the Hamiltonian is introduced, a variational principle problem is solved within an appropriate trial space. However, when considering realistic systems, these theories are difficult to be applied, the computational cost being one of the reasons. For nuclear systems, due to the presence of the short-range repulsive core, such theories lead to quite inaccurate results. It is concluded that in general, the nuclear many-body problem manifests several non-perturbative features with respect to the independent particle models. Even for the soft-core interactions, which allows for a perturbative description of the nuclear many-body problem, the lowest order is not sufficient to reach a convergent solution. Therefore, in nuclear physics, a different direction, namely the nuclear energy density functional (EDF), was adopted to treat still rigorously the problem of strongly interacting nucleons. This approach has many common features with the density functional theory, which was proposed initially for the description of electronic systems. The basic idea is to map the original interacting problem into an approach based on an independent particle description. DFT is based on the work of Hohenberg and Kohn(H-K) [61], which states that the problem of interacting particles within an external statical potential can be reduced to a non-interacting problem, where the energy is a functional of the local density. In the non-interacting problem, the particle move within a local effective potential, which can be expressed as a functional of the local density. The minimum of this functional, obtained variationally, coincides with the ground state energy of the interacting problem, while the corresponding density matches the local density of the initial system. Hohenberg and Kohn prove the existence of an unique functional of the density which determines exactly the external potential, and thus the ground-state energy, but gives no hint whatsoever on how this functional looks like. To construct the exact functional, several degrees of approximation have been proposed, including local density approximation (LDA), gradient expansion approximation (GEA) or generalized gradient approximation (GGA), where higher orders of density gradients were added.

The ideas behind density functional theory can be also applied to nucleons interacting trough the strong force within nuclear systems. In contrast to electronic systems, the *self bound* nature of the nuclei makes the original H-K work not entirely applicable (since there

is no external potential that confines the nucleons), thus, the energy density functional has been rather empirically introduced in the 70's [62]. Consequently, this implies the necessity to develop nuclear energy density functionals, in which the energy of the system is described in terms of proton and neutron densities.

Two phenomenological functionals of energy, namely the Gogny and Skyrme ones, are based on effective nucleon-nucleon interactions and are suitable for the description of nuclear matter properties. In particular, the effective nucleon-nucleon interaction in the Skyrme approach can be represented as a sum of two-body and three-body interactions [63]

$$V = \sum_{i<j} V_{ij} + \sum_{i<j<k} V_{ijk} \ . \tag{3.1}$$

The zero-range two-body operators, V_{ij}, in the above equation have the following form [64, 65]:

$$\begin{aligned} V_{ij} = {} & t_0 \, (1 + x_0 P_\sigma) \, \delta(\mathbf{r}_i - \mathbf{r}_j) + \frac{1}{2} \, t_1 \, (1 + x_1 P_\sigma) \big[(\mathbf{k}')^2 \, \delta(\mathbf{r}_i - \mathbf{r}_j) + \delta(\mathbf{r}_i - \mathbf{r}_j) \, \mathbf{k}^2 \big] \\ & + \ t_2 (1 + x_2 P_\sigma) \, \mathbf{k}' \, \delta(\mathbf{r}_i - \mathbf{r}_j) \, \mathbf{k} + \frac{1}{6} \, t_3 \, (1 + x_3 P_\sigma) \, \delta(\mathbf{r}_i - \mathbf{r}_j) \, \rho^\alpha \big(\frac{\mathbf{r}_i + \mathbf{r}_j}{2} \big) \\ & + i \, t_4 \, (\sigma_i + \sigma_j) \ [\mathbf{k}' \times \delta(\mathbf{r}_i - \mathbf{r}_j) \, \mathbf{k}] \ , \end{aligned} \tag{3.2}$$

with $\mathbf{k}$ being the operator of the relative momentum:

$$\mathbf{k} = \frac{1}{2i} \, \big(\nabla_i - \nabla_j \big) \ , \tag{3.3}$$

acting on the right direction, and with $\mathbf{k}'$:

$$\mathbf{k}' = - \frac{1}{2i} \, \big(\nabla_i - \nabla_j \big) \ , \tag{3.4}$$

acting on the left direction. The spin exchange operator, P_σ, has the form:

$$P_\sigma = \frac{1}{2} \big(1 + \sigma_i \cdot \sigma_j \big) \ . \tag{3.5}$$

In the above sum, the first term is associated to the central-part of the interaction, the terms with t_1 and t_2 characterise the non-local interaction, while the term with t_4 is related to the spin-orbit interaction. The three-body operators, V_{ijk}, correspond also to a zero-range interaction:

$$V_{ijk} = t_3 \, \delta(\mathbf{r}_i - \mathbf{r}_j) \, \delta(\mathbf{r}_i - \mathbf{r}_k) \ , \tag{3.6}$$

and, which, integrated over the coordinates of one of the particles, generates a two-body contact interaction dependent on the local density. The ground state energy of the system, considering the wave function to be a single Slater determinant, can be derived using the Hartree-Fock method:

$$E_0 = \langle \psi | T + V | \psi \rangle = \int d^3 r \ \mathscr{E}(\mathbf{r}) \ , \tag{3.7}$$

where $\mathscr{E}(\mathbf{r}) = \mathscr{E}_{kin}(\mathbf{r}) + \mathscr{E}_{pot}(\mathbf{r})$ represents the energy density functional. Even if, in this case, the functional was obtained from an effective interaction and a many-body method, there are several subtle differences between HF and EDF approach. In any case, the coefficients factorizing various terms, local density and density gradient dependent, are adjusted by requiring that a set of experimental properties are reproduced. Therefore, these coefficients encode more physics than those provided within HF theory. For example, for our Skyrme functional, the coefficients are fixed requiring that the saturation density, the binding energy at saturation, the incompressibility modulus, the symmetry energy at saturation and other properties are reproduced.

Knowing the energy density, one can also find the main ingredient required within the transport model, namely, the mean field potential, $U = \delta\mathscr{E}_{pot}(\mathbf{r})/\delta\rho(\mathbf{r})$. Consequently, employing the energy density functional technique allows us to obtain a self-consistent nuclear mean-field, subsequently used in the description of the dynamics of nuclear excitations, in particular the dipolar response. The dynamics of the nuclear systems is described using a semi-classical transport approach based on two coupled Landau-Vlasov kinetic equations for protons and neutrons. In the next section we shall describe in detail the properties of the energy density functional which will be employed into the transport model.

3.1 Energy density functional for nuclear systems

The energy density functional, from a thermodynamical point of view, can be seen as the nuclear equation of state (EOS) at zero temperature. Nuclear matter is an ideal system which contains two components, neutrons and protons, and, as a result, the EOS depends on both proton and neutron densities. Alternatively, it is possible to introduce other degrees of freedom, total or isoscalar density ($\rho_{isoscalar} = \rho = \rho_n + \rho_p$) and isospin or isovector density ($\rho_{isovector} = \rho_i = \rho_n - \rho_p$). In this case, the total energy per nucleon can be written as [66, 67]:

$$\frac{E}{A}(\rho, I) = \frac{E}{A}(\rho) + \frac{E_{sym}}{A}(\rho)\, I^2 \,, \tag{3.8}$$

where $\frac{E}{A}(\rho)$ describes the properties of symmetric nuclear matter, for which the isospin parameter:

$$I = \frac{\rho_i}{\rho} = \frac{N-Z}{A} \,, \tag{3.9}$$

becomes zero. It is obvious that the relation between the total energy per nucleon and the volume energy density provided by the energy density functional, $\mathscr{E}(\rho)$, is:

$$\mathscr{E}(\rho) = \mathscr{E}_{\rm kin} + \mathscr{E}_{\rm pot} = \frac{E(\rho)}{V} = \frac{E(\rho)}{A}\,\frac{A}{V} = \rho\,\frac{E}{A}(\rho) \,. \tag{3.10}$$

The pressure of the system, at zero temperature, is given by:

$$P = -\,\frac{\partial E}{\partial V} \,. \tag{3.11}$$

If, instead of the volume, we consider as the variable the density, $\rho = A/V$, considering that the total number of nucleons remains constant, we can write:

$$\mathrm{d}V = -\frac{V^2}{A}\,\mathrm{d}\rho\,, \tag{3.12}$$

and, consequently, we obtain the pressure as:

$$P = \frac{A}{V^2}\,\frac{dE}{d\rho} = \frac{A^2}{V^2}\,\frac{d(E/A)}{d\rho} = \rho^2\,\frac{d\varepsilon}{d\rho}\,, \tag{3.13}$$

with $\varepsilon = E/A = \varepsilon_{kin} + \varepsilon_{pot}$. At saturation density (equilibrium) the pressure should be equal to zero, $P(\rho_0) = 0$. An important thermodynamical response function is the compressibility, β :

$$\beta = -\frac{1}{V}\,\frac{\partial V}{\partial P} = \frac{1}{\rho}\,\frac{\partial \rho}{\partial P}\,, \tag{3.14}$$

which characterises the variation of the nuclear density with the pressure. Considering its inverse form, while taking into account Eq. (3.11), we have:

$$\beta^{-1} = V\,\frac{\partial^2 E}{\partial V^2} = \rho^3\,\frac{d^2(E/A)}{d\rho^2} = \rho^3\,\frac{d^2\varepsilon}{d\rho^2}\,, \tag{3.15}$$

where we used the density as variable instead of the volume. We can now define the nuclear incompressibility modulus, K:

$$K = \frac{9}{\rho}\,\beta^{-1} = 9\,\rho^2\,\frac{d^2\,\varepsilon}{d\rho^2}\,. \tag{3.16}$$

At saturation, the nuclear incompressibility modulus is a measure of the curvature parameter of the EOS, as a function of the density. Moreover, it can also be linked to the sound velocity which propagates in nuclear matter. Taking into account the experimental information, we shall require that, at saturation, the symmetric nuclear matter has the following properties: (i) the equilibrium density $\rho_0 = 0.16$ fm^{-3}, (ii) the energy per nucleon $E/A(\rho_0) = -16$ MeV/nucleon, while (iii) the incompressibility modulus corresponds to a soft-EOS $K(\rho_0) = 201$ MeV, and information about its value can be obtained from giant monopole resonances studies [64].

Returning to Eq. (3.10), for the kinetic part, taking into account the dependence of the density on the Fermi momentum, $\rho_{n,p} = \dfrac{k_{Fn,p}^3}{3\pi^2}$, we can write:

$$\begin{aligned}
\mathscr{E}_{\mathrm{kin}} &= \int_0^{\rho_n} \frac{p_{F,n}^2(\rho')}{2m}\,\mathrm{d}\rho' + \int_0^{\rho_p} \frac{p_{F,p}^2(\rho')}{2m}\,\mathrm{d}\rho' \\
&= \frac{\hbar^2}{2m}\,(3\pi^2)^{2/3}\left[\int_0^{\rho_n} {\rho'_n}^{2/3}\,\mathrm{d}\rho'_n + \int_0^{\rho_p} {\rho'_p}^{2/3}\,\mathrm{d}\rho'_p\right] \\
&= \frac{3}{5}\,\frac{\hbar^2}{2m}\,(3\pi^2)^{2/3}\left[\rho_n^{5/3} + \rho_p^{5/3}\right]\,.
\end{aligned} \tag{3.17}$$

Considering now the isospin parameter, $I = (N - Z)/A$, and

$$\rho_n = \frac{\rho}{2}\,(1 + I) \tag{3.18a}$$

$$\rho_p = \frac{\rho}{2}\,(1 - I)\,, \tag{3.18b}$$

we have

$$\mathscr{E}_{kin} = \frac{3}{5}\,\frac{\hbar^2}{2m}\,(3\pi^2)^{2/3}\,\frac{1}{2^{5/3}}\,\rho^{5/3}\big[(1+I)^{5/3}+(1-I)^{5/3}\big]\,. \tag{3.19}$$

Thus, we can write:

$$\frac{E}{A}(\rho,I)_{\rm kin} = \frac{\mathscr{E}_{\rm kin}}{\rho} = \frac{3}{5}\,\varepsilon_F(\rho)\,\frac{1}{2}\,\big[(1+I)^{5/3}+(1-I)^{5/3}\big]\,, \tag{3.20}$$

with the Fermi energy:

$$\varepsilon_F(\rho) = \frac{\hbar^2}{2m}\Big(\frac{3\pi^2}{2}\Big)^{2/3}\rho^{2/3}\,. \tag{3.21}$$

Now, if we recall the symmetry energy coefficient definition, $a_{\rm sym} = E_{\rm sym}/A = \varepsilon_{\rm sym}$ (see Eq. 3.8)), in the Bethe-Weizsäcker mass formula [68]:

$$a_{\rm sym} = \frac{1}{2}\,\frac{\partial^2}{\partial I^2}\,\frac{E}{A}(\rho,I)\bigg|_{I=0}\,, \tag{3.22}$$

we obtain the kinetic contribution to the symmetry energy:

$$\begin{aligned}\big(\varepsilon_{\rm sym}\big)_{\rm kin} &= \frac{3}{5}\,\varepsilon_F(\rho)\,\frac{1}{4}\,\frac{\partial^2}{\partial I^2}\,\big[(1+I)^{5/3}+(1-I)^{5/3}\big]\bigg|_{I=0}\\ &= \frac{3}{5}\,\varepsilon_F(\rho)\,\frac{1}{4}\,\frac{4\cdot 5}{9} = \frac{1}{3}\,\varepsilon_F(\rho)\,.\end{aligned} \tag{3.23}$$

Comparing with a value for a_{sym} provided by the Bethe-Weizsäcker formula, $a_{sym} = 28 \to 32$ MeV, we observe that the kinetic contribution, essentially related to the Pauli correlations, represents less than a half. The rest of the contribution to the symmetry energy is the result of the properties of the nucleon-nucleon interaction, specifically, the interaction in the isovector channel:

$$\varepsilon_{\rm sym} \equiv \frac{E_{\rm sym}}{A}(\rho) = \big(\varepsilon_{\rm sym}\big)_{\rm kin} + \big(\varepsilon_{\rm sym}\big)_{\rm pot}\,. \tag{3.24}$$

For example, for a simplified Skyrme-like force [68]:

$$V_{ij} = t_0\,(1+x_0P_\sigma)\,\delta(\mathbf{r}_i-\mathbf{r}_j) + \frac{1}{6}\,t_3\,(1+x_3P_\sigma)\Big(\rho\frac{\mathbf{r}_i+\mathbf{r}_j}{2}\Big)^{\sigma-1}\,\delta(\mathbf{r}_i-\mathbf{r}_j)\,, \tag{3.25}$$

with the coefficients:

$$t_0 = -2973\ \text{MeV}\cdot\text{fm}^3 \tag{3.26a}$$

$$t_3 = 19034\ \text{MeV}\cdot\text{fm}^{(3\times\sigma)} \tag{3.26b}$$

$$x_0 = 0.025\,,\quad x_3 = 0\,,\quad \sigma = \frac{7}{6}\,, \tag{3.26c}$$

the interaction contribution to the energy density functional has the form:

$$\mathscr{E}_{pot}(\rho,\rho_i) = \frac{E_{pot}}{V} = \frac{E_{pot}}{A}\,\frac{A}{V} = \frac{A}{2}\,\frac{\rho^2}{\rho_0} + \frac{B}{\sigma+1}\,\frac{\rho^{\sigma+1}}{\rho_0^\sigma} + \frac{C(\rho)}{2}\,\frac{\rho_i^2}{\rho_0}\,, \tag{3.27}$$

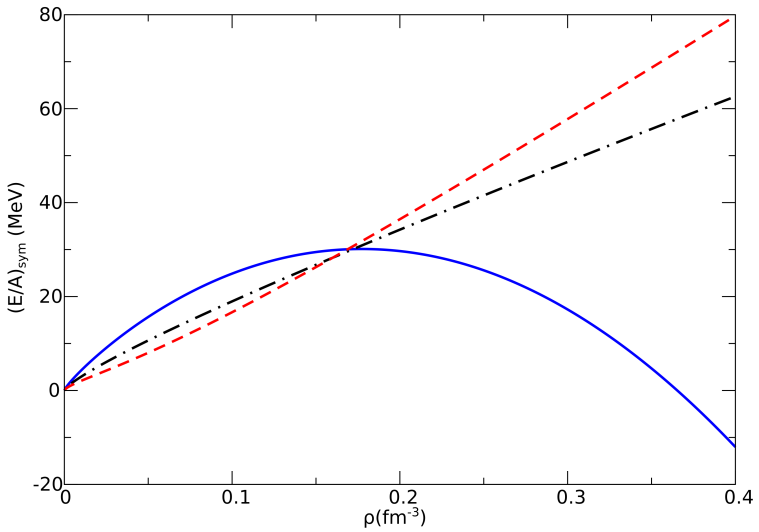

Figure 3.1: Graphical representation of the density dependence of the symmetry energy per nucleon, $\frac{E_{\rm sym}}{A}$, (expressed in Eq. (3.32)) for different parametrizations of the symmetry energy: solid blue for *asy-soft*, dot-dashed black for *asy-stiff* and dashed red for *asy-superstiff*, the isospin parameter I corresponding to ^{132}Sn isotope.

where:

$$A = \frac{3}{4}\, t_0\, \rho_0 \,, \tag{3.28}$$

$$B = \frac{\sigma+1}{16}\, t_3\, \rho_0^{\sigma} \,, \tag{3.29}$$

$$C(\rho) = -\frac{1}{4}\,\rho_0 \Big[t_0(1+2x_0) + \frac{t_3}{6}\,(1+2x_3)\rho^{\sigma-1} \Big] \,. \tag{3.30}$$

Consequently, in this case, the potential part of the symmetry energy is:

$$\begin{aligned} \Big(\frac{E_{\rm sym}}{A}\Big)_{\rm pot} I^2 &= \frac{1}{\rho}\,\frac{C(\rho)}{2}\,\frac{\rho_i^2}{\rho_0} \\ \Big(\frac{E_{\rm sym}}{A}\Big)_{\rm pot} \frac{\rho_i^2}{\rho^2} &= \frac{1}{\rho}\,\frac{C(\rho)}{2}\,\frac{\rho_i^2}{\rho_0} \\ \Big(\frac{E_{\rm sym}}{A}\Big)_{\rm pot} &= \big(\varepsilon_{\rm sym}\big)_{\rm pot} = \frac{C(\rho)}{2}\,\frac{\rho}{\rho_0} \,, \end{aligned} \tag{3.31}$$

and finally we obtain:

$$\varepsilon_{\rm sym} \equiv \frac{E_{\rm sym}}{A}(\rho) = \big(\varepsilon_{\rm sym}\big)_{\rm kin} + \big(\varepsilon_{\rm sym}\big)_{\rm pot} = \frac{1}{3}\,\varepsilon_F(\rho) + \frac{C(\rho)}{2}\,\frac{\rho}{\rho_0} \,. \tag{3.32}$$

Around the saturation point, the symmetry energy dependence on density is characterized by the values of the coefficients L and $K_{\rm sym}$ appearing in the expansion up to the second order of $\varepsilon_{\rm sym}(\rho)$ [66, 69]:

$$\varepsilon_{\rm sym}(\rho) = \varepsilon_{\rm sym}(\rho_0) + \frac{L}{3}\left(\frac{\rho-\rho_0}{\rho_0}\right) + \frac{K_{\rm sym}}{18}\left(\frac{\rho-\rho_0}{\rho_0}\right)^2 \,, \tag{3.33}$$

where L represents the slope parameter and $K_{\rm sym}$ represents the curvature of the nuclear symmetry energy at saturation density. More specifically, the slope parameter is defined as:

$$L = 3\,\rho_0\,\left.\frac{d\varepsilon_{\rm sym}}{d\rho}\right|_{\rho=\rho_0}\,, \tag{3.34}$$

and the curvature parameter as:

$$K_{\rm sym} = 9\,\rho_0^2\,\left.\frac{d^2\varepsilon_{\rm sym}}{d^2\rho}\right|_{\rho=\rho_0}\,. \tag{3.35}$$

It is useful to link the slope and curvature parameters to other physical properties which are more meaningful. We can express the slope parameter, L, in terms of the *symmetry pressure*:

$$L = \frac{3}{\rho_0}\,P_{\rm sym}(\rho_0)\,, \tag{3.36}$$

where

$$P_{\rm sym} = \rho^2\,\left.\frac{d\varepsilon_{\rm sym}}{d\rho}\right|_{\rho=\rho_0}\,, \tag{3.37}$$

For asymmetric nuclear matter characterised by the isospin parameter, I, the shift of the equilibrium density and incompressibility can be expressed in terms of these two coefficients:

$$\Delta\rho_0(I) = \frac{3\,\rho_0\,L}{K(I=0)}\,I^2 < 0\,, \tag{3.38}$$

and

$$\Delta K(I) = (K_{\rm sym} - 6\,L)\,I^2 < 0\,. \tag{3.39}$$

Now, in the spirit of EDF formalism, in the following Chapters we shall resume to a potential energy density defined by Eq. (3.27). The mean-field potentials for protons (neutrons) can be expressed as the functional derivative of $\mathscr{E}_{pot}$ with respect to the proton (neutron) density [68, 70]:

$$U_p = \frac{\delta\mathscr{E}_{\rm pot}}{\delta\rho_p} = A\,\frac{\rho}{\rho_0} + B\Big(\frac{\rho}{\rho_0}\Big)^{\sigma} - C(\rho)\,\frac{\rho_i}{\rho_0} + \frac{1}{2}\,\frac{dC(\rho)}{d\rho}\,\frac{\rho_i^2}{\rho_0}\,, \tag{3.40}$$

$$U_n = \frac{\delta\mathscr{E}_{\rm pot}}{\delta\rho_n} = A\,\frac{\rho}{\rho_0} + B\Big(\frac{\rho}{\rho_0}\Big)^{\sigma} + C(\rho)\,\frac{\rho_i}{\rho_0} + \frac{1}{2}\,\frac{dC(\rho)}{d\rho}\,\frac{\rho_i^2}{\rho_0}\,. \tag{3.41}$$

A commonly used parametrization for the isoscalar mean-field channel, corresponding to a so-called "hard EOS", characterised by a large value of incompressibility ($K(\rho_0) = 380$ MeV) is given by:

$$U_{n,p} = -124\ {\rm MeV}\,\frac{\rho}{\rho_0} + 70.5\ {\rm MeV}\,\Big(\frac{\rho}{\rho_0}\Big)^2\,. \tag{3.42}$$

However, experimental indications favors a "soft EOS" with $K(\rho_0) = 201$ MeV:

$$U_{n,p} = -356.8\ {\rm MeV}\,\frac{\rho}{\rho_0} + 303.9\ {\rm MeV}\,\Big(\frac{\rho}{\rho_0}\Big)^{7/6}\,, \tag{3.43}$$

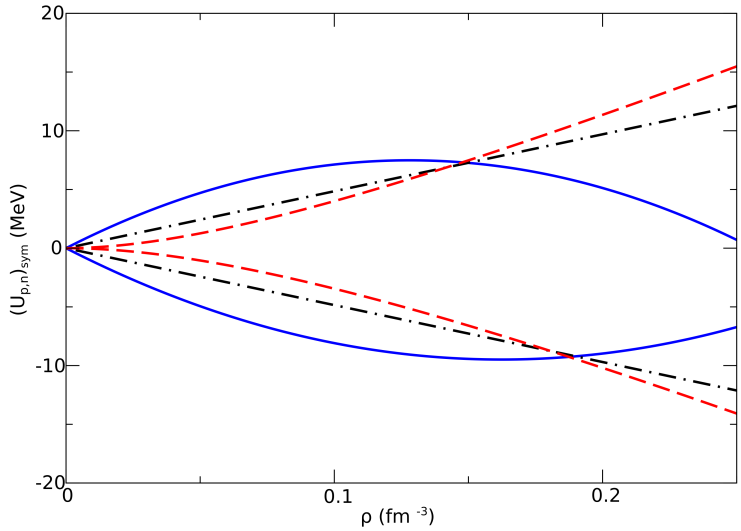

Figure 3.2: Graphical representation of the density dependence of the symmetry contribution to the mean field, $(U_{p,n})_{\rm sym}$, for protons (see Eq. (3.40)) - lower curves and for neutrons (see Eq. (3.41)) - upper curves, for different parametrizations of the symmetry energy: solid blue line for *asy-soft*, dot-dashed black line for *asy-stiff* and dashed red line for *asy-superstiff*, the isospin parameter I corresponding to ^{132}Sn isotope.

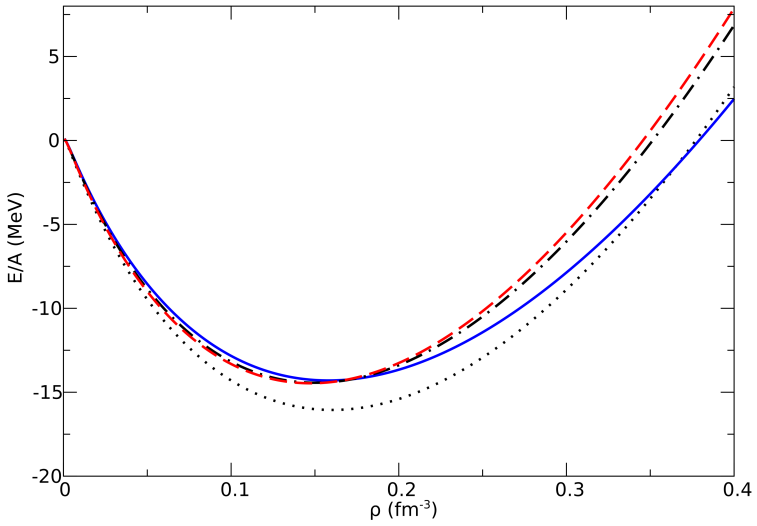

Figure 3.3: Graphical representation of the density dependence of the energy per nucleon, $\frac{E}{A}$, (expressed in Eq. (3.8)) for different parametrizations of the symmetry energy: solid blue line for *asy-soft*, dot-dashed black line for *asy-stiff* and dashed red line for *asy-superstiff*, the isospin parameter I corresponding to ^{132}Sn isotope, and for symmetric nuclear matter, $\frac{E}{A}\big|_{I=0}$: dotted black line.

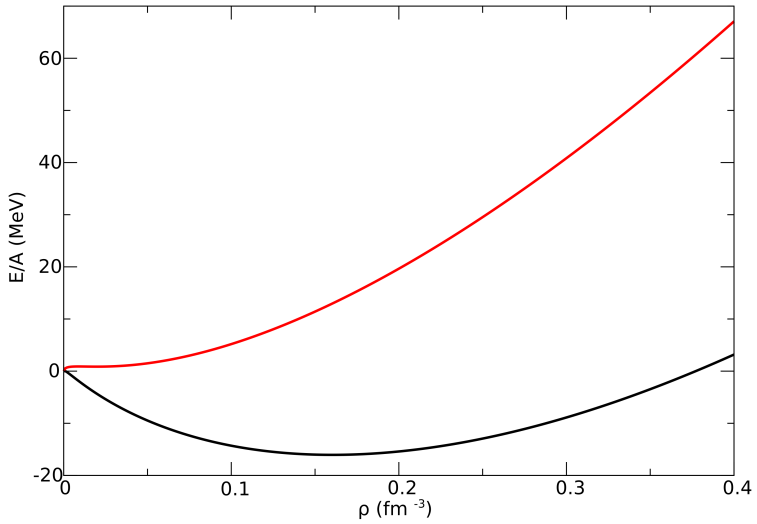

Figure 3.4: Graphical representation of the density dependence of the energy per nucleon in symmetric nuclear matter, $\frac{E}{A}\big|_{I=0}$ (black line), and in neutron matter, $\frac{E}{A}\big|_{I=1}$, for an *asy-stiff* parametrization of the symmetry term, i.e. $C = 32\ MeV$ (red line).

which we will employ in our numerical simulations.

However, the knowledge of the equation of state for asymmetric nuclear matter beyond normal conditions remains still poor. Based on the philosophy of EDF, while keeping the value of symmetry energy at saturation almost the same, we shall allow for three different dependences with density away from equilibrium. For the *asy-soft* EOS we imply a SKM* parametrisation, in which the symmetry term manifests an almost flat dependence around saturation density, and a slow decrease towards higher densities (a small slope parameter, L). For the *asy-stiff* EOS the dependence on the density of $C(\rho)$ is constant (i.e $C(\rho)$ = constant $\approx$ 32 MeV), and thus, the symmetry term will linearly increase with respect to the nuclear density. Lastly, for the *asy-superstiff* EOS, the symmetry term increases rapidly around saturation density, proportional to $\frac{\rho^2}{\rho_0(\rho+\rho_0)}$ (see also Fig. 3.1). It becomes clear that, away from the saturation density, $\rho_0 = 0.16$ fm^{-3}, the mean field perceived by protons and neutrons are different for the three equations of state introduced (see also Fig. 3.2).

Lastly, we represent in Fig. 3.3 the density dependence of the energy per nucleon for an isospin parameter corresponding to ^{132}Sn isotope, and in Fig. 3.4 the density dependence of the energy per nucleon in symmetric nuclear matter.

3.2 Landau-Vlasov kinetic equations

This section is devoted to an analysis of the basic features of the Landau-Vlasov equation. In the first part, by employing the Wigner transform, we prove that the Vlasov equation for one-body distribution function represents the semi-classical approximation of the time dependent Hartree-Fock equations. We will closely follow the work of Bertsch and Das Gupta [71], and, for consistency, in addition, several detailed proofs will be presented.

Then, this equation will be solved analytically in the linear approximation. The solution represents a quantum collective mode named zero-sound. Both the isoscalar and isovector modes in nuclear matter are described and the role of the symmetry energy in the later case will be addressed.

To deduce the Vlasov equation, we shall first express the time dependent HF equations in terms of the one-body *density matrix*. This is defined as:

$$\rho_{ji} = \langle\psi|a_i^\dagger a_j|\psi\rangle \ , \tag{3.44}$$

where $|\psi\rangle$ is a single determinant representing the many-body wave function, while the annihilation and creation operators, $a_i, a_i^\dagger$, refers to an arbitrary single-particle complete basis. The time derivative of the matrix elements, ρ_{ji}, is given by:

$$\dot{\rho}_{ji} = \frac{\partial}{\partial t}\big(\langle\psi|a_i^\dagger a_j|\psi\rangle\big) = \frac{\partial}{\partial t}\langle\psi|a_i^\dagger a_j|\psi\rangle + \langle\psi|a_i^\dagger a_j\frac{\partial}{\partial t}|\psi\rangle \ . \tag{3.45}$$

Using the time-dependent Schrödinger equation:

$$\frac{\partial}{\partial t}\,|\psi\rangle = \frac{1}{i\hbar}\,H|\psi\rangle \ , \tag{3.46}$$

and its adjoint conjugate, one can write Eq. (3.45):

$$\dot{\rho}_{ji} = \frac{1}{i\hbar}\,\langle\psi|[a_i^\dagger a_j, H]|\psi\rangle = \frac{1}{i\hbar}\,\langle\psi|[a_i^\dagger, H]a_j + a_i^\dagger[a_j, H]|\psi\rangle \ . \tag{3.47}$$

Here the exact Hamiltonian, H, is expressed as a sum between the kinetic and potential energy operators, in the occupation number representation:

$$H = T + V = \sum_{pq} t_{pq}\ a_p^\dagger\, a_q + \frac{1}{2}\sum_{prqs} v_{prqs}\ a_p^\dagger\, a_r^\dagger\, a_s\, a_q \ , \tag{3.48}$$

where t_{pq} and v_{prqs} represent one-body and two-body matrix elements respectively. To obtain the time derivative of the density matrix, we have to evaluate the commutators of the creation and annihilation operators with the kinetic and potential energy operators. One should keep in mind that for fermions, the following fundamental anti-commutation relations hold:

$$\{a_i, a_j\} = 0 \ ; \qquad \{a_i^\dagger, a_j^\dagger\} = 0 \ ; \qquad \{a_i^\dagger, a_j\} = \delta_{ij} \ . \tag{3.49}$$

For the kinetic energy commutators, we have:

$$\begin{aligned}[a_i^\dagger, T] &= \sum_{pq} t_{pq}\,[a_i^\dagger, a_p^\dagger a_q] = \sum_{pq} t_{pq}\big(\{a_i^\dagger, a_p^\dagger\}a_q - a_p^\dagger\{a_q, a_i^\dagger\}\big) \\ &= -\sum_{pq} t_{pq}\ a_p^\dagger\,\delta_{qi} = -\sum_{p} t_{pi}\ a_p^\dagger \ ,\end{aligned} \tag{3.50}$$

and

$$\begin{aligned}[a_j, T] &= \sum_{pq} t_{pq}[a_j, a_p^\dagger a_q] = \sum_{pq} t_{pq}\big(\{a_j, a_p^\dagger\}a_q - a_p^\dagger\{a_q, a_j\}\big) \\ &= \sum_{pq} t_{pq}a_q\delta_{jp} = \sum_{p} t_{jp}a_p \ .\end{aligned} \tag{3.51}$$

Consequently, the kinetic energy contribution to the time derivative of the density matrix will be:

$$
\begin{aligned}
(\dot{\rho}_{ji})_{\rm kin} &= \frac{1}{i\hbar}\sum_p \langle\psi|\big\{ -t_{pi}\,a_p^\dagger\,a_j + t_{jp}\,a_i^\dagger\,a_p\big\}|\psi\rangle \\
&= \frac{1}{i\hbar}\sum_p (t_{jp}\,\rho_{pi} - \rho_{jp}\,t_{pi}) = \frac{1}{i\hbar}\,\langle j|\big(T\rho - \rho T\big)|i\rangle\ . \qquad (3.52)
\end{aligned}
$$

For the commutators involving the potential energy, we need to evaluate the following commutators:

$$
\begin{aligned}
[a_i^\dagger, a_p^\dagger a_r^\dagger a_s a_q] &= \{a_p^\dagger a_r^\dagger a_s, a_i^\dagger\}a_q - a_p^\dagger a_r^\dagger a_s\{a_q, a_i^\dagger\} \\
&= a_p^\dagger a_r^\dagger\{a_s, a_i^\dagger\}a_q - [a_p^\dagger a_r^\dagger, a_i^\dagger]\,a_s, a_q - a_p^\dagger a_r^\dagger a_s\ \delta_{qi} \\
&= a_p^\dagger a_r^\dagger a_q\ \delta_{si} - a_p^\dagger a_r^\dagger a_s\ \delta_{qi}\ , \qquad (3.53)
\end{aligned}
$$

and

$$
\begin{aligned}
[a_j, a_p^\dagger a_r^\dagger a_s a_q] &= \{a_p^\dagger a_r^\dagger a_s, a_j\}a_q - a_p^\dagger a_r^\dagger a_s\{a_q, a_j\} \\
&= a_p^\dagger a_r^\dagger\{a_s, a_j\}a_q - [a_p^\dagger a_r^\dagger, a_j]a_s a_q \\
&= -a_p^\dagger\{a_r^\dagger, a_j\}a_s a_q + \{a_p^\dagger, a_j\}a_r^\dagger a_s a_q \\
&= a_p^\dagger a_s a_q\ \delta_{pj} - a_p^\dagger a_s a_q\ \delta_{rj}\ . \qquad (3.54)
\end{aligned}
$$

Consequently, the potential energy contribution to the time variation of the density matrix can be written:

$$
\begin{aligned}
(\dot{\rho}_{ji})_{\rm pot} &= \frac{1}{i\hbar}\langle\psi|\frac{1}{2}\sum_{prqs} v_{prqs}\big[(a_p^\dagger a_r^\dagger a_q\,\delta_{si} - a_p^\dagger a_r^\dagger a_s\,\delta_{qi})a_j \\
&\quad + a_i^\dagger(a_r^\dagger a_s a_q\,\delta_{pj} - a_p^\dagger a_s a_q\,\delta_{rj})\big]\psi\rangle \\
&= \frac{1}{2i\hbar}\langle\psi|\sum_{prq} v_{prqi}a_p^\dagger a_r^\dagger a_q a_j - \sum_{prs} v_{pris}a_p^\dagger a_r^\dagger a_s a_j \\
&\quad + \sum_{rqs} v_{jrqs}a_i^\dagger a_r^\dagger a_s a_q - \sum_{pqs} v_{pjqs}a_i^\dagger a_p^\dagger a_s a_q|\psi\rangle \\
&= \frac{1}{2i\hbar}\langle\psi|\sum_{prq}(v_{prqi} - v_{priq})a_p^\dagger a_r^\dagger a_q a_j + \sum_{rqs}(v_{jrqs} - v_{rjqs})a_i^\dagger a_r^\dagger a_s a_q|\psi\rangle \\
&= \frac{1}{2i\hbar}\Big(\sum_{prq}(v_{prqi} - v_{priq})\langle\psi|a_p^\dagger a_r^\dagger a_q a_j|\psi\rangle + \sum_{rqs}(v_{jrqs} - v_{rjqs})\langle\psi|a_i^\dagger a_r^\dagger a_s a_q|\psi\rangle\Big)\ . \qquad (3.55)
\end{aligned}
$$

We shall now proof that for any Slater determinant, $|\psi\rangle = b_1^\dagger ... b_i^\dagger ... b_N^\dagger|0\rangle$, where b_i are associated with any single-particle complete basis, the following relation holds:

$$
\langle\psi|a_p^\dagger a_r^\dagger a_q a_s|\psi\rangle = \rho_{qr}\rho_{sp} - \rho_{sr}\rho_{qp}\ . \qquad (3.56)
$$

We observe that the creation and annihilation operators, a, can be related to the operators, b, trough a unitary transformation:

$$a_p^\dagger = \sum_l u_{pl}^* \, b_l^\dagger \; ; \qquad a_q = \sum_l u_{ql} \, b_l \; . \tag{3.57}$$

Consequently, one can write:

$$\begin{aligned} \langle\psi|a_p^\dagger \, a_r^\dagger \, a_q \, a_s|\psi\rangle = & \sum_{lm} u_{pl}^* \, u_{rm}^* \, u_{ql} \, u_{sm} \, \langle\psi|b_l^\dagger \, b_m^\dagger \, b_l \, b_m|\psi\rangle \\ & + \sum_{lm} u_{pl}^* \, u_{rm}^* \, u_{qm} \, u_{sl} \, \langle\psi|b_l^\dagger \, b_m^\dagger \, b_m \, b_l|\psi\rangle \; . \end{aligned} \tag{3.58}$$

A rearrangement of the creation and annihilation operators leads to:

$$\langle\psi|b_l^\dagger \, b_m^\dagger \, b_l \, b_m|\psi\rangle = \langle\psi|b_l^\dagger(\, \delta_{lm} - b_l \, b_m^\dagger)b_m|\psi\rangle = \langle\psi|\, \delta_{lm} b_l^\dagger \, b_m|\psi\rangle - \langle\psi|b_l^\dagger \, b_l \, b_m^\dagger \, b_m|\psi\rangle \; , \tag{3.59}$$

and

$$\langle\psi|\, b_l^\dagger \, b_m^\dagger \, b_m \, b_l \, |\psi\rangle = -\langle\psi|\, b_l^\dagger \, b_m^\dagger \, b_l \, b_m \, |\psi\rangle \; . \tag{3.60}$$

Eventually, the substitution of Eqs. (3.59) and (3.60) into Eq. (3.58), and keeping in mind that $|\psi\rangle$ is a Slater determinant, leads to:

$$\begin{aligned} \langle\psi|a_p^\dagger a_r^\dagger a_q a_s|\psi\rangle &= -\sum_{lm} u_{pl}^* u_{rm}^* u_{ql} u_{sm} \langle\psi|b_l^\dagger b_l|\psi\rangle\langle\psi|b_m^\dagger b_m|\psi\rangle \\ &\quad + \sum_{lm} u_{pl}^* u_{rm}^* u_{qm} u_{sl} \langle\psi|b_l^\dagger b_l|\psi\rangle\langle\psi|b_m^\dagger b_m|\psi\rangle \\ &= -\langle\psi|\sum_l u_{pl}^* b_l^\dagger \sum_l u_{ql} b_l|\psi\rangle\langle\psi|\sum_m u_{rm}^* b_m^\dagger \sum_m u_{sm} b_m|\psi\rangle \\ &\quad + \langle\psi|\sum_l u_{pl}^* b_l^\dagger \sum_l u_{sl} b_l|\psi\rangle\langle\psi|\sum_m u_{rm}^* b_m^\dagger \sum_m u_{qm} b_m|\psi\rangle \\ &= -\langle\psi|a_p^\dagger a_q|\psi\rangle\langle\psi|a_r^\dagger a_s|\psi\rangle + \langle\psi|a_p^\dagger a_s|\psi\rangle\langle\psi|a_r^\dagger a_q|\psi\rangle \\ &= \rho_{qr}\rho_{sp} - \rho_{sr}\rho_{qp} \; . \end{aligned} \tag{3.61}$$

Based on the previous result, one can further write the potential energy contribution as:

$$(\dot{\rho}_{ji})_{\rm pot} = \frac{1}{2i\hbar}\Big\{ \sum_{prq}(v_{prqi} - v_{priq})(\rho_{qr}\rho_{jp} - \rho_{jr}\rho_{qp}) + \sum_{rqs}(v_{jrqs} - v_{rjqs})(\rho_{sr}\rho_{qi} - \rho_{qr}\rho_{si})\Big\} \; . \tag{3.62}$$

If we now introduce the self-consistent Hartree-Fock potential [50, 71]:

$$\langle p|U|q\rangle = \sum_{rs}(v_{prqs} - v_{rpqs})\rho_{sr} \; , \tag{3.63}$$

we obtain:

$$\begin{aligned} (\dot{\rho}_{ji})_{\rm pot} &= \frac{1}{2i\hbar}\Big\{ \sum_q \langle j|U|q\rangle \, \rho_{qi} + \sum_s \langle j|U|s\rangle \, \rho_{si} - \sum_p \langle p|U|i\rangle \, \rho_{jp} - \sum_r \langle r|U|i\rangle \, \rho_{jr}\Big\} \\ &= \frac{1}{i\hbar}\sum_\alpha \big\{ \langle j|U|\alpha\rangle \, \rho_{\alpha i} - \rho_{j\alpha}\langle\alpha|U|i\rangle\big\} \; . \end{aligned} \tag{3.64}$$

We sum up the kinetic and potential contributions:

$$(\dot{\rho}_{ji})_{\rm kin} = \frac{1}{i\hbar}\sum_{\alpha}\left(\langle j|T|\alpha\rangle\,\rho_{\alpha i} - \rho_{j\alpha}\,\langle\alpha|T|i\rangle\right)\,, \tag{3.65}$$

$$(\dot{\rho}_{ji})_{\rm pot} = \frac{1}{i\hbar}\sum_{\alpha}\left(\langle j|U|\alpha\rangle\,\rho_{\alpha i} - \rho_{j\alpha}\,\langle\alpha|U|i\rangle\right)\,, \tag{3.66}$$

and thus, we arrive to the time-dependent Hartree-Fock equation for the density matrix:

$$\begin{aligned}(\dot{\rho}_{ji})_{\rm total} &= \frac{1}{i\hbar}\sum_{\alpha}\left(\langle j|T+U|\alpha\rangle\,\rho_{\alpha i} - \rho_{j\alpha}\,\langle\alpha|T+U|i\rangle\right)\\ &= \frac{1}{i\hbar}\,\langle j|\big(H\rho-\rho H\big)|i\rangle\,.\end{aligned} \tag{3.67}$$

For example, if we consider the density matrix elements in the position representation:

$$\rho_{\mathbf{r}\mathbf{r}'} = \sum_{\alpha}\psi_{\alpha}(\mathbf{r})\;\psi^{*}_{\alpha}(\mathbf{r}')\,, \tag{3.68}$$

with $|\alpha\rangle$ denoting any complete single-particle basis, and the time derivative of the density matrix written as:

$$\dot{\rho}_{\mathbf{r}\mathbf{r}'} = \sum_{\alpha}\left\{\frac{\partial\psi_{\alpha}(\mathbf{r})}{\partial t}\,\psi^{*}_{\alpha}(\mathbf{r}') + \psi_{\alpha}(\mathbf{r})\,\frac{\partial\psi^{*}_{\alpha}(\mathbf{r}')}{\partial t}\right\}\,, \tag{3.69}$$

the TDHF equations in the position representation (see Eq.(3.67)) can be written as:

$$\begin{aligned}\dot{\rho}_{\mathbf{r}\mathbf{r}'} &= \frac{1}{i\hbar}\int \mathrm{d}^3r''\Big(\langle\mathbf{r}|H|\mathbf{r}''\rangle\,\rho_{\mathbf{r}''\mathbf{r}'} - \rho_{\mathbf{r}\mathbf{r}''}\,\langle\mathbf{r}''|H|\mathbf{r}'\rangle\Big)\\ &= \frac{1}{i\hbar}\sum_{\alpha}\int \mathrm{d}^3r''\Big(\langle\mathbf{r}|H|\mathbf{r}''\rangle\,\psi_{\alpha}(\mathbf{r}'')\,\psi^{*}_{\alpha}(\mathbf{r}') - \psi_{\alpha}(\mathbf{r})\,\psi^{*}_{\alpha}(\mathbf{r}'')\,\langle\mathbf{r}''|H|\mathbf{r}'\rangle\Big)\,.\end{aligned} \tag{3.70}$$

From Eqs. (3.69) and (3.70), taking into account that the Hamiltonian, H, is hermitian, we conclude that:

$$\frac{\partial\psi_{\alpha}(\mathbf{r})}{\partial t} = \frac{1}{i\hbar}\int \mathrm{d}^3r'\;\langle\mathbf{r}|H|\mathbf{r}'\rangle\,\psi_{\alpha}(\mathbf{r}')\,. \tag{3.71}$$

To arrive at the Vlasov equation we have to consider the Wigner transform of the density matrix. Working with the density matrix in the position representation, $\rho_{\mathbf{r}'\mathbf{r}''}$, this is defined as a kind of Fourier transform:

$$f(\mathbf{r},\mathbf{p}) \equiv \frac{1}{(2\pi\hbar)^3}\,\rho_{\rm Wigner}(\mathbf{r},\mathbf{p}) = \frac{1}{(2\pi\hbar)^3}\int \mathrm{d}^3s\;\mathrm{e}^{-\frac{i}{\hbar}\mathbf{p}\cdot\mathbf{s}}\;\rho_{\mathbf{r}+\mathbf{s}/2,\mathbf{r}-\mathbf{s}/2}\,, \tag{3.72}$$

with respect to the relative distance $\mathbf{r}'-\mathbf{r}''$. We chose the notation $f(\mathbf{r},\mathbf{p})$ to stress the analogy with the classical one-body phase-space distribution function. Indeed, if

one integrates the distribution function $f(\mathbf{r},\mathbf{p})$ over momentum space one gets the local density:

$$\begin{aligned}\int \mathrm{d}^3p\; f(\mathbf{r},\mathbf{p}) &= \frac{1}{(2\pi\hbar)^3}\iint \mathrm{d}^3p\;\mathrm{d}^3s\;\mathrm{e}^{-\frac{i}{\hbar}\mathbf{p}\cdot\mathbf{s}}\;\rho_{\mathbf{r}+\mathbf{s}/2,\mathbf{r}-\mathbf{s}/2}\\ &= \frac{1}{(2\pi\hbar)^3}\int \mathrm{d}^3s\;\rho_{\mathbf{r}+\mathbf{s}/2,\mathbf{r}-\mathbf{s}/2}\int \mathrm{d}^3p\;\mathrm{e}^{-\frac{i}{\hbar}\mathbf{p}\cdot\mathbf{s}}\\ &= \int \mathrm{d}^3s\;\rho_{\mathbf{r}+\mathbf{s}/2,\mathbf{r}-\mathbf{s}/2}\;\delta(-\mathbf{s}) = \rho_{\mathbf{rr}} = \rho(\mathbf{r})\;. \end{aligned} \tag{3.73}$$

Concerning the normalization factor, this definition for $f(\mathbf{r},\mathbf{p})$ is also preferred by Bertsch and Das Gupta [71] and Brink and Di Toro [72]. Other authors (see for example the work of Kolomietz and Shlomo [73]) define the function $f(\mathbf{r},\mathbf{p})$ to be just the Wigner transform (i.e. $f(\mathbf{r},\mathbf{p}) = \rho_{\mathrm{Wigner}}(\mathbf{r},\mathbf{p})$). In this case the constant $\dfrac{1}{(2\pi\hbar)^3}$ appears when an integration over momentum space occurs.

We mention that the distribution function can be expressed also as a Fourier transform with respect to the relative momenta, when one works with a momentum representation of the density matrix, $\rho_{\mathbf{p}'\mathbf{p}''}$:

$$\rho_{\mathbf{p}'\mathbf{p}''} = \langle\psi|\, a^\dagger_{\mathbf{p}''}\, a_{\mathbf{p}'}\,|\psi\rangle\;. \tag{3.74}$$

Indeed, one can expand the creation and annihilation operators, $a^\dagger_{\mathbf{r}}, a_{\mathbf{r}}$, in terms of any complete basis:

$$a^\dagger_{\mathbf{r}} = \sum_i \langle\mathbf{r}|i\rangle^*\, a^\dagger_i = \sum_i \langle i|\mathbf{r}\rangle\, a^\dagger_i\;. \tag{3.75}$$

One can thus write:

$$\int \mathrm{d}^3r\;\langle\mathbf{r}|j\rangle\, a^\dagger_{\mathbf{r}} = \sum_i \int \mathrm{d}^3r\;\langle i|\mathbf{r}\rangle\;\langle\mathbf{r}|j\rangle\, a^\dagger_i = a^\dagger_j\;. \tag{3.76}$$

Considering now $a^\dagger_j$ to be related to the momentum basis, we can express the creation and annihilation operators:

$$a^\dagger_{\mathbf{p}} = \int \mathrm{d}^3r\;\langle\mathbf{r}|\mathbf{p}\rangle\; a^\dagger_{\mathbf{r}} = \frac{1}{(2\pi\hbar)^{3/2}}\int \mathrm{d}^3r\;\mathrm{e}^{\frac{i}{\hbar}\mathbf{p}\cdot\mathbf{r}}\; a^\dagger_{\mathbf{r}}\;, \tag{3.77}$$

$$a_{\mathbf{p}} = \int \mathrm{d}^3r\;\langle\mathbf{p}|\mathbf{r}\rangle\; a_{\mathbf{r}} = \frac{1}{(2\pi\hbar)^{3/2}}\int \mathrm{d}^3r\;\mathrm{e}^{-\frac{i}{\hbar}\mathbf{p}\cdot\mathbf{r}}\; a_{\mathbf{r}}\;. \tag{3.78}$$

If we assume that:

$$f(\mathbf{r},\mathbf{p}) = \frac{1}{(2\pi\hbar)^3}\int \mathrm{d}^3\mathbf{q}\;\mathrm{e}^{\frac{i}{\hbar}\mathbf{q}\cdot\mathbf{r}}\;\rho_{\mathbf{p}+\mathbf{q}/2,\mathbf{p}-\mathbf{q}/2}\;, \tag{3.79}$$

and, in this equation we insert the creation and annihilation operators, Eqs. (3.77)

and (3.78), we obtain:

$$\begin{aligned} f(\mathbf{r},\mathbf{p}) &= \frac{1}{(2\pi\hbar)^6}\int \mathrm{d}^3\mathbf{q}\, \mathrm{e}^{\frac{i}{\hbar}\mathbf{q}\cdot\mathbf{r}}\, \langle\psi| \iint \mathrm{d}^3r_1\, \mathrm{d}^3r_2\, \mathrm{e}^{-\frac{i}{\hbar}(\mathbf{p}+\frac{\mathbf{q}}{2})\mathbf{r}_1}\, \mathrm{e}^{\frac{i}{\hbar}(\mathbf{p}-\frac{\mathbf{q}}{2})\mathbf{r}_2}\, a^\dagger_{\mathbf{r}_2}\, a_{\mathbf{r}_1}\, |\psi\rangle \\ &= \frac{1}{(2\pi\hbar)^6}\int \mathrm{d}^3\mathbf{q}\, \mathrm{e}^{\frac{i}{\hbar}\mathbf{q}\cdot\mathbf{r}} \iint \mathrm{d}^3r_1\, \mathrm{d}^3r_2\, \mathrm{e}^{-\frac{i}{\hbar}(\mathbf{p}+\frac{\mathbf{q}}{2})\mathbf{r}_1}\, \mathrm{e}^{\frac{i}{\hbar}(\mathbf{p}-\frac{\mathbf{q}}{2})\mathbf{r}_2}\, \rho_{\mathbf{r}_1,\mathbf{r}_2} \\ &= \frac{1}{(2\pi\hbar)^6}\int \mathrm{d}^3\mathbf{q}\, \mathrm{e}^{\frac{i}{\hbar}\mathbf{q}(\mathbf{r}-\frac{\mathbf{r}_1+\mathbf{r}_2}{2})} \iint \mathrm{d}^3r_1\, \mathrm{d}^3r_2\, \mathrm{e}^{-\frac{i}{\hbar}\mathbf{p}(\mathbf{r}_1-\mathbf{r}_2)}\, \rho_{\mathbf{r}_1,\mathbf{r}_2} \\ &= \frac{1}{(2\pi\hbar)^3}\iint \mathrm{d}^3r_1\, \mathrm{d}^3r_2\, \delta\Big(\mathbf{r}-\frac{\mathbf{r}_1+\mathbf{r}_2}{2}\Big)\, \mathrm{e}^{-\frac{i}{\hbar}\mathbf{p}(\mathbf{r}_1-\mathbf{r}_2)}\, \rho_{\mathbf{r}_1,\mathbf{r}_2}\ . \end{aligned} \tag{3.80}$$

Making the following substitution:

$$\mathbf{s} = \mathbf{r}_1 - \mathbf{r}_2\ , \qquad \mathbf{r} = \frac{\mathbf{r}_1+\mathbf{r}_2}{2}\ , \tag{3.81}$$

one has:

$$f(\mathbf{r},\mathbf{p}) = \frac{1}{(2\pi\hbar)^3}\int \mathrm{d}^3\mathbf{s}\, \mathrm{e}^{-\frac{i}{\hbar}\mathbf{p}\cdot\mathbf{s}}\, \rho_{\mathbf{r}+\mathbf{s}/2,\mathbf{r}-\mathbf{s}/2}\ , \tag{3.82}$$

which is exactly the definition for the distribution function in terms of the density matrix in the position representation, therefore making our initial assumption valid. This new form of the distribution function, helps us to show that, when integrated over coordinate space:

$$\begin{aligned} \int \mathrm{d}^3r\ f(\mathbf{r},\mathbf{p}) &= \frac{1}{(2\pi\hbar)^3}\iint \mathrm{d}^3p\, \mathrm{d}^3\mathbf{q}\, \mathrm{e}^{\frac{i}{\hbar}\mathbf{q}\cdot\mathbf{r}}\, \rho_{\mathbf{p}+\mathbf{q}/2,\mathbf{p}-\mathbf{q}/2} \\ &= \frac{1}{(2\pi\hbar)^3}\int \mathrm{d}^3\mathbf{q}\, \rho_{\mathbf{p}+\mathbf{q}/2,\mathbf{p}-\mathbf{q}/2} \int \mathrm{d}^3r\ \mathrm{e}^{\frac{i}{\hbar}\mathbf{q}\cdot\mathbf{r}} \\ &= \int \mathrm{d}^3\mathbf{q}\, \rho_{\mathbf{p}+\mathbf{q}/2,\mathbf{p}-\mathbf{q}/2}\, \delta(\mathbf{q}) = \rho_{\mathbf{pp}} = \rho(\mathbf{p})\ , \end{aligned} \tag{3.83}$$

the local density in momentum space is obtained.

Now, we are in the position to derive the Vlasov equation. Using the TDHF equations (Eqs. (3.67)) as well as the two definitions for the Wigner transforms of the density matrices (Eqs. (3.72) and (3.79)) one can express the time derivative of the distribution function as a sum two terms: one kinetic, in which we will use the momentum representation for $f(\mathbf{r},\mathbf{p})$, and with $|\alpha\rangle$ representing momentum states:

$$\begin{aligned} \Big(\frac{\partial f(\mathbf{r},\mathbf{p})}{\partial t}\Big)_{\text{kin}} &= \frac{1}{(2\pi\hbar)^3}\int \mathrm{d}^3\mathbf{q}\, \mathrm{e}^{\frac{i}{\hbar}\mathbf{q}\cdot\mathbf{r}}\, \dot\rho_{\mathbf{p}+\mathbf{q}/2,\mathbf{p}-\mathbf{q}/2} \\ &= \frac{1}{(2\pi\hbar)^3}\int \mathrm{d}^3\mathbf{q}\, \mathrm{e}^{\frac{i}{\hbar}\mathbf{q}\cdot\mathbf{r}}\, \frac{1}{i\hbar}\int \mathrm{d}^3\boldsymbol{\alpha}\Big(\langle\mathbf{p}+\frac{\mathbf{q}}{2}|T|\alpha\rangle\rho_{\alpha,\mathbf{p}-\frac{\mathbf{q}}{2}} - \rho_{\mathbf{p}+\frac{\mathbf{q}}{2},\alpha}\langle\alpha|T|\mathbf{p}-\frac{\mathbf{q}}{2}\rangle\Big)\ , \end{aligned} \tag{3.84}$$

and one potential, where the position representation will be used, and with $|\alpha\rangle$ representing position states:

$$\begin{aligned} \Big(\frac{\partial f(\mathbf{r},\mathbf{p})}{\partial t}\Big)_{\text{pot}} &= \frac{1}{(2\pi\hbar)^3}\int \mathrm{d}^3\mathbf{s}\, \mathrm{e}^{-\frac{i}{\hbar}\mathbf{p}\cdot\mathbf{s}}\, \dot\rho_{\mathbf{r}+\mathbf{s}/2,\mathbf{r}-\mathbf{s}/2} \\ &= \frac{1}{(2\pi\hbar)^3}\int \mathrm{d}^3\mathbf{q}\, \mathrm{e}^{-\frac{i}{\hbar}\mathbf{p}\cdot\mathbf{s}}\, \frac{1}{i\hbar}\int \mathrm{d}^3\boldsymbol{\alpha}\, \Big(\langle\mathbf{r}+\frac{\mathbf{s}}{2}|U|\alpha\rangle\, \rho_{\alpha,\mathbf{r}-\frac{\mathbf{s}}{2}} - \rho_{\mathbf{r}+\frac{\mathbf{s}}{2},\alpha}\, \langle\alpha|U|\mathbf{r}-\frac{\mathbf{s}}{2}\rangle\Big)\ . \end{aligned} \tag{3.85}$$

The kinetic term can be evaluated as follows:

$$\begin{aligned}\Big(\frac{\partial f(\mathbf{r},\mathbf{p})}{\partial t}\Big)_{\rm kin} &= \frac{1}{(2\pi\hbar)^3}\,\frac{1}{i\hbar}\iint \mathrm{d}^3\mathbf{q}\;\mathrm{d}^3\boldsymbol{\alpha}\;\mathrm{e}^{\frac{i}{\hbar}\mathbf{q}\cdot\mathbf{r}}\Big\{\frac{\alpha^2}{2m}\;\delta\big(\boldsymbol{\alpha}-(\mathbf{p}+\frac{\mathbf{q}}{2})\big)\;\rho_{\boldsymbol{\alpha},\mathbf{p}-\frac{\mathbf{q}}{2}} \\ &\qquad -\frac{(\mathbf{p}-\frac{\mathbf{q}}{2})^2}{2m}\;\rho_{\mathbf{p}-\frac{\mathbf{q}}{2},\alpha}\;\delta\big(\alpha-(\mathbf{p}-\frac{\mathbf{q}}{2})\big)\Big\} \\ &= \frac{1}{(2\pi\hbar)^3}\,\frac{1}{i\hbar}\int \mathrm{d}^3\mathbf{q}\;\mathrm{e}^{\frac{i}{\hbar}\mathbf{q}\cdot\mathbf{r}}\;\rho_{\mathbf{p}+\frac{\mathbf{q}}{2},\mathbf{p}-\frac{\mathbf{q}}{2}}\Big[\frac{(\mathbf{p}+\frac{\mathbf{q}}{2})^2}{2m}-\frac{(\mathbf{p}-\frac{\mathbf{q}}{2})^2}{2m}\Big] \\ &= \frac{1}{(2\pi\hbar)^3}\,\frac{1}{i\hbar}\int \mathrm{d}^3\mathbf{q}\;\mathrm{e}^{\frac{i}{\hbar}\mathbf{q}\cdot\mathbf{r}}\;\frac{\mathbf{p}\cdot\mathbf{q}}{m}\;\rho_{\mathbf{p}+\frac{\mathbf{q}}{2},\mathbf{p}-\frac{\mathbf{q}}{2}} = -\frac{\mathbf{p}}{m}\cdot\nabla_{\mathbf{r}}\;f(\mathbf{r},\mathbf{p})\;. \end{aligned} \tag{3.86}$$

To evaluate the potential term we first consider the mean field potential to be local (i.e. $\langle\mathbf{r}|U|\mathbf{r}'\rangle = U(\mathbf{r})\delta(\mathbf{r}-\mathbf{r}')$):

$$\begin{aligned}\Big(\frac{\partial f(\mathbf{r},\mathbf{p})}{\partial t}\Big)_{\rm pot} &= \frac{1}{(2\pi\hbar)^3}\,\frac{1}{i\hbar}\iint \mathrm{d}^3\mathbf{s}\;\mathrm{d}^3\boldsymbol{\alpha}\;\mathrm{e}^{-\frac{i}{\hbar}\mathbf{p}\cdot\mathbf{s}}\;\Big\{U\big(\mathbf{r}+\frac{\mathbf{s}}{2}\big)\;\delta\big(\mathbf{r}+\frac{\mathbf{s}}{2}-\boldsymbol{\alpha}\big)\;\rho_{\boldsymbol{\alpha},\mathbf{r}-\frac{\mathbf{s}}{2}} \\ &\qquad -\rho_{\mathbf{r}+\frac{\mathbf{s}}{2},\boldsymbol{\alpha}}\;U(\boldsymbol{\alpha})\;\delta\big(\boldsymbol{\alpha}-(\mathbf{r}-\frac{\mathbf{s}}{2})\big)\Big\} \\ &= \frac{1}{(2\pi\hbar)^3}\,\frac{1}{i\hbar}\iint \mathrm{d}^3\mathbf{s}\;\mathrm{e}^{-\frac{i}{\hbar}\mathbf{p}\cdot\mathbf{s}}\Big[U(\mathbf{r}+\frac{\mathbf{s}}{2})-U(\mathbf{r}-\frac{\mathbf{s}}{2})\Big]\rho_{\mathbf{r}+\frac{\mathbf{s}}{2},\mathbf{r}-\frac{\mathbf{s}}{2}}\;. \end{aligned} \tag{3.87}$$

It is worth noting that the above equations retain the full quantum mechanical picture. If we expand to the lowest order

$$\begin{aligned}U(\mathbf{r}+\tfrac{\mathbf{s}}{2})-U(\mathbf{r}-\tfrac{\mathbf{s}}{2}) &= U(\mathbf{r})+(\mathbf{r}+\tfrac{\mathbf{s}}{2}-\mathbf{r})\cdot\nabla_{\mathbf{r}}U(\mathbf{r})+\ldots \\ &\quad -U(\mathbf{r})-(\mathbf{r}-\tfrac{\mathbf{s}}{2}-\mathbf{r})\cdot\nabla_{\mathbf{r}}U(\mathbf{r})-\ldots \\ &\approx \mathbf{s}\cdot\nabla_{\mathbf{r}}U(\mathbf{r})\;,\end{aligned}$$

the previous statement will not hold anymore, and we get:

$$\begin{aligned}\Big(\frac{\partial f(\mathbf{r},\mathbf{p})}{\partial t}\Big)_{\rm pot} &= \frac{1}{(2\pi\hbar)^3}\,\frac{1}{i\hbar}\iint \mathrm{d}^3\mathbf{s}\;\mathrm{e}^{-\frac{i}{\hbar}\mathbf{p}\cdot\mathbf{s}}\;\big(\mathbf{s}\cdot\nabla_{\mathbf{r}}U(\mathbf{r})\big)\;\rho_{\mathbf{r}+\frac{\mathbf{s}}{2},\mathbf{r}-\frac{\mathbf{s}}{2}} \\ &= \nabla_{\mathbf{r}}U(\mathbf{r})\cdot\nabla_{\mathbf{p}}f(\mathbf{r},\mathbf{p})\;.\end{aligned} \tag{3.88}$$

Summing up these the kinetic and potential contributions:

$$\begin{aligned}\frac{\partial f(\mathbf{r},\mathbf{p})}{\partial t} &= \Big(\frac{\partial f(\mathbf{r},\mathbf{p})}{\partial t}\Big)_{\rm kin}+\Big(\frac{\partial f(\mathbf{r},\mathbf{p})}{\partial t}\Big)_{\rm pot} \\ &= -\frac{\mathbf{p}}{m}\cdot\nabla_{\mathbf{r}}f(\mathbf{r},\mathbf{p})+\nabla_{\mathbf{r}}U(\mathbf{r})\cdot\nabla_{\mathbf{p}}f(\mathbf{r},\mathbf{p})\;,\end{aligned} \tag{3.89}$$

we obtain the Vlasov equation:

$$\frac{\partial f(\mathbf{r},\mathbf{p})}{\partial t}+\frac{\mathbf{p}}{m}\cdot\nabla_{\mathbf{r}}f(\mathbf{r},\mathbf{p})-\nabla_{\mathbf{r}}U(\mathbf{r})\cdot\nabla_{\mathbf{p}}f(\mathbf{r},\mathbf{p})=0\;. \tag{3.90}$$

One should note that Eq. (3.90) is obtained within the lowest order, and if one would include in the expansion of the local potential, $U(\mathbf{r}\pm\frac{\mathbf{s}}{2})$ all higher order terms (see Eq. (3.88)), one would arrive to the TDHF limit. As previously noted, $f(\mathbf{r},\mathbf{p})$ can be viewed

as the quantum mechanical analogue to the classical phase-space distribution function. In the semi-classical limit given by the Vlasov equation, the quantum effects enter through the Pauli correlations contained into the distribution function, included already from the initial conditions, which should characterise the initial distribution of the quantum system. Moreover, as a transport equation, the Vlasov equation, verifies the Liouville theorem (i.e. the volume in phase-space is conserved), so, at any later time, the Pauli principle will hold. We also mention that into the transport equations, the first quantum effects can be included as additional terms which contain second order powers of Plank constant, and depend on third order derivatives.

3.2.1 Isoscalar response

In the following example, we employ the Vlasov equation to illustrate the isoscalar response in nuclear matter, within a microscopic model based on one component. We shall consider small deviations from the equilibrium distribution function:

$$f(\mathbf{r},\mathbf{p},t) = f^0(E) + \delta f(\mathbf{r},\mathbf{p},t) \; , \tag{3.91}$$

with

$$f^0(E) = \frac{\gamma}{(2\pi\hbar)^3}\,\Theta(E-E_F) \; , \tag{3.92}$$

the equilibrium Fermi-Dirac distribution function at zero temperature. γ is the degeneracy factor, equal to two, accounting for spin up and spin down nucleons. The local variation of the density can be expressed in terms of the small deviation of the distribution function from the equilibrium, δf:

$$\delta\rho(\mathbf{r}) = \int \mathrm{d}^3p\; \delta f(\mathbf{r},\mathbf{p},t) \; . \tag{3.93}$$

The linearized Vlasov equation (3.90) becomes:

$$\frac{\partial\,\delta f}{\partial t} + \frac{\mathbf{p}}{m}\cdot\nabla_{\mathbf{r}}\delta f - \nabla_{\mathbf{r}}\delta U(\rho(\mathbf{r}))\cdot\nabla_{\mathbf{p}} f^0 = 0 \; , \tag{3.94}$$

with the potential variation satisfying $\delta U(\rho(\mathbf{r})) = \dfrac{\partial U}{\partial\rho}\,\delta\rho$, and thus:

$$\nabla_{\mathbf{r}}\delta U(\rho(\mathbf{r})) = \frac{\partial U}{\partial\rho}\;\nabla_{\mathbf{r}}\delta\rho \; . \tag{3.95}$$

We search for a plane-wave solution to Eq. (3.94) of the following form:

$$\delta f(\mathbf{r},\mathbf{p},t) = \frac{\gamma}{(2\pi\hbar)^3}\sum_{\mathbf{k}} A_{\mathbf{k}}(\mathbf{p})\;\mathrm{e}^{\,i(\mathbf{kr}-\omega t)} \; . \tag{3.96}$$

Consequently, for the variation of the distribution function we have:

$$\frac{\partial\,\delta f}{\partial t} = \frac{\gamma}{(2\pi\hbar)^3}\sum_{\mathbf{k}}(-i\omega)\;A_{\mathbf{k}}(\mathbf{p})\;\mathrm{e}^{\,i(\mathbf{kr}-\omega t)} \; , \tag{3.97}$$

$$\nabla_{\mathbf{r}}\delta f = \frac{\gamma}{(2\pi\hbar)^3}\sum_{\mathbf{k}}(i\mathbf{k})\;A_{\mathbf{k}}(\mathbf{p})\;\mathrm{e}^{\,i(\mathbf{kr}-\omega t)} \; . \tag{3.98}$$

With the help of Eq. (3.93), one can write:

$$\begin{aligned}\nabla_{\mathbf{r}}\delta\rho &= \nabla_{\mathbf{r}}\int \frac{\gamma}{(2\pi\hbar)^3}\sum_{\mathbf{k}} A_{\mathbf{k}}(\mathbf{p})\, \mathrm{e}^{\,i(\mathbf{kr}-\omega t)}\, \mathrm{d}^3p \\ &= \sum_{\mathbf{k}} (i\mathbf{k})\Big[\frac{\gamma}{(2\pi\hbar)^3}\int A_{\mathbf{k}}(\mathbf{p})\, \mathrm{d}^3p\Big]\, \mathrm{e}^{\,i(\mathbf{kr}-\omega t)} \\ &= \sum_{\mathbf{k}} (i\mathbf{k})\, \rho_{\mathbf{k}}\, \mathrm{e}^{\,i(\mathbf{kr}-\omega t)}\,, \end{aligned} \tag{3.99}$$

with

$$\rho_{\mathbf{k}} = \frac{\gamma}{(2\pi\hbar)^3}\int A_{\mathbf{k}}(\mathbf{p})\, \mathrm{d}^3p\,, \tag{3.100}$$

and

$$\delta\rho(\mathbf{r}) = \sum_{\mathbf{k}} \rho_{\mathbf{k}}\, \mathrm{e}^{\,i(\mathbf{kr}-\omega t)}\,. \tag{3.101}$$

Consequently, for the last term of Eq. (3.94) we have:

$$\begin{aligned}\nabla_{\mathbf{r}}\delta U\cdot\nabla_{\mathbf{p}} f^0 = \nabla_{\mathbf{r}}\Big(\frac{\partial U}{\partial\rho}\delta\rho\Big)\cdot\nabla_{\mathbf{p}} f^0 &= \frac{\partial U}{\partial\rho}\,\nabla_{\mathbf{r}}\delta\rho\cdot\nabla_{\mathbf{p}} f^0 \\ &= \frac{\partial U}{\partial\rho}\,(i\mathbf{k})\sum_{\mathbf{k}}\rho_{\mathbf{k}}\,\mathrm{e}^{\,i(\mathbf{kr}-\omega t)}\cdot\frac{\gamma}{(2\pi\hbar)^3}\big(-\frac{\mathbf{p}}{m}\,\delta(E-E_F)\big)\,,\end{aligned} \tag{3.102}$$

and thus, the Vlasov equation becomes:

$$\frac{\gamma}{(2\pi\hbar)^3}\sum_{\mathbf{k}}\Big((-i\omega)\,A_{\mathbf{k}}(\mathbf{p}) + i\mathbf{k}\cdot\frac{\mathbf{p}}{m}\,A_{\mathbf{k}}(\mathbf{p}) + \frac{\partial U}{\partial\rho}\,(i\mathbf{k})\cdot\frac{\mathbf{p}}{m}\,\rho_{\mathbf{k}}\,\delta(E-E_F)\Big)\,\mathrm{e}^{\,i(\mathbf{kr}-\omega t)} = 0\,. \tag{3.103}$$

For the above equation to be true, we should have:

$$A_{\mathbf{k}}(\mathbf{p})\Big(\frac{\mathbf{k}\cdot\mathbf{p}}{m}-\omega\Big) + \frac{\mathbf{k}\cdot\mathbf{p}}{m}\,\frac{\partial U}{\partial\rho}\,\rho_{\mathbf{k}}\,\delta(E-E_F) = 0\,, \tag{3.104}$$

or, equivalently:

$$A_{\mathbf{k}}(\mathbf{p}) + \frac{\partial U}{\partial\rho}\,\rho_{\mathbf{k}}\,\delta(E-E_F)\,\frac{\mathbf{k}\cdot\mathbf{p}/m}{\mathbf{k}\cdot\mathbf{p}/m-\omega} = 0\,. \tag{3.105}$$

The above equation represents an homogeneous system of equations for the $A_{\mathbf{k}}(\mathbf{p})$ amplitudes. From the condition to have non-trivial solutions, the dispersion relation will be derived. Indeed, if we integrate over momentum space and consider $\dfrac{\mathbf{k}\cdot\mathbf{p}}{m} = \dfrac{k\,p\,\cos\theta}{m}$ with $\theta = (\widehat{\mathbf{k},\mathbf{p}})$, we obtain:

$$\int \mathrm{d}^3p\,\frac{\gamma}{(2\pi\hbar)^3}\,A_{\mathbf{k}}(\mathbf{p}) + \frac{\partial U}{\partial\rho}\,\rho_{\mathbf{k}}\int \mathrm{d}^3p\,\frac{\gamma}{(2\pi\hbar)^3}\,\delta(E-E_F)\,\frac{\mathbf{k}\cdot\mathbf{p}/m}{\mathbf{k}\cdot\mathbf{p}/m-\omega} = 0\,, \tag{3.106}$$

or, equivalently:

$$\rho_{\mathbf{k}}\Big(1+\frac{\partial U}{\partial\rho}\,\frac{\gamma}{(2\pi\hbar)^3}\iiint\frac{k\,p\,\cos\theta/m}{k\,p\cos\theta/m-\omega}\,\delta(E-E_F)\,p^2\sin\theta\,\mathrm{d}p\,\mathrm{d}\theta\,\mathrm{d}\phi\Big)=0\,. \quad (3.107)$$

One can express the delta-Dirac function in terms of absolute values of the momenta:

$$\delta(E-E_F)=\delta\Big(\frac{p^2}{2m}-\frac{p_F^2}{2m}\Big)=2\,m\,\delta(p^2-p_F^2)=2\,m\,\frac{1}{2\,p_F}\big[\delta(p+p_F)+\delta(p-p_F)\big]$$
$$=\frac{m}{p_F}\,\delta(p-p_F)\,, \quad (3.108)$$

since there are no negative absolute momenta, and the first delta function cancels. The integral in Eq. (3.107), over momenta, becomes:

$$\int\frac{k\,p\,\cos\theta/m}{k\,p\,\cos\theta/m-\omega}\,\delta(E-E_F)\,p^2\,\mathrm{d}p=\int\frac{\cos\theta}{\cos\theta-\omega\,\dfrac{m}{k\,p}}\,\frac{m}{p_F}\,\delta(p-p_F)\,p^2\,\mathrm{d}p$$
$$=\frac{\cos\theta}{\cos\theta-\omega\,\dfrac{m}{k\,p_F}}\,m\,p_F$$
$$=\frac{\cos\theta}{\cos\theta-\dfrac{\omega}{k\,v_F}}\,m\,p_F=\frac{\cos\theta}{\cos\theta-s}\,m\,p_F\,, \quad (3.109)$$

with $s=\dfrac{\omega}{kv_F}$. Now, we shall solve the integral over the polar angle θ:

$$\int_0^\pi\frac{-\cos\theta}{\cos\theta-s}\,\mathrm{d}(\cos\theta)=\int_1^{-1}\frac{-x}{x-s}\,\mathrm{d}x=\int_{-1}^1\frac{x-s+s}{x-s}\,\mathrm{d}x=2+s\int_{-1}^1\frac{1}{x-s}\,\mathrm{d}x$$
$$=2-s\,\ln\frac{s+1}{s-1}=2\Big(1-\frac{s}{2}\,\ln\frac{s+1}{s-1}\Big)\,, \quad (3.110)$$

Considering now Eqs. (3.109) and (3.110), Eq. (3.107) requires:

$$1+\frac{\partial U}{\partial\rho}\,\frac{\gamma}{(2\pi\hbar)^3}\,2\,\Big(1-\frac{s}{2}\,\ln\frac{s+1}{s-1}\Big)\,mp_F\,2\pi=0\,. \quad (3.111)$$

This equation can also be written in the following form:

$$\frac{s}{2}\,\ln\frac{s+1}{s-1}=1+\frac{1}{F^0}\,. \quad (3.112)$$

The solution of this equation gives the collective mode velocity in terms of Fermi velocity units. This collective mode named *zero-sound* is a pure quantum mode which depends on the interaction through the the Landau parameter, F^0, representing the product between $\dfrac{\partial U}{\partial\rho}$ and the single-particle density of states at Fermi level, $N(0)$:

$$N(0)=\int\mathrm{d}^3p\,\frac{\gamma}{(2\pi\hbar)^3}\,\delta(E-E_F)=\frac{\gamma}{(2\pi\hbar)^3}\int\mathrm{d}p\,\mathrm{d}\Omega\,p^2\,\frac{m}{p_F}\,\delta(p-p_F)$$
$$=\frac{\gamma}{(2\pi\hbar)^3}\,4\pi\,m\,p_F=\frac{\gamma\,m\,p_F}{2\pi^2\hbar^3}\,. \quad (3.113)$$

We remark that this mode propagates even at zero temperature and in the absence of any particle collisions, being therefore completely different from the hydrodynamical sound-wave, which requires the local equilibrium. This can only be established trough two-body collisions, which, at zero temperature, are inhibited due to Pauli blocking. The mode manifests as a periodic egg-like shape oscillations in momentum space and at zero-temperature involves only particles only at the Fermi surface.

3.2.2 Isovectorial response

Using a similar procedure, we can obtain an isovector zero-sound mode in symmetric nuclear matter, based on a set of two coupled Vlasov equations for both protons and neutrons:

$$\frac{\partial f_p}{\partial t} + \frac{\mathbf{p}}{m} \cdot \nabla_{\mathbf{r}} f_p - \nabla_{\mathbf{r}} U_p \cdot \nabla_{\mathbf{p}} f_p = 0 \ , \tag{3.114a}$$

$$\frac{\partial f_n}{\partial t} + \frac{\mathbf{p}}{m} \cdot \nabla_{\mathbf{r}} f_n - \nabla_{\mathbf{r}} U_n \cdot \nabla_{\mathbf{p}} f_n = 0 \ . \tag{3.114b}$$

We again consider small deviations of the distribution functions from equilibrium:

$$f_p(\mathbf{r}, \mathbf{p}, t) = f_p^0(E) + \delta f_p(\mathbf{r}, \mathbf{p}, t) \ , \tag{3.115a}$$

$$f_n(\mathbf{r}, \mathbf{p}, t) = f_n^0(E) + \delta f_n(\mathbf{r}, \mathbf{p}, t) \ , \tag{3.115b}$$

with $f_p^0(E) = f_n^0(E) = \dfrac{\gamma}{(2\pi\hbar)^3}\, \Theta(E - E_F)$ representing the statical Fermi-Dirac solutions for protons and neutrons. Within the linear approximation, Eqs. (3.114) become:

$$\frac{\partial\, \delta f_p}{\partial t} + \frac{\mathbf{p}}{m} \cdot \nabla_{\mathbf{r}} \delta f_p - \nabla_{\mathbf{r}} \delta U_p \cdot \nabla_{\mathbf{p}} f_p^0 = 0 \ , \tag{3.116a}$$

$$\frac{\partial\, \delta f_n}{\partial t} + \frac{\mathbf{p}}{m} \cdot \nabla_{\mathbf{r}} \delta f_n - \nabla_{\mathbf{r}} \delta U_n \cdot \nabla_{\mathbf{p}} f_n^0 = 0 \ . \tag{3.116b}$$

Considering a Skyrme-like parametrization of the mean-field potentials for protons and neutrons (see Eqs. (3.40) and (3.41)):

$$\delta U_p = \frac{A}{\rho_0}(\delta\rho_n + \delta\rho_p) + \frac{B}{\rho_0}(\delta\rho_n + \delta\rho_p)^\sigma + \frac{C}{\rho_0}(\delta\rho_p - \delta\rho_n) \ , \tag{3.117a}$$

$$\delta U_n = \frac{A}{\rho_0}(\delta\rho_n + \delta\rho_p) + \frac{B}{\rho_0}(\delta\rho_n + \delta\rho_p)^\sigma + \frac{C}{\rho_0}(\delta\rho_n - \delta\rho_p) \ , \tag{3.117b}$$

with C taken to be density independent (i.e. as for the *asy-stiff* parametrisation). For the isovector variation $\delta f = \delta f_p - \delta f_n$, one has:

$$\frac{\partial\, \delta f}{\partial t} + \frac{\mathbf{p}}{m} \cdot \nabla_{\mathbf{r}} \delta f - \nabla_{\mathbf{r}} (\delta U_p - \delta U_n) \cdot \Big(- \frac{\mathbf{p}}{m}\, \delta(E - E_F) \Big) = 0 \ , \tag{3.118}$$

where

$$(\delta U_p - \delta U_n) = 2\, \frac{C}{\rho_0}\, (\delta\rho_p - \delta\rho_n) = 2\, \frac{C}{\rho_0} \int \mathrm{d}^3 p\, \gamma\, \delta f \ . \tag{3.119}$$

Again, we search for a plane-wave solution:

$$\delta f(\mathbf{r},\mathbf{p},t) = \frac{\gamma}{(2\pi\hbar)^3}\sum_{\mathbf{k}} A_{\mathbf{k}}(\mathbf{p})\, \mathrm{e}^{\,i(\mathbf{k}\mathbf{r}-\omega t)}\ , \tag{3.120}$$

and, consequently, Eq. (3.118) becomes:

$$\frac{\gamma}{(2\pi\hbar)^3}\sum_{\mathbf{k}}\Big[(-i\omega)A_{\mathbf{k}}(\mathbf{p})+i\mathbf{k}\cdot\frac{\mathbf{p}}{m}A_{\mathbf{k}}(\mathbf{p})+2\,\frac{C}{\rho_0}\,i\mathbf{k}\cdot\frac{\mathbf{p}}{m}\,\rho_{\mathbf{k}}\,\delta(E-E_F)\Big]\,\mathrm{e}^{\,i(\mathbf{k}\cdot\mathbf{r}-\omega t)} = 0\ . \tag{3.121}$$

This requires that the following equation should be satisfied:

$$A_{\mathbf{k}}(\mathbf{p}) + 2\,\frac{\partial C}{\rho_0}\,\rho_{\mathbf{k}}\,\delta(E-E_F)\,\frac{\mathbf{k}\cdot\mathbf{p}/m}{\mathbf{k}\cdot\mathbf{p}/m-\omega} = 0\ . \tag{3.122}$$

To obtain the dispersion relation we again integrate over momentum space:

$$\int \mathrm{d}^3p\ \frac{\gamma}{(2\pi\hbar)^3}\ A_{\mathbf{k}}(\mathbf{p}) + 2\,\frac{C}{\rho_0}\,\frac{\gamma}{(2\pi\hbar)^3}\ \rho_{\mathbf{k}}\int \mathrm{d}^3p\ \delta(E-E_F)\,\frac{\mathbf{k}\cdot\mathbf{p}/m}{\mathbf{k}\cdot\mathbf{p}/m-\omega} = 0\ , \tag{3.123}$$

which will lead us to:

$$\begin{aligned} 1 + 2\,\frac{C}{\rho_0}\,\frac{\gamma}{(2\pi\hbar)^3}\ 2\Big(1-\frac{s}{2}\,\ln\frac{s+1}{s-1}\Big)\ m\,p_F\ 2\pi = 0\ , \\ \frac{C}{\rho_0}\,\frac{\gamma}{(2\pi\hbar)^3}\ 8\pi\ m\,p_F\,\Big(\frac{s}{2}\,\ln\frac{s+1}{s-1}-1\Big) = 1\ . \end{aligned} \tag{3.124}$$

Since the equilibrium density, ρ_0, can be expressed in terms of Fermi momentum :

$$\begin{aligned} \rho_0 &= \int \mathrm{d}^3p\ f^0(E) = \int \mathrm{d}^3p\ \big(f_p^0(E)+f_n^0(E)\big) \\ &= \int \mathrm{d}^3p\ \frac{2\gamma}{(2\pi\hbar)^3}\,\Theta(E-E_F) = \frac{2\gamma}{(2\pi\hbar)^3}\int p^2\ \mathrm{d}p\ \mathrm{d}\Omega\ \Theta(E-E_F) \\ &= \frac{2\gamma}{(2\pi\hbar)^3}\ 4\pi\int_0^{E_F} 2\,m\,E\ \frac{m}{\sqrt{2mE}}\ \mathrm{d}E = \frac{2\gamma}{(2\pi\hbar)^3}\ 4\pi\sqrt{2}\ m^{3/2}\,\frac{E_F^{3/2}}{3/2} \\ &= \frac{2\gamma}{(2\pi\hbar)^3}\ 4\pi\,\frac{p_F^3}{3}\ , \end{aligned} \tag{3.125}$$

we will have:

$$\frac{s}{2}\,\ln\frac{s+1}{s-1} - 1 = \frac{2\,E_F}{3\,C}\ . \tag{3.126}$$

The isovector collective mode velocity will depend now on the symmetry energy through the value of the parameter C. For $C = 32$ MeV, corresponding to an *asy-stiff* parametrisation, the solution $s = \dfrac{\omega}{k\,v_F} \approx 1.08$ is obtained (see Fig. 3.5). Again, the isovector zero sound mode is a quantum collective motion different from the hydrodynamical (or first sound) mode, which is driven by the pressure gradient, and so, requiring the local thermodynamical equilibrium. In finite nuclei, this zero sound mode will correspond to the GDR. Considering a wave-number k, determined by the dimension of the tin isotope ^{132}Sn, the energy of the phonon would be $\hbar\,\omega \approx 15.15$ MeV, quite close to the experimental results.

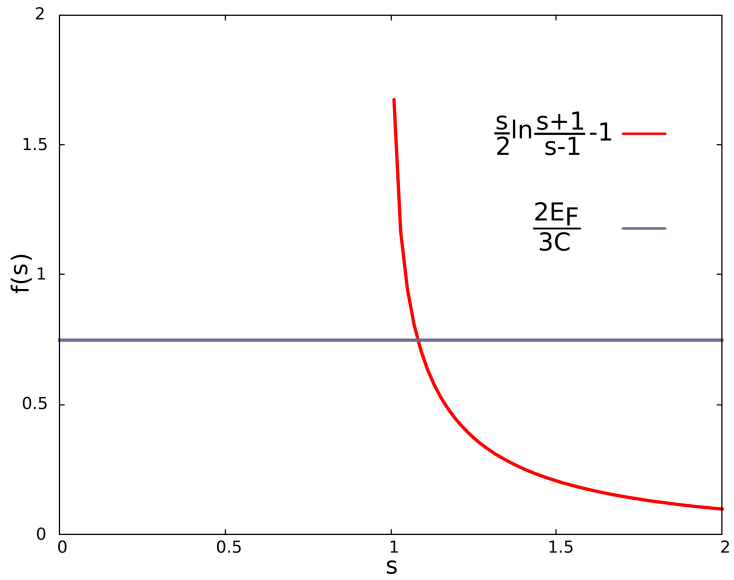

Figure 3.5: Graphical representation for the *zero sound* solution in Eq. (3.126), $s = \dfrac{\omega}{k\, v_F} \approx 1.08$, with $E_F \approx 36$ MeV at saturation density $\rho_0 = 0.16$ fm^{-3} (see Eq. (3.21)), and an *asy-stiff* parametrization for the symmetry term, $C = 32$ MeV.

Chapter 4

Vlasov approach to dipole modes in neutron rich nuclei

In the previous Chapter, we proved that the Vlasov equation:

$$\frac{\partial f(\mathbf{r},\mathbf{p})}{\partial t} + \frac{\mathbf{p}}{m} \cdot \nabla_{\mathbf{r}} f(\mathbf{r},\mathbf{p}) - \nabla_{\mathbf{r}} U(\mathbf{r}) \cdot \nabla_{\mathbf{p}} f(\mathbf{r},\mathbf{p}) = 0 \,, \tag{4.1}$$

represents the semi-classical limit of the TDHF equations. It describes the dynamical evolution of the one-body distribution function, $f(\mathbf{r},\mathbf{p},t)$, of a fermionic system, in the presence of a self-consistent mean-field, $U(\mathbf{r})$. When applied to nuclear matter, we showed that it predicts the existence of a new class of collective motions, namely the zero-sound, which can propagate even at zero-temperature. In this Chapter our goal is to extend the application of this equation to finite fermionic systems, namely atomic nuclei.

Along the first section we describe the basic ingredients required to implement numerically the Vlasov equation. Our approach will be based on the so-called test particle method, which we will briefly describe in the following. Once the principles of this method are presented, we shall expose the structure of the numerical program devoted to integrate the transport equation. Then, we shall investigate various static properties of the neutron rich tin isotope, ^{132}Sn. We test the capability of the program to reproduce some features of the neutron skin also in relation to the symmetry energy parametrization employed. Finally we explore the dipole response of various neutron rich nuclei, focusing on the properties of the collective modes, pygmy, core, and GDR vibrations, suggested by the HOSM in Chapter 2. We shall inquire in detail the dependence of these features on the symmetry energy parametrization as well as on the nuclear mass.

4.1 The test particle method

The essential task of the transport approach is to provide the value of the one-body distribution function at any time. Once this quantity is known, the expectation values of any one-body observable, $A(\mathbf{r},\mathbf{p})$, can be evaluated as an integral over phase-space. In particular, the total number of nucleons, A, is:

$$\iint \mathrm{d}^3r \; \mathrm{d}^3p \; f(\mathbf{r},\mathbf{p},t) = A \,. \tag{4.2}$$

The test particle method starts from the observation that the Gaussian functions generate, as coherent states, a super-complete basis. Then, the following expansion for the distribution function is valid:

$$f(\mathbf{r},\mathbf{p},t) = \frac{1}{(2\pi\hbar)^3}\int \mathrm{d}^3r_0\ \mathrm{d}^3p_0\ \omega(\mathbf{r}_0,\mathbf{p}_0,0)\ g(\mathbf{r}-\mathbf{r}_0,\mathbf{p}-\mathbf{p}_0,t) \equiv\ \omega(\mathbf{r},\mathbf{p},0)\ g(\mathbf{r},\mathbf{p},t)\ , \tag{4.3}$$

where $g(\mathbf{r}-\mathbf{r}_0,\mathbf{p}-\mathbf{p}_0,t)$ corresponds to a product of Gaussian functions in coordinate and momentum space, centered in $\mathbf{r}_0$ and $\mathbf{p}_0$ respectively, while $\omega(\mathbf{r}_0,\mathbf{p}_0,0)$ represents the corresponding weight in the expansion of g. In our numerical implementation, this expansion is discretized into a sum over a sufficiently large number of Gaussian functions [74, 75]:

$$f(\mathbf{r},\mathbf{p},t) = \frac{1}{\mathcal{N}}\,\frac{1}{(2\pi\hbar)^3}\,\frac{1}{(4\pi^2\chi\phi)^{3/2}}\sum_i^N \exp\left(-\frac{(\mathbf{r}-\mathbf{r}_i(t))^2}{2\,\chi}\right)\exp\left(-\frac{(\mathbf{p}-\mathbf{p}_i(t))^2}{2\,\phi}\right)\ . \tag{4.4}$$

Here, $\mathbf{r}_i(t)$ and $\mathbf{p}_i(t)$ represent the centroid positions in coordinate and momentum space of the i-Gaussian function, which define an individual test particle, while $\mathcal{N}$ indicates the number of test particles per nucleon. Consequently, the total number of test particles used, will be $N = A\cdot\mathcal{N}$.

The Gaussian functions which appear in Eq. (4.4) are normalized as follows:

$$g_\chi(\mathbf{r}-\mathbf{r}_i) = \frac{1}{(2\pi\chi)^{3/2}}\ \exp\left(-\frac{(\mathbf{r}-\mathbf{r}_i)^2}{2\chi}\right)\ , \tag{4.5a}$$

$$g_\phi(\mathbf{p}-\mathbf{p}_i) = \frac{1}{(2\pi\phi)^{3/2}}\ \exp\left(-\frac{(\mathbf{p}-\mathbf{p}_i)^2}{2\phi}\right)\ , \tag{4.5b}$$

so that one has:

$$\int \mathrm{d}^3r\ g_\chi(\mathbf{r}-\mathbf{r}_i) = 1\ , \tag{4.6a}$$

$$\int \mathrm{d}^3p\ g_\phi(\mathbf{p}-\mathbf{p}_i) = 1\ . \tag{4.6b}$$

Let us observe that the gradients of the distribution function, as well as the time derivative can be expressed as follows:

$$\nabla_{\mathbf{r}} f(\mathbf{r},\mathbf{p},t) = \frac{1}{\mathcal{N}}\,\frac{1}{(2\pi\hbar)^3}\,\frac{1}{(4\pi^2\chi\phi)^{3/2}} \times\sum_i^N\Big[-\frac{(\mathbf{r}-\mathbf{r}_i)}{\chi}\Big]\ \exp\left(-\frac{(\mathbf{r}-\mathbf{r}_i)^2}{2\chi}\right)\ \exp\left(-\frac{(\mathbf{p}-\mathbf{p}_i)^2}{2\phi}\right)\ , \tag{4.7a}$$

$$\nabla_{\mathbf{p}} f(\mathbf{r},\mathbf{p},t) = \frac{1}{\mathcal{N}}\,\frac{1}{(2\pi\hbar)^3}\,\frac{1}{(4\pi^2\chi\phi)^{3/2}} \times\sum_i^N\Big[-\frac{(\mathbf{p}-\mathbf{p}_i)}{\phi}\Big]\ \exp\left(-\frac{(\mathbf{r}-\mathbf{r}_i)^2}{2\chi}\right)\ \exp\left(-\frac{(\mathbf{p}-\mathbf{p}_i)^2}{2\phi}\right)\ , \tag{4.7b}$$

and

$$\frac{\partial}{\partial t} f(\mathbf{r},\mathbf{p},t) = \frac{1}{\mathcal{N}} \frac{1}{(2\pi\hbar)^3} \frac{1}{(4\pi^2\chi\phi)^{3/2}} \times \sum_i^N \left[\frac{(\mathbf{r}-\mathbf{r}_i)}{\chi} \frac{\partial \mathbf{r}_i}{\partial t} \exp\left(-\frac{(\mathbf{r}-\mathbf{r}_i)^2}{2\chi} \right) \exp\left(-\frac{(\mathbf{p}-\mathbf{p}_i)^2}{2\phi} \right) + \frac{(\mathbf{p}-\mathbf{p}_i)}{\phi} \frac{\partial \mathbf{p}_i}{\partial t} \exp\left(-\frac{(\mathbf{r}-\mathbf{r}_i)^2}{2\chi} \right) \exp\left(-\frac{(\mathbf{p}-\mathbf{p}_i)^2}{2\phi} \right) \right] . \quad (4.8)$$

Substituting these expressions into the Vlasov equation (Eq. (3.90)), we find that the centroids of each Gaussian, $\mathbf{r}_i$ and $\mathbf{p}_i$ must satisfy Hamilton equations, that is:

$$\frac{\partial \mathbf{r}_i}{\partial t} = \frac{\mathbf{p}_i}{m} , \quad (4.9a)$$

$$\frac{\partial \mathbf{p}_i}{\partial t} = -\nabla_{\mathbf{r}_i} U(\mathbf{r}_i) . \quad (4.9b)$$

One can observe that the local density obtained by integrating the distribution function over momenta, appears as a contribution from all the test particles:

$$\begin{aligned} \rho(\mathbf{r}) &= \int \mathrm{d}^3p \; f(\mathbf{r},\mathbf{p},t) \\ &= \frac{1}{\mathcal{N}} \frac{1}{(2\pi\hbar)^3} \sum_{i=1}^N g_\chi(\mathbf{r}-\mathbf{r}_i(t)) \int \mathrm{d}^3p \; g_\phi(\mathbf{p}-\mathbf{p}_i(t)) \\ &= \frac{1}{\mathcal{N}} \frac{1}{(2\pi\hbar)^3} \sum_{i=1}^N g_\chi(\mathbf{r}-\mathbf{r}_i(t)) . \end{aligned} \quad (4.10)$$

More generally, the average value of an arbitrary physical quantity, $A(\mathbf{r},\mathbf{p})$, can be expressed:

$$\begin{aligned} \langle A(\mathbf{r},\mathbf{p}) \rangle &= \int \mathrm{d}^3r \; \mathrm{d}^3p \; A(\mathbf{r},\mathbf{p}) f(\mathbf{r},\mathbf{p},t) \\ &= \frac{1}{\mathcal{N}} \frac{1}{(2\pi\hbar)^3} \sum_i^N \int \mathrm{d}^3r \; \mathrm{d}^3p \; A(\mathbf{r},\mathbf{p}) \; g_\chi(\mathbf{r}-\mathbf{r}_i) \; g_\phi(\mathbf{p}-\mathbf{p}_i) \\ &= \frac{1}{\mathcal{N}} \frac{1}{(2\pi\hbar)^3} \sum_i^N \langle A(\mathbf{r},\mathbf{p}) \rangle_i , \end{aligned} \quad (4.11)$$

where $\langle A(\mathbf{r},\mathbf{p}) \rangle_i$ represents the contribution of an individual Gaussian. This contribution is obtained by the convolution of A with the corresponding Gaussians in coordinate and momentum space:

$$\langle A(\mathbf{r},\mathbf{p}) \rangle_i = \int \mathrm{d}^3r \; \mathrm{d}^3p \; A(\mathbf{r},\mathbf{p}) \; g_\chi(\mathbf{r}-\mathbf{r}_i(t)) \; g_\phi(\mathbf{p}-\mathbf{p}_i(t)) . \quad (4.12)$$

Consequently, for the average density, $\langle\rho\rangle$, we get:

$$\langle\rho\rangle = \int \mathrm{d}^3r\ \mathrm{d}^3p\ \rho(\mathbf{r})\ f(\mathbf{r},\mathbf{p},t) = \frac{1}{\mathcal{N}}\ \frac{1}{(2\pi\hbar)^3} \sum_i^N \langle\rho(\mathbf{r})\rangle_i$$
$$= \frac{1}{\mathcal{N}^2}\ \frac{1}{(2\pi\hbar)^6} \sum_{i,j}^N g_{2\chi}(\mathbf{r}_i - \mathbf{r}_j)\ , \tag{4.13}$$

since,

$$\begin{aligned}
\langle\rho(\mathbf{r})\rangle_i &= \int \mathrm{d}^3r\ \mathrm{d}^3p\ \rho(\mathbf{r})\ g_\chi(\mathbf{r}-\mathbf{r}_i)\ g_\phi(\mathbf{p}-\mathbf{p}_i) \\
&= \int \mathrm{d}^3r\ \rho(\mathbf{r})\ g_\chi(\mathbf{r}-\mathbf{r}_i) \\
&= \frac{1}{\mathcal{N}}\ \frac{1}{(2\pi\hbar)^3} \sum_j^N \int \mathrm{d}^3r\ g_\chi(\mathbf{r}-\mathbf{r}_j)\ g_\chi(\mathbf{r}-\mathbf{r}_i) \\
&= \frac{1}{\mathcal{N}}\ \frac{1}{(2\pi\hbar)^3} \sum_j^N \frac{1}{(2\pi\chi)^3} \int \mathrm{d}^3r\ \mathrm{e}^{-\frac{(\mathbf{r}-\mathbf{r}_j)^2}{2\chi}}\ \mathrm{e}^{-\frac{(\mathbf{r}-\mathbf{r}_i)^2}{2\chi}} \\
&= \frac{1}{\mathcal{N}}\ \frac{1}{(2\pi\hbar)^3} \sum_j^N \frac{1}{(2\pi\chi)^3} \int \mathrm{d}^3r\ \exp\left(-\frac{2(\mathbf{r}-\frac{\mathbf{r}_i+\mathbf{r}_j}{2})^2}{2\chi}\right)\ \exp\left(-\frac{(\mathbf{r}_i-\mathbf{r}_j)^2}{4\chi}\right) \\
&= \frac{1}{\mathcal{N}}\ \frac{1}{(2\pi\hbar)^3} \sum_j^N \frac{1}{(2\pi\chi)^3}\ \sqrt{\pi\chi}\ \exp\left(-\frac{(\mathbf{r}_i-\mathbf{r}_j)^2}{4\chi}\right) \\
&= \frac{1}{\mathcal{N}}\ \frac{1}{(2\pi\hbar)^3} \sum_j^N \frac{1}{(4\pi\chi)^{3/2}}\ \exp\left(-\frac{(\mathbf{r}_i-\mathbf{r}_j)^2}{4\chi}\right) \\
&= \frac{1}{\mathcal{N}}\ \frac{1}{(2\pi\hbar)^3} \sum_j^N g_{2\chi}(\mathbf{r}_i-\mathbf{r}_j)\ .
\end{aligned} \tag{4.14}$$

Into the calculations we also need to evaluate $\langle\rho^\gamma(\mathbf{r})\rangle_i$, for which we shall make the following approximation:

$$\langle\rho^\gamma(\mathbf{r})\rangle_i \approx \langle\rho(\mathbf{r})\rangle_i^\gamma\ . \tag{4.15}$$

Solving the Hamilton equations will require also the gradients of the average value of the density carried by a Gaussian i:

$$\begin{aligned}
\frac{\partial}{\partial x_i}\langle\rho(\mathbf{r})\rangle_i &= \frac{1}{\mathcal{N}}\ \frac{1}{(2\pi\hbar)^3} \sum_j^N \frac{\partial}{\partial x_i}\ g_{2\chi}(\mathbf{r}_i-\mathbf{r}_j) \\
&= \frac{1}{\mathcal{N}}\ \frac{1}{(2\pi\hbar)^3}\ \frac{1}{(4\pi\chi)^{3/2}} \sum_j^N \frac{\partial}{\partial x_i}\ \exp\left(-\frac{(\mathbf{r}_i-\mathbf{r}_j)^2}{4\chi}\right) \\
&= \frac{1}{\mathcal{N}}\ \frac{1}{(2\pi\hbar)^3}\ \frac{1}{(4\pi\chi)^{3/2}} \sum_j^N \frac{x_j - x_i}{2\chi}\ \exp\left(-\frac{(\mathbf{r}_i-\mathbf{r}_j)^2}{4\chi}\right)\ .
\end{aligned} \tag{4.16}$$

For $\dfrac{\partial}{\partial x_i}\langle\rho^\gamma(\mathbf{r})\rangle_i$ we also make the approximation:

$$\frac{\partial}{\partial x_i}\,\langle\rho^\gamma(\mathbf{r})\rangle_i \approx \frac{\partial}{\partial x_i}\,\langle\rho(\mathbf{r})\rangle_i^\gamma = \gamma\,\langle\rho^\gamma(\mathbf{r})\rangle_i^{\gamma-1}\,\frac{\partial}{\partial x_i}\,\langle\rho(\mathbf{r})\rangle_i\ . \tag{4.17}$$

Consequently, for the isoscalar part of the mean field:

$$U(\rho) = A\,\frac{\rho}{\rho_0} + B\,\frac{\rho}{\rho_0}^{\gamma} \equiv t_0\,\rho + t_3\,\rho^\gamma\ , \tag{4.18}$$

the convolution over Gaussian i can be expressed:

$$\langle U(\rho)\rangle_i = t_0\,\langle\rho(\mathbf{r})\rangle_i + t_3\,\langle\rho(\mathbf{r})\rangle_i^\gamma\ , \tag{4.19}$$

while the derivative with respect to coordinate x_i is:

$$\frac{\partial}{\partial x_i}\,\langle U(\rho)\rangle_i = t_0\,\frac{\partial}{\partial x_i}\,\langle\rho(\mathbf{r})\rangle_i + t_3\,\frac{\partial}{\partial x_i}\,\langle\rho(\mathbf{r})\rangle_i^\gamma\ . \tag{4.20}$$

The numerical integration of the Hamilton equations is achieved employing a second order Runge-Kutta algorithm [76], which is briefly discussed in the following.

We start from a first order differential equation, satisfied by the function $y(x)$:

$$\frac{dy}{dx} = f\big(x, y(x)\big)\ . \tag{4.21}$$

We are interested in the solution of the above equation, knowing the initial condition (i.e. $y_0 = y(x=0)$), at a particular value of x, let us say $x = 1$. The idea now is to divide the interval $[0,1]$ into equally spaced subintervals with the length $h = 1/N$ with the number of intervals, N, eing sufficiently large. The next step is to develop a recursion formula which will relate y_n (with $y_n = y(x_n = nh)$) to y_m, with $m = n-1, n-2, n-3, \ldots$. An exact recursion formula can be achieved by integrating Eq. (4.21), so that:

$$y_{n+1} - y_n = \int_{x_n}^{x_{n+1}} \mathrm{d}x\ f(x,y)\ . \tag{4.22}$$

The second order Runge-Kutta algorithm is obtained by approximating $f(x,y)$ in the above integral by a Taylor expansion about the mid-point of the integration interval:

$$f(x,y) = f(x_{n+1/2}, y_{n+1/2}) + (x - x_{n+1/2})\ \left.\frac{df}{dx}\right|_{x=(n+1/2)h}\ . \tag{4.23}$$

From Eqs. (4.21), (4.22) and (4.23) we get:

$$\begin{aligned}
y_{n+1} - y_n &= \int_{x_n}^{x_{n+1}} \mathrm{d}x\ \big(f(x_{n+1/2}, y_{n+1/2}) + (x - x_{n+1/2})\,y_{n+1/2}\big) \\
&= hf(x_{n+1/2}, y_{n+1/2}) + \frac{x_{n+1}^2 - x_n^2}{2}\,y_{n+1/2} - (x_{n+1} - x_n)\,x_{n+1/2}\,y_{n+1/2} \\
&= hf(x_{n+1/2}, y_{n+1/2}) + \frac{(x_{n+1} - x_n)(x_{n+1} + x_n)}{2}\,y_{n+1/2} - hx_{n+1/2}\,y_{n+1/2} \\
&= hf(x_{n+1/2}, y_{n+1/2}) + h\,\frac{(x_{n+1} + x_n)}{2}\,y_{n+1/2} - hx_{n+1/2}y_{n+1/2} \\
&= hf(x_{n+1/2}, y_{n+1/2})\ ,
\end{aligned} \tag{4.24}$$

so

$$y_{n+1} = y_n + hf(x_{n+1/2}, y_{n+1/2}) + \mathcal{O}(h^3) \ , \tag{4.25}$$

which is just the second order Runge-Kutta approximation. Thus, the propagation of the test particles in Eq. (4.9) will be expressed as follows (with $h = \delta t$ and $x_n = t$):

$$\mathbf{p}_i(t + \delta t) = \mathbf{p}_i(t) - \delta t \ \nabla U(\mathbf{r}_i, t + \delta t/2) \ , \tag{4.26}$$

$$\mathbf{r}_i(t + \delta t/2)) = \mathbf{r}_i(t - \delta t/2) + \delta t \ \mathbf{p}_i(t)/m \ . \tag{4.27}$$

Solving these equations we reconstruct the distribution function at any instant in terms of the Gaussian functions.

Now we are in the position to describe the structure of the numerical code devoted to solve the two coupled Vlasov equations for protons and neutrons. Essentially, the program has three main parts, and an overview is presented in Fig. (4.1). In the first part, the ground-state for the system is constructed. In the second part, the time integration is implemented. The third part of the program, at specified time intervals, extracts physical information of interest which characterise various properties of the system.

For the initialization, the program reads from the input file, the number of neutrons and protons, the widths of Gaussian functions in coordinate and momentum space, χ and ϕ, the number of test particles per nucleon, $\mathcal{N}$, the integration time step, the total evolution time, the time interval at which the subroutine CLUSTER is called, the EOS choice in isoscalar and isovector channels. In the isovector sector we consider *asy-stiff* parametrisation *isy=1*, *asy-soft* parametrisation *isy=2*, and *asy-superstiff* parametrisation *isy=3*. We performed several trial runs with various number of test particles per nucleon, to observe the stability of the calculations. To achieve a good spanning of the phase-space we decided to work mainly with $\mathcal{N} = 1200$ test particles per nucleon, which represents a balanced compromise between accuracy and computation speed. The integration time step is 0.5 fm/c, and the analysis time interval is 1 fm/c. The system evolution if followed for at least 630 fm/c.

The nucleus ground state preparation is performed within a subroutine named GROUND, following the steps described below [77]. Within a volume in phase-space, $V_{0ps} = V_0(\mathbf{r}) \cdot V_0(\mathbf{p})$, obtained from a sphere in coordinate space of radius $1.5\,A^{1/3}$ fm and a sphere in momentum space of radius $1.45\,\hbar$ MeV/c (with $\hbar = 197.33$ MeV $\cdot$ fm/c), a number, $N_{\rm tot} = 4\ \dfrac{V_{0ps}}{(2\pi\hbar)^3}\ \mathcal{N}$ of Gaussian functions equal to the total number of states, is randomly generated. Starting from some initial guess for the values of Fermi energies of protons and neutrons, a linear interpolation of Fermi levels is obtained. After that, the energies of all the nucleons are situated below the final Fermi levels. Once the new Fermi levels are obtained, a new random generation of test particles is performed until a number of proton Gaussians, $\mathcal{N} \cdot Z$ with energy less than proton Fermi level, and a number of neutron Gaussians, $\mathcal{N} \cdot N$ with energy less than neutron Fermi level are obtained. With this initial positions of the Gaussians in coordinate and momentum space, one can construct the initial distribution functions, $f(\mathbf{r}, \mathbf{p}, t = 0)$ (see Eq. (4.4)) for protons and neutrons.

The second part of the program, the subroutine PROPAG, acomplishes the time evolution of the system, integrating the Vlasov equation which, in agreement with our previous discussions, is reduced to the integration of the Hamilton equations for the centroids of the Gaussians entering into the definition of the distribution functions (see Eq. (4.9))

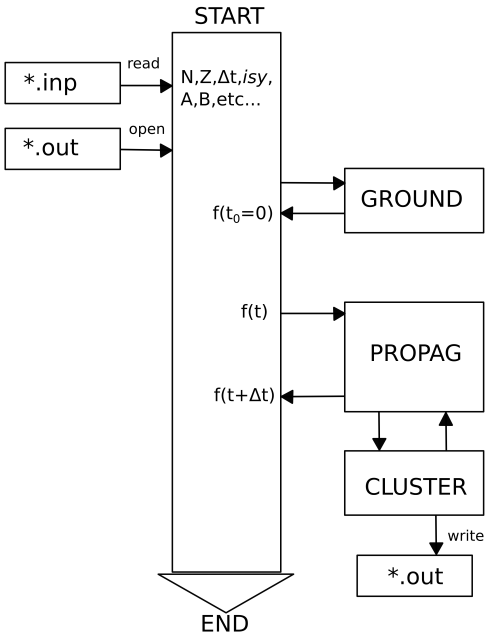

Figure 4.1: Schematic overview of the program structure.

for protons and neutrons. Using the Runge-Kutta method the integration of Hamilton equations is accomplished evaluating at each time step the contributions to the gradient of the nuclear mean field and Coulomb interactions among protons. Once the new positions of Gaussians are known the new distribution functions are reconstructed. Then, the physical properties of interest (dipole moments, quadrupole moments, local densities in the real and momentum space, energies) are calculated into the subroutine named CLUSTER, based on relations as those introduced in the beginning of the Section.

4.2 Static properties within Vlasov dynamics

We shall first investigate the ground state properties of the neutron-rich nucleus ^{132}Sn. The ground state configuration is obtained as the stationary solution of the Vlasov equations for protons and neutrons. Since we neglect the two-body collision effects, the main ingredient would be the nuclear mean field. We shall employ a Skyrme-like parametrization for the nuclear mean field (see. Eqs. (3.40), (3.41) and (3.43)), as well as the Coulomb interaction potential between the protons. The values of the coefficients $A = -356.8$ MeV, $B = 303.9$ MeV, $\sigma = 7/6$, lead to the following properties of symmetric nuclear matter: the saturation density $\rho_0 = 0.16$ fm^{-3}, the binding energy $E_B = -16$ MeV/nucleon, and the compressibility modulus of "soft EOS" type, $K = 201$ MeV. The effective nucleon mass is taken equal to the bare mass, 940 MeV. For the isovector channel we employ three different parametrizations, namely *asy-soft*, *asy-stiff* and *asy-superstiff*, which we previously discussed.

The system is left to freely evolve in the absence of any external perturbation. The equilibrium distribution functions of the Vlasov equations are obtained. Then, one can

evaluate the local proton and neutron densities:

$$\rho_p(\mathbf{r},t) = \int \mathrm{d}^3p\ f_p(\mathbf{r},\mathbf{p},t)\ , \tag{4.28}$$

$$\rho_n(\mathbf{r},t) = \int \mathrm{d}^3p\ f_n(\mathbf{r},\mathbf{p},t)\ , \tag{4.29}$$

as well as the proton and neutron mean square radii:

$$\langle r_p^2\rangle = \frac{1}{N_p}\int \mathrm{d}^3r\ r^2\,\rho_p(\mathbf{r},t)\ , \tag{4.30}$$

$$\langle r_n^2\rangle = \frac{1}{N_n}\int \mathrm{d}^3r\ r^2\,\rho_n(\mathbf{r},t)\ . \tag{4.31}$$

Then one can calculate the neutron skin thickness defined as:

$$\Delta R_{np} = R_n - R_p = \sqrt{\langle r_n^2\rangle} - \sqrt{\langle r_p^2\rangle}\ . \tag{4.32}$$

In Table. 4.1 we report the values of the protons and neutrons rms radii, as well as the skin thickness, for the three different parametrizations of $C(\rho)$. The values of the symmetry energy per nucleon at saturation:

$$\frac{E_{sym}}{A}(\rho_0) = \frac{1}{3}\,\varepsilon_F(\rho) + \frac{C(\rho)}{2}\,\frac{\rho}{\rho_0}\bigg|_{\rho=\rho_0}\ , \tag{4.33}$$

as well as the slope parameter:

$$L = 3\,\rho_0\,\frac{dE_{sym}/A}{d\rho}\bigg|_{\rho=\rho_0}\ , \tag{4.34}$$

are also reported in Table. 4.1 for the three asy-EOS. One can see that the neutron skin thickness increases with the slope parameter, an effect linked to the *symmetry pressure*. This is consistent with the findings of Yoshida and Sagawa [12]. Moreover, the values obtained with our semi-classical approach for the protons and neutrons rms radii as well as the skin thickness, are in reasonable agreement with the ones obtained in the framework of relativistic mean field or Skyrme Hartree-Fock theories [78]. A good agreement is also remarked when our findings are compared with the results obtained with similar effective interactions, within various theoretical models [79]. The radial extensions as well as the radial density profiles (see Fig. 4.2) for protons and neutrons, are quite consistent with those obtained using other theoretical methods [78, 30]. Nevertheless, while in our semi-classical calculations, a constant density profile is predicted in the internal region below 4 fm, in more sophisticated quantum approaches, such as Hartree-Fock-Bogolyubov [30], some oscillations of proton and neutron densities show up. However, our semi-classical approach is able to disentangle the symmetry energy effects in the nuclear ground state, consistent with the predictions of more elaborate approaches.

The stability of the ground state was also checked, and, as can be seen from Fig. 4.2 the system manifests very small amplitude fluctuations around the average values of neutron and proton rms radii. Moreover, the number of test particles escaping from

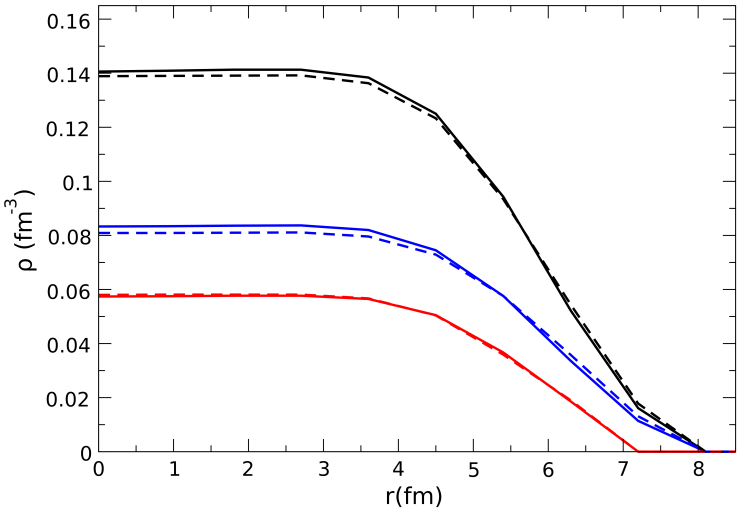

Figure 4.2: Graphical representation of the radial density profiles for the neutrons (blue lines in the middle), protons (lower red lines) and total (upper black lines) for *asy-soft* (solid lines) and *asy-superstiff* (dashed lines) parametrisations of the EOS.

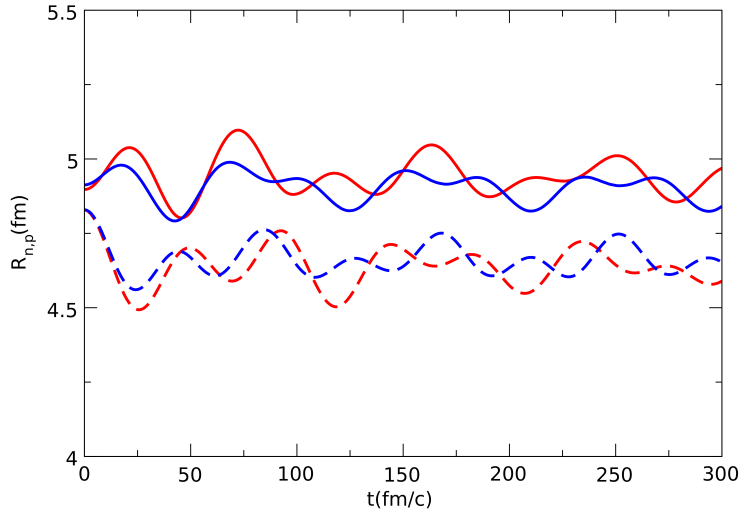

Figure 4.3: Time evolution of proton (dashed lines) and neutron (solid lines) radii for *asy-soft* (blue) and *asy-superstiff* (red) parametrisations of the EOS, in the ground state.

asy-EOS	E_{sym}/A (MeV)	L(MeV)	R_n(fm)	R_p(fm)	$\Delta R_{np}(fm)$
asy-soft	29.9	14.4	4.90	4.65	0.25
asy-stiff	28.3	72.6	4.95	4.65	0.30
asy-superstiff	28.3	96.6	4.96	4.65	0.31

Table 4.1: The dependence on the equation of state (EOS) for the symmetry energy at saturation, the slope parameter, neutrons rms radius, protons rms radius and neutron skin thickness.

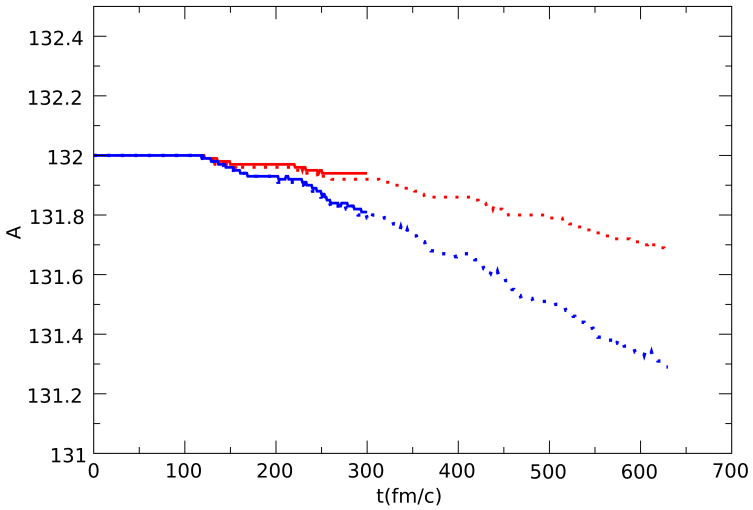

Figure 4.4: Time evolution of the mass number, A, for the ground state (solid lines) and for an evolution of the ^{132}Sn nucleus after a "pygmy-like" excitation (dotted lines), for *asy-soft* (blue) and *asy-superstiff* (red) parametrisations of the EOS.

the system within 300 fm/c is less then 0.2 nucleons (see Fig. 4.2), while the energy conservation is satisfied within a limit less than 1%.

Summarizing the main findings of these Section, we conclude that our semi-classical approach provides quite reasonable description of the ground state, in agreement with other many-body approaches, and in the range inferred by experimental observations. Moreover, the sensitivity of the neutron skin to the symmetry-energy, also predicted by other works, motivate us to extend our investigation to the dipole response in neutron rich nuclei.

4.3 Pygmy and Giant dipole modes in exotic nuclei

Inspired by the main conclusions of the HOSM, in this Section we explore both the oscillations of the nuclear skin against the core, associated to the pygmy mode, and the out of phase oscillations of all protons against all neutrons, associated to the GDR mode.

To inquire on the collective properties of the pygmy dipole mode, after $t = t_0 =$ 30 fm/c from the initialisation, we excite the system by boosting along z direction all the excess neutrons, and in opposite direction all the core nucleons in such a way that the center of mass of the nucleus remains at rest. We shall call this a "pygmy-like" excitation. The excess neutrons, $N_e = 32$, for the case of ^{132}Sn isotope, are identified as the most distant neutrons from the center of mass. Later on, we shall consider a different initial excitation, where all the neutrons are boosted along z direction, and in opposite direction all the protons, in such a way that the center of mass remains at rest. We shall call this a "GDR-like" excitation.

We mention that, in order to check the stability of our numerical procedure during the time evolution, we analyze the number of test particles escaping from the system. On average this number corresponds to less than a neutron(see also Fig. 4.2), while, the total energy conservation is satisfied within 1.5%.

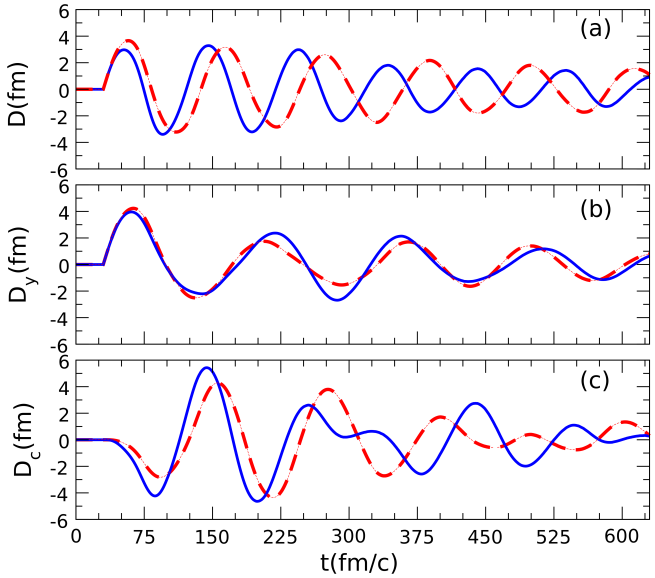

Figure 4.5: Graphical representation of the time evolution of the total dipole D (a), pygmy dipole D_y (b), and of core dipole D_c (c), for *asy-soft* (solid blue lines) and *asy-superstiff* (dashed red lines) EOS, for a "pygmy-like" initial excitation with $N_e = 32$ excess neutrons considered in the excitation.

In all cases, after the initial boost, the system is left to evolve for at least 600 fm/c, and the time dependence of the collective coordinates associated with the pygmy, $\mathbf{Y}$, core, $\mathbf{X}_c$, and giant dipole modes, $\mathbf{X}$, is obtained, by numerically solving the Vlasov equation for protons and neutrons respectively. We recall that $\mathbf{Y}$ accounts for the distance between the center of mass of the core and the center of mass of the excess neutrons, $\mathbf{X}_c$ accounts for the distance between the center of mass of the protons and the center of mass of the neutrons within the core, while $\mathbf{X}$ accounts for the distance between the center of mass of the protons and the center of mass of all the neutrons.

In Fig. 4.5 we plot the time evolution of the total dipole, D, pygmy dipole, D_y, and core dipole, D_c, moments (for definitions see Eq. (2.71 from Chapter 2)), following a "pygmy-like" excitation for two parametrizations of the EOS. One can observe that while D_y approaches its maximum value, a symmetry energy dependent oscillatory motion of the core dipole, D_c, initiates. Within the HOSM, the core Hamiltonian, H_c and pygmy Hamiltonian, H_y are independent (i.e. commute). Thus, one would expect, in agreement with Eq. (2.71) that in a "pygmy-like" excitation, the core would remain inert, and the total dipole, D, would be determined only by the pygmy dipole, D_y. However, our semi-classical approach based on two coupled Vlasov equations for protons and neutrons, as observed, provides a different scenario, in which the core becomes excited. The coupling of the core is symmetry energy dependent, since, the larger the slope parameter, L, is, the more delayed is the isovector core response. This can be explained by the fact that a larger L corresponds to a larger neutron presence in the surface (see also Fig. 4.2), and so, a smaller coupling to the core is expected. Additionally, we clearly remark that the pygmy dipole oscillations are quite independent of the symmetry energy parametrization. At variance, the total dipole, D, is evidently affected by the isovector part of the interaction, and is influenced by the existence of the isovector core oscillations. The fastest vibrations

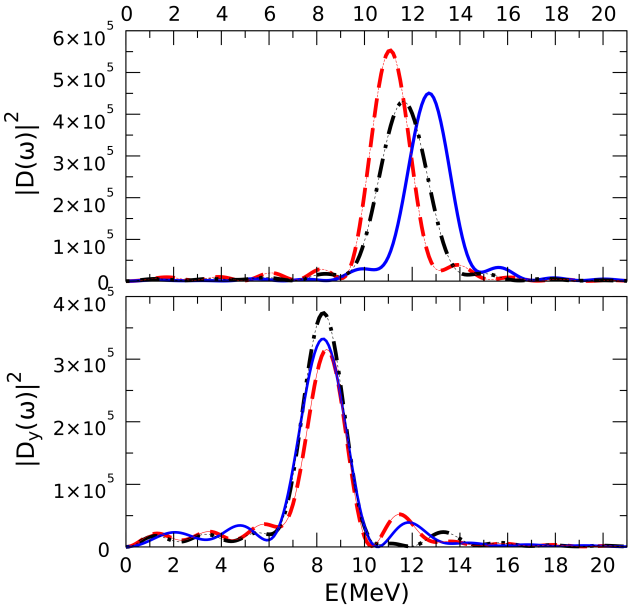

Figure 4.6: Graphical representation of the power spectrum of total dipole (a) and pygmy dipole D_y (b) (in fm^4/c^2), for *asy-soft* (solid blue lines), *asy-stiff* (dot-dashed black lines) and *asy-superstiff* (dashed red lines) EOS, for a "pygmy-like" initial excitation.

of the total dipole are observed for the *asy-soft* EOS, and looking at Fig. 3.1, one can see that this case corresponds to the largest value for the symmetry energy below saturation, and lowest L. In contrast, the pygmy dipole vibrations are not affected by the value of the symmetry energy below saturation, revealing the isoscalar-like nature of this mode.

Let us remind that a comparison of HOSM predictions with the experimental data, concerning the exhausted EWSR by the pygmy mode, suggested that a part of the excess neutrons could remain bound to the core. This seems to be confirmed by our self-consistent transport simulations, because the core does not remain inert (see Fig. 4.5). Later on, we shall present other evidences of this hypothesis. To estimate the energy centroid associated with each collective dipole mode, we calculate the power spectrum of the pygmy dipole, $D_y(t)$:

$$|D_y(\omega)|^2 = \left| \int_{t_0}^{t_{max}} \mathrm{d}t \; D_y(t) \; \mathrm{e}^{-i\omega t} \right|^2 , \tag{4.35}$$

and of the total dipole, $D(t)$:

$$|D(\omega)|^2 = \left| \int_{t_0}^{t_{max}} \mathrm{d}t \; D(t) \; \mathrm{e}^{-i\omega t} \right|^2 , \tag{4.36}$$

for each of the three asy-EOS parametrizations employed (see Figs. 4.6 and 4.7).

Confirming the qualitative observation, the position of the GDR centroid shifts towards larger values when one moves from *asy-superstiff* (largest slope parameter) to *asy-soft* (lowest slope parameter). The energy centroid corresponding to the pygmy mode is situated well below the GDR one, quite insensitive to the symmetry energy density parametrization. The PDR peak, for all the three cases is situated at $\sim$ 8.5 MeV,

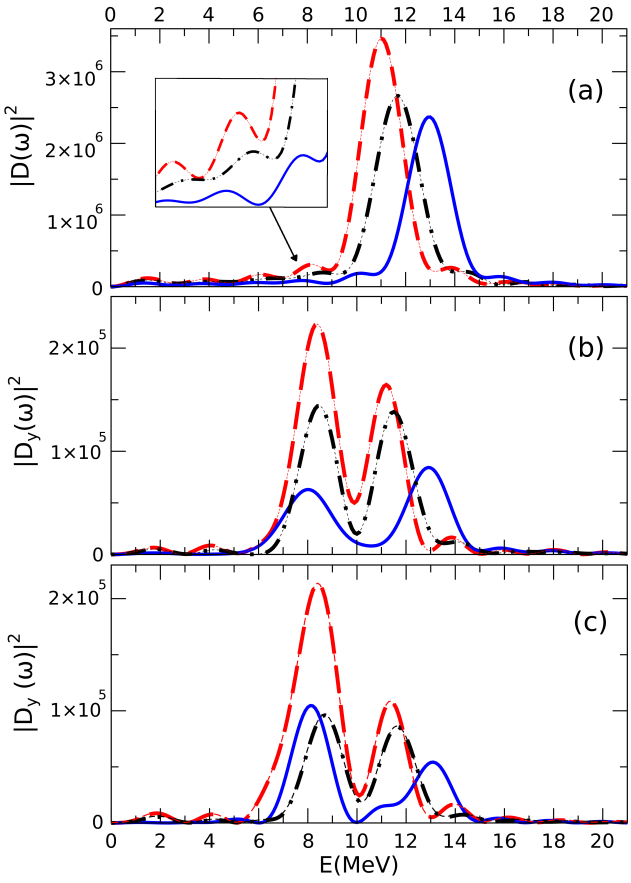

Figure 4.7: Graphical representation of the power spectrum of total dipole (a), pygmy dipole D_y with $N_y = N_e = 32$ skin neutrons (b) and pygmy dipole D_y with $N_y = 10$ skin neutrons (in $\mathrm{fm}^4/\mathrm{c}^2$), for *asy-soft* (solid blue lines), *asy-stiff* (dot-dashed black lines) and *asy-superstiff* (dashed red lines) EOS, for a "GDR-like" initial excitation.

clearly showing the isoscalar-like nature of this mode. A similar conclusion for Ni isotopes was reported within a relativistic mean-field approach by Liang *et al.* [80]. While, within the schematic HOSM all dipole modes are degenerate, with an energy $E = 41 \cdot A^{-1/3}$ MeV ≈ 8 MeV for ^{132}Sn isotope, in the semi-classical approach, the GDR energy is pushed up by the isovector interaction. Consequently, the dipole response can be explained in terms of the isoscalar-like (PDR) and isovector-like (GDR) modes, as expected in asymmetric systems [81, 82]. Moreover, both isoscalar-like and isovector-like modes are excited under a "pygmy-like" excitation.

To check the influence of the initial conditions on the dipole response let us now consider a "GDR-like" excitation, with the initial energy close to the value associated with first GDR excited state, i.e. ~ 15 MeV. Now, even though the initial conditions favors the isovector-like mode, a sizeable contribution in the pygmy region is evidenced. The low lying energy response seems to be symmetry energy dependent, as can be seen by comparing the total dipole Fourier spectra for the three parametrisations, shown in Fig. 4.7 (a). This is even better evidenced from the Fourier power spectrum of the pygmy dipole mode, as depicted in Fig. 4.7 (b). We mention that the result shown in Fig. 4.7 (b) was obtained considering that the number of skin neutrons which determine the pygmy dipole, is equal to the number of excess neutrons, i.e. $N_y = N_e = 32$. The part of the power spectrum of the pygmy dipole, situated at energies associated to GDR, indicates, however, that not all excess nucleons are coupled to the pygmy mode. A fraction of them seems to be coupled to the core dynamics, consistent with the HOSM suggestion. We tested further this suggestion, considering a new set of calculations, in which the number of excess neutrons contributing to the pygmy dipole is reduced to $N_y = 10$, the most peripheral out of the $N_e = 32$ neutrons. The power spectrum of the pygmy dipole in this case, is reported in Fig. 4.7 (c). An enhancement of the response in the pygmy region can be clearly remarked, simultaneously with the reduction of the response in the GDR region. In other words, the relative weight increases in the pygmy region when the $\mathbf{Y}$ coordinate is constructed with $N_y = 10$ most distant neutrons. Moreover, a part of the excess neutrons are involved in an isovector-like motion and the relative weight is symmetry energy dependent. One notices that in the case of *asy-superstiff* parametrization more neutrons are involved in the pygmy-like motion, since the slope parameter gives a larger skin size in this case.

Since a part of the neutrons that belong to the skin always contribute to the GDR mode, an EWSR value lower than the HOSM predictions corresponding to $N_y = N_e = 32$ is expected. Consequently, this explains why in the Fourier power spectrum of the total dipole, D, a weak response is seen at the pygmy frequency.

From this investigation the question on how to appropriately excite the pygmy dipole resonance arises, and, in this respect, nuclear rather than electromagnetic probes can induce neutron skin excitations closer to our first class of initial conditions (i.e. the "pygmy-like" ones) [83, 84]. Calvayrac *et al.* [85] showed that, in the case of "GDR-like" initial excitation, one can relate the strength function to the imaginary part of the Fourier transform of the total dipole, $D(\omega)$, and consequently, the corresponding cross-section can be calculated. In this respect, let us assume the nucleus under the photon-excitation driven by a classical field. Considering a very fast process, we can write the perturbation as:

$$V_{ext} = \eta\, \delta(t)\, \mathbf{D} \equiv \eta\, \delta(t)\, \frac{NZ}{A}\mathbf{X}\,, \tag{4.37}$$

with η being the perturbation strength, and $\mathbf{D}$ being the dipole operator. The effect of this perturbation corresponds to a dipolar velocity field superimposed on the ground state, $|\Phi_0\rangle$, so that the new state is [85]:

$$|\Phi(0)\rangle = \mathrm{e}^{i\eta\mathbf{D}}\,|\Phi_0\rangle\ . \tag{4.38}$$

The expectation value of the collective momenta, $\mathbf{P}$, can be written as follows:

$$\begin{aligned}\langle\Phi(0)|\mathbf{P}|\Phi(0)\rangle &= \langle\Phi_0|\,\mathrm{e}^{-i\eta\mathbf{D}}\,\mathbf{P}\,\mathrm{e}^{i\eta\mathbf{D}}\,|\Phi_0\rangle \\ &= \langle\Phi_0|\,\mathrm{e}^{-i\eta\mathbf{D}}\,\mathrm{e}^{i\eta\mathbf{D}}\,\mathbf{P}\,|\Phi_0\rangle + \langle\Phi_0|\,\mathrm{e}^{-i\eta\mathbf{D}}\,[\mathbf{P},\mathrm{e}^{i\eta\mathbf{D}}]|\Phi_0\rangle \\ &= \langle\Phi_0|\,\mathrm{e}^{-i\eta\mathbf{D}}\,[\mathbf{P},\mathrm{e}^{i\eta\mathbf{D}}]|\Phi_0\rangle\ ,\end{aligned} \tag{4.39}$$

since the expectation value of the collective momenta in the ground state, $\langle\Phi_0|\mathbf{P}|\Phi_0\rangle$, should be zero. The commutator in Eq. (4.39) can be expressed as:

$$[\mathbf{P},\mathrm{e}^{i\eta\mathbf{D}}] = -\,i\,\hbar\,\frac{\partial}{\partial x}\,\mathrm{e}^{i\eta\mathbf{D}} = \hbar\,\eta\,\frac{NZ}{A}\,\mathrm{e}^{i\eta\mathbf{D}}\ , \tag{4.40}$$

and consequently, Eq. (4.39) becomes:

$$\langle\Phi(0)|\mathbf{P}|\Phi(0)\rangle = \langle\Phi_0|\,\mathrm{e}^{-i\eta\mathbf{D}}\,\hbar\,\eta\,\frac{NZ}{A}\,\mathrm{e}^{i\eta\mathbf{D}}|\Phi_0\rangle = \hbar\,\eta\,\frac{NZ}{A}\ . \tag{4.41}$$

Now it is possible to relate the value for the strength of the perturbation, η, to the expectation value of the initial collective momenta, induced by the perturbation:

$$\langle\mathbf{P}\rangle = \sqrt{2\,m\,\frac{NZ}{A}\,\hbar\,\omega_0} \equiv \sqrt{2\,\mu\,\hbar\,\omega_0} = \hbar\,\eta\,\frac{NZ}{A}\ , \tag{4.42}$$

with ω_0 being the frequency of the undamped harmonic oscillator. Consequently, we find the perturbation strength as:

$$\eta = \sqrt{\frac{2\,m\,A\,\omega_0}{NZ\,\hbar}}\ . \tag{4.43}$$

To estimate the strength function, $S(E)$, we shall now consider the Fourier transform of a weakly damped total dipole, $D(t) = D_0\ \sin(\omega_0 t)\,\mathrm{e}^{-\gamma t}$, with γ sufficiently small:

$$D(\omega) = \int_0^\infty D_0\,\sin(\omega_0 t)\,\mathrm{e}^{-\gamma t}\,\mathrm{e}^{i\omega t}\,\mathrm{d}t\ . \tag{4.44}$$

Using an exponential representation of the sine function (e.g. $\sin(\omega_0 t) = (\mathrm{e}^{i\omega_0 t} - \mathrm{e}^{-i\omega_0 t})/2i$) we obtain:

$$D(\omega) = \frac{D_0}{2i}\left(\frac{1}{i(\omega-\omega_0)-\gamma} - \frac{1}{i(\omega+\omega_0)-\gamma}\right)\ . \tag{4.45}$$

Considering now that the damping factor is sufficiently small, $\gamma \to 0$, and since the imaginary part of the $\dfrac{1}{\omega_0 \pm \omega}$ can be written using the δ-Dirac function as $i\pi\delta(\omega_0 \pm \omega)$ [85], the imaginary part of the Fourier transformed dipole becomes:

$$\mathscr{I}\,(D(\omega)) = D_0\,\frac{\pi}{2}\,\delta(\omega-\omega_0)\ , \tag{4.46}$$

and, consequently, the strength function, $S(\omega)$, is:

$$S(\omega) = \frac{\mathscr{I}(D(\omega))}{\pi\,\eta} = \frac{1}{2}\,\frac{D_0}{\eta}\,\delta(\omega-\omega_0)\;. \tag{4.47}$$

To evaluate the amplitude, D_0, we express the energy stored in a harmonic oscillator as:

$$\hbar\omega_0 = \frac{1}{2}\,k\,\mathbf{X}^2 = \frac{1}{2}\,\mu\,\omega_0^2\,\frac{D_0^2}{NZ/A} = \frac{1}{2}\,m\,\frac{NZ}{A}\,\omega_0^2\,\frac{D_0^2}{NZ^2/A}\;, \tag{4.48}$$

and one has:

$$D_0 = \sqrt{\frac{2\hbar}{m\,\omega_0}\frac{NZ}{A}}\;. \tag{4.49}$$

Therefore, using Eq. (4.43), we have:

$$\frac{D_0}{\eta} = \sqrt{\frac{2\hbar}{m\,\omega_0}\frac{NZ}{A}}\,\sqrt{\frac{NZ}{A}\,\frac{\hbar}{2\,m\,\omega_0}} = \frac{\hbar}{m\,\omega_0}\,\frac{NZ}{A} = \frac{\hbar^2}{m\,E_0}\,\frac{NZ}{A}\;. \tag{4.50}$$

Now, within a constant of $\dfrac{4\pi^2e^2}{\hbar c}$, the total cross section for the dipole absorption, σ_D, can be expressed:

$$\begin{aligned}\sigma_D &\sim \int_0^\infty E\;S(E)\;\mathrm{d}E = \int_0^\infty E\;\frac{S(\omega)}{\hbar}\;\mathrm{d}E = \int_0^\infty E\;\frac{1}{2}\,\frac{D_0}{\eta}\,\frac{\delta(\omega-\omega_0)}{\hbar}\;\mathrm{d}E\\ &= \int_0^\infty E\;\frac{1}{2}\,\frac{D_0}{\eta}\,\delta(E-E_0)\;\mathrm{d}E = \frac{1}{2}\;E_0\;\frac{D_0}{\eta} = \frac{\hbar^2}{2m}\;\frac{NZ}{A}\;,\end{aligned} \tag{4.51}$$

showing that, indeed, with the strength function obtained as the imaginary part of the dipole Fourier transform, we recover the known value for the EWSR.

Returning to our simulations, we assume that a number of ten oscillations (See also Fig. 4.8) in the presence of Landau damping will provide an approximate, yet reliable estimate of the strength function. In Fig. 4.9 the dipolar cross-section, $\sigma(E)$, is plotted for two different asy-EOS, using the information provided by the numerical simulations, and following the prescription described above. The numerically obtained value for the total cross section represents more than 90% of the theoretical value presented in Eq. (4.51).

Now, we estimate the total strength associated with PDR, integrating the cross section over the PDR region (i.e. between ~ 6 MeV and ~ 9 MeV). Our calculations show that the fraction of the EWSR exhausted by the pygmy mode represents 2.8% for *asy-soft*, 4.5% for *asy-stiff* and 4.6% for *asy-superstiff* respectively, and consequently, a good agreement with the experimental value of $\sim 4\%$ reported by Adrich et. al [8] is achieved. These values again confirm that not all the excess neutrons participate to the pygmy oscillations. The EWSR exhausted by the pygmy mode is proportional to the skin thickness, in agreement with the results obtained by Inakura *et al.* [86]. We conclude that while the skin thickness does not affect the position of the PDR centroid, it influences the amount of EWSR exhausted by the pygmy mode.

In the final part of this Section we extend the previous analysis to other neutron rich nuclei, from the lighter ^{48}Ca and ^{68}Ni to heavier ^{208}Pb, in order to study the mass

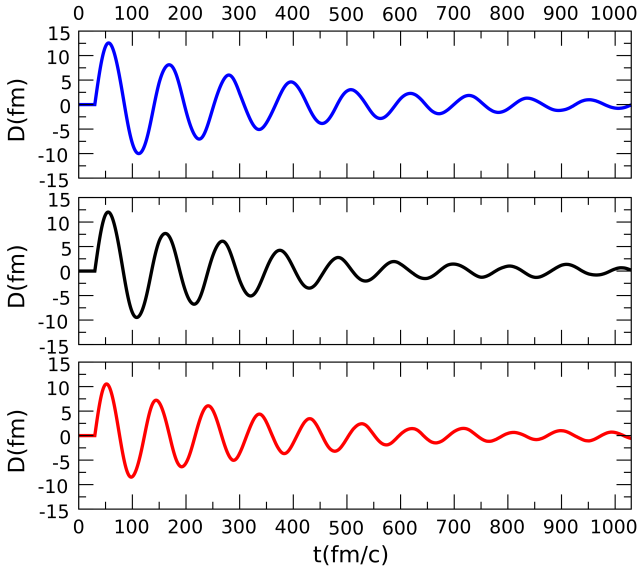

Figure 4.8: Graphical representation of the time evolution of the total dipole D for *asy-soft* (blue lines - top), *asy-stiff* (black lines - middle) and *asy-superstiff* (red lines - bottom) EOS, for a "GDR-like" initial excitation. The initial energy associated with the kinetic part of the collective energy is 9 MeV.

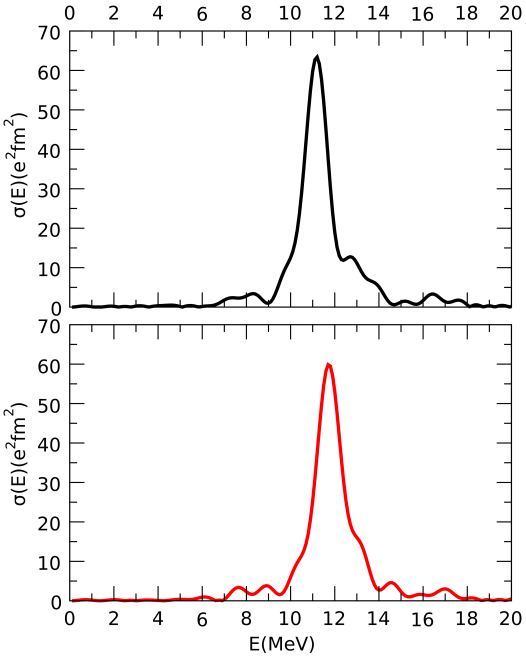

Figure 4.9: Graphical representation of the cross section, $\sigma(E)$, dependence on the energy, for *asy-stiff* (black lines - top) and *asy-superstiff* (red lines - bottom) EOS.

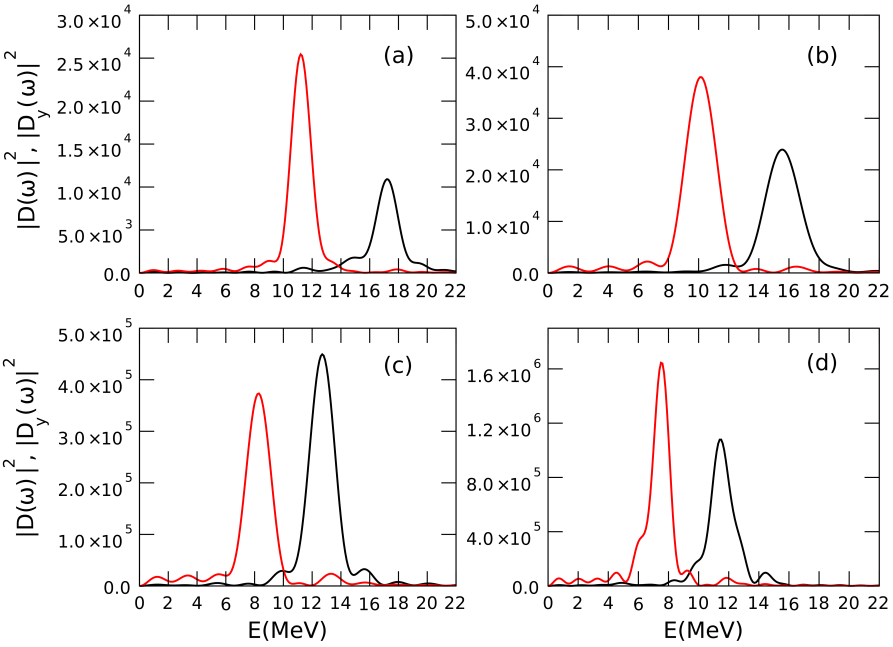

Figure 4.10: Power spectrum for the pygmy (red lines) and giant (black lines) modes, reported with our semi-classical approach, using the *asy-soft* EOS for ^{48}Ca (a), ^{68}Ni (b), ^{132}Sn (c) and for ^{208}Pb (d).

dependence of the PDR. For these systems, as already discussed in the Introduction, theoretical and experimental data are available.

Considering "pygmy-like" excitations, we identified the pygmy and GDR response, as shown in Fig. 4.10. The mass dependence of the pygmy energy centroid is plotted in Fig. 4.11, together with the experimentally reported values and the predictions of other theoretical models. We notice a surprisingly good agreement with the experimental data.

Hartmann *et al.* [19], within a high resolution photon scattering approach up to 10 MeV studied the calcium isotopes, ^{40}Ca and ^{48}Ca. A concentration of the low-lying dipole strength between 7 to 9 MeV, for ^{48}Ca isotope, was identified. Our theoretical estimations for the energy centroid of the pygmy mode is around $\sim$ 11.5 MeV (see Fig. 4.11), suggesting that part of the low-lying dipole response can be detected experimentally also above 10 MeV. Moreover, the theoretical predictions made within density functional theory formalism by Chambers *et al.* [34] suggest that the centroid energy for the pygmy mode lies around $\sim$ 7.5 MeV, lower than our predictions. All these comments show that further investigations, both theoretical and experimental are required.

Quite recently, using the virtual photon scattering technique, Wieland et al. [22] reported the existence of a peak in the dipole response centered at approximately 11 eV, attributed to the low lying dipole response of the neutron rich nickel isotope, ^{68}Ni. This peak is found to be well below the GDR centroid, whose energy lies near 17 MeV. With our semi-classical approach based on two coupled Landau-Vlasov equations, the energy centroids for the nickel isotope, ^{68}Ni, are reported at $\sim$ 10 MeV and $\sim$ 16 MeV for PDR and GDR respectively. By means of a random phase approximation approach with various types of interactions used, Roca-Maza *et al.* [33], report the pygmy centroid to range from

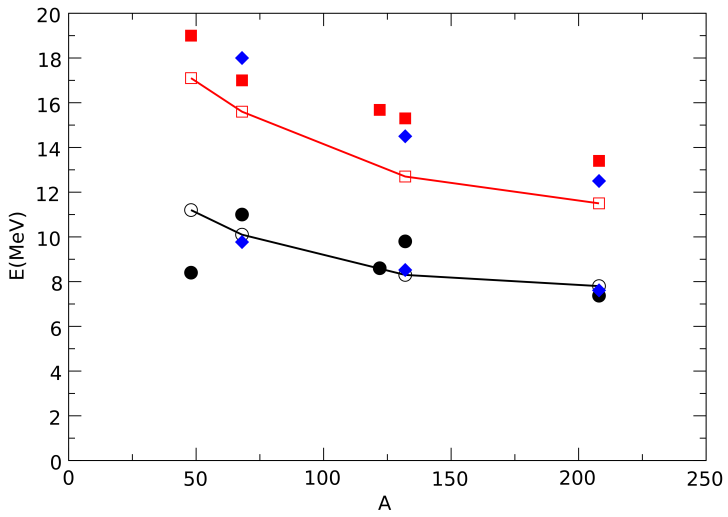

Figure 4.11: Mass dependence of the energy centroids for pygmy (circles) and giant (squares) modes, reported with our semi-classical approach, using the *asy-soft* EOS (empty circles/squares) and within a RPA formalism [33] (blue diamonds). Experimental values (full circles/squares) are reported from Ref. [19] for ^{48}Ca, from Ref. [22] for ^{68}Ni, from Ref. [8] for ^{132}Sn and from Ref. [25] for ^{208}Pb.

9.3 MeV (using the SLy5 force) to 10.45 MeV (using the SkI3 force), and therefore, in good agreement with our prediction. In the same study [33], the energy centroid corresponding to the PDR for the tin, ^{132}Sn, and lead, ^{208}Pb, isotopes ranges from 8.52 MeV (using the SGII force) to 9.23 MeV (with SkI3) for tin, and from 7.61 MeV (SGII) to 8.01 MeV (SkI3) for lead, and consequently, in quite good accordance with the centroids obtained within our approach (see Fig. 4.11). Simmilar results are obtained within the relativistic RPA framework by Piekarewicz [2], which reported a pygmy centroid around $\sim$ 8 MeV (with various models employed, i.e. FSUGold, FSUGold', NL3 and NL3'), while for GDR a peak ranging from 14.46 MeV (NL3') to 16.59 MeV (FSUGold') is obtained. Moreover, the theoretical predictions are in line with experimental data obtained by Adrich *et al.* [8] for ^{132}Sn within a Coulomb dissociation technique following an in-flight fission of a ^{238}U beam, and by Tamii *et al.* [25] for ^{208}Pb, within a polarized proton inelastic scattering at very forward angles approach.

Concluding, we remark that the results obtained with our approach for PDR are in quite good agreement with other experimental or theoretical works, while, for the GDR case a qualitative agreement is achieved too. A mass parametrisation of the PDR centroid of $42 \cdot A^{-1/3}$ MeV is obtained. This parametrisation is close to the HOSM energy for degenerate dipole modes in the absence of isovector interaction, pointing again to an isoscalar character of PDR. This is in agreement with our previous observation concerning the insensitivity of PDR centroid to the density parametrisation of the nuclear mean field in the isovector channel.

Chapter 5

Conclusions and perspectives

In summary, within this thesis, we explored new aspects of the dipole motions in neutron rich nuclei. The existence of a collective pygmy dipole mode in these systems is evidenced within both harmonic oscillator shell model (HOSM) and a semi-classical, self-consistent microscopic approach based on two Landau-Vlasov equations (for protons and neutrons) involving Skyrme-like mean-fields. We provided both qualitative arguments resulting from the power spectrum analysis of different dipolar degrees of freedom as well as quantitative, by estimating the exhausted EWSR associated with this mode. The HOSM predicts an upper limit for the energy weighted sum rule exhausted by the pygmy mode, $f_y = \frac{N_e Z}{N A_c}$, where N_e represents the number of neutrons in excess, while A_c is the mass number of the core. A comparative analysis of our results for several neutron rich isotopes (i.e. calcium, nickel, tin and lead) with experimental data, shows that, if all excess neutrons are considered to take part in the pygmy-type oscillations, this fraction f_y overestimates the experimental values. Considering that a part from the excess neutrons are bound to the core, if less neutrons are considered in the skin, $N_y < N_e$, then the Thomas-Reiche-Kuhn sum rule diminishes, and the corresponding fraction $f_y = \frac{N_y Z}{N A_c}$ approaches the experimental data. We verified this hypothesis within a self consistent semi-classical model based on kinetic Vlasov equations. In this approach we first focused our attention on the doubly-magic tin isotope, ^{132}Sn. From the transport simulations we predict that the energy centroid that corresponds to the PDR is located around 8.5 MeV. This centroid is situated well below the GDR peak (which is located at 13 MeV for an *asy-soft* parametrization of the asy-EOS), and is insensitive to the symmetry parametrization employed, revealing the isoscalar-like character of the pygmy mode. However, since the slope parameter varies with the three different parametrizations employed for the symmetry energy (*asy-soft*, *asy-stiff* and *asy-superstiff*) the number of neutrons on the nuclear surface is affected, and thus, the neutrons participating in the pygmy mode varies as well. Consequently, the EWSR exhausted by the pygmy mode varies from 2.8% for *asy-soft* to 4.5% for *asy-stiff* and 4.6% for *asy-superstiff*, proportional to the slope parameter, L. We stress that this behaviour can be also related to the S-J component of the dipole dynamics in medium-heavy nuclei, where the dipole motion cannot be fully described by a pure G-T component.

Lastly, within the same semi-classical approach, the mass dependence of the PDR and GDR energy centroids is obtained. We extract a parametrisation $42 \cdot A^{-1/3}$ MeV,

for the pygmy and $62 \cdot A^{-1/3}$ MeV, for the giant modes respectively, in good agreement with experimental data (in special for the case of PDR). We stress that our transport model employing an energy density functional can be extended to include additional correlation effects by considering terms depending on density gradients, accounting for additional nucleon-nucleon correlations. Moreover, we would like to mention that such self-consistent, transport approaches, can be valuable in exploring the collective response of other mesoscopic systems where similar normal modes may manifest, see [87] for a time-dependent approach to the surface and volume plasmons in Buckminsterfullerene and [88] for a study of out-of-phase dipolar oscillation of the thermal cloud and Bose-Einstein condensate.

Bibliography

[1] J. Gaardhøje, A. Bruce, and B. Herskind, "Nuclear collective motion under extreme conditions: The GDR at very high spin and temperature," *Nucl. Phys. A*, vol. 482, no. 1–2, pp. 121 – 139, 1988.

[2] J. Piekarewicz, "Pygmy dipole resonance as a constraint on the neutron skin of heavy nuclei," *Phys. Rev. C*, vol. 73, p. 044325, Apr 2006.

[3] S. Abrahamyan, Z. Ahmed, H. Albataineh, K. Aniol, D. S. Armstrong, W. Armstrong, T. Averett, B. Babineau, A. Barbieri, V. Bellini, R. Beminiwattha, J. Benesch, F. Benmokhtar, T. Bielarski, W. Boeglin, A. Camsonne, M. Canan, P. Carter, G. D. Cates, C. Chen, J.-P. Chen, O. Hen, F. Cusanno, M. M. Dalton, R. De Leo, K. de Jager, W. Deconinck, P. Decowski, X. Deng, A. Deur, D. Dutta, A. Etile, D. Flay, G. B. Franklin, M. Friend, S. Frullani, E. Fuchey, F. Garibaldi, E. Gasser, R. Gilman, A. Giusa, A. Glamazdin, J. Gomez, J. Grames, C. Gu, O. Hansen, J. Hansknecht, D. W. Higinbotham, R. S. Holmes, T. Holmstrom, C. J. Horowitz, J. Hoskins, J. Huang, C. E. Hyde, F. Itard, C.-M. Jen, E. Jensen, G. Jin, S. Johnston, A. Kelleher, K. Kliakhandler, P. M. King, S. Kowalski, K. S. Kumar, J. Leacock, J. Leckey, J. H. Lee, J. J. LeRose, R. Lindgren, N. Liyanage, N. Lubinsky, J. Mammei, F. Mammoliti, D. J. Margaziotis, P. Markowitz, A. McCreary, D. McNulty, L. Mercado, Z.-E. Meziani, R. W. Michaels, M. Mihovilovic, N. Muangma, C. Muñoz Camacho, S. Nanda, V. Nelyubin, N. Nuruzzaman, Y. Oh, A. Palmer, D. Parno, K. D. Paschke, S. K. Phillips, B. Poelker, R. Pomatsalyuk, M. Posik, A. J. R. Puckett, B. Quinn, A. Rakhman, P. E. Reimer, S. Riordan, P. Rogan, G. Ron, G. Russo, K. Saenboonruang, A. Saha, B. Sawatzky, A. Shahinyan, R. Silwal, S. Sirca, K. Slifer, P. Solvignon, P. A. Souder, M. L. Sperduto, R. Subedi, R. Suleiman, V. Sulkosky, C. M. Sutera, W. A. Tobias, W. Troth, G. M. Urciuoli, B. Waidyawansa, D. Wang, J. Wexler, R. Wilson, B. Wojtsekhowski, X. Yan, H. Yao, Y. Ye, Z. Ye, V. Yim, L. Zana, X. Zhan, J. Zhang, Y. Zhang, X. Zheng, and P. Zhu, "Measurement of the Neutron Radius of ^{208}Pb through Parity Violation in Electron Scattering," *Phys. Rev. Lett.*, vol. 108, p. 112502, Mar 2012.

[4] S. Karataglidis, K. Amos, B. A. Brown, and P. K. Deb, "Discerning the neutron density distribution of ^{208}Pb from nucleon elastic scattering," *Phys. Rev. C*, vol. 65, p. 044306, Mar 2002.

[5] N. Fukunishi, T. Otsuka, and I. Tanihata, "Neutron-skin and proton-skin formations in exotic nuclei far from stability," *Phys. Rev. C*, vol. 48, pp. 1648–1655, Oct 1993.

[6] I. Tanihata, D. Hirata, T. Kobayashi, S. Shimoura, K. Sugimoto, and H. Toki, "Revelation of thick neutron skins in nuclei," *Phys. Lett. B*, vol. 289, no. 3–4, pp. 261 – 266, 1992.

[7] P. G. Hansen and B. Jonson, "The neutron halo of extremely neutron-rich nuclei," *Europhys. Lett.*, vol. 4, no. 4, p. 409, 1987.

[8] P. Adrich, A. Klimkiewicz, M. Fallot, K. Boretzky, T. Aumann, D. Cortina-Gil, U. D. Pramanik, T. W. Elze, H. Emling, H. Geissel, M. Hellström, K. L. Jones, J. V. Kratz, R. Kulessa, Y. Leifels, C. Nociforo, R. Palit, H. Simon, G. Surówka, K. Sümmerer, and W. Waluś, "Evidence for Pygmy and Giant Dipole Resonances in ^{130}Sn and ^{132}Sn," *Phys. Rev. Lett.*, vol. 95, p. 132501, Sep 2005.

[9] B. Özel, J. Enders, P. von Neumann-Cosel, I. Poltoratska, A. Richter, D. Savran, S. Volz, and A. Zilges, "Systematics of the pygmy dipole resonance in stable tin isotopes from resonant photon scattering," *Nucl. Phys. A*, vol. 788, no. 1–4, pp. 385 – 388, 2007.

[10] A. Klimkiewicz, N. Paar, P. Adrich, M. Fallot, K. Boretzky, T. Aumann, D. Cortina-Gil, U. D. Pramanik, T. W. Elze, H. Emling, H. Geissel, M. Hellström, K. L. Jones, J. V. Kratz, R. Kulessa, C. Nociforo, R. Palit, H. Simon, G. Surówka, K. Sümmerer, D. Vretenar, and W. Waluś, "Nuclear symmetry energy and neutron skins derived from pygmy dipole resonances," *Phys. Rev. C*, vol. 76, p. 051603, Nov 2007.

[11] A. Carbone, G. Colò, A. Bracco, L.-G. Cao, P. F. Bortignon, F. Camera, and O. Wieland, "Constraints on the symmetry energy and neutron skins from pygmy resonances in ^{68}Ni and ^{132}Sn," *Phys. Rev. C*, vol. 81, p. 041301, Apr 2010.

[12] S. Yoshida and H. Sagawa, "Isovector nuclear matter properties and neutron skin thickness," *Phys. Rev. C*, vol. 73, p. 044320, Apr 2006.

[13] S. Yoshida and H. Sagawa, "Neutron skin thickness and equation of state in asymmetric nuclear matter," *Phys. Rev. C*, vol. 69, p. 024318, Feb 2004.

[14] P.-G. Reinhard and W. Nazarewicz, "Information content of a new observable: The case of the nuclear neutron skin," *Phys. Rev. C*, vol. 81, p. 051303, May 2010.

[15] N. Paar, "The quest for novel modes of excitation in exotic nuclei," *J. Phys. G: Nucl. Part. Phys.*, vol. 37, no. 6, p. 064014, 2010.

[16] N. Paar, D. Vretenar, E. Khan, and G. Colò, "Exotic modes of excitation in atomic nuclei far from stability," *Rep. Prog. Phys.*, vol. 70, no. 5, p. 691, 2007. `http://stacks.iop.org/0034-4885/70/i=5/a=R02`.

[17] D. Sarchi, P. Bortignon, and G. Colò, "Dipole states in stable and unstable nuclei," *Phys. Lett. B*, vol. 601, no. 1–2, pp. 27 – 33, 2004.

[18] S. Ottini-Hustache, N. Alamanos, F. Auger, B. Castel, Y. Blumenfeld, V. Chiste, N. Frascaria, A. Gillibert, C. Jouanne, V. Lapoux, F. Marie, W. Mittig, J. C. Roynette, and J. A. Scarpaci, "Anomalous $E1$ and $E2$ strengths in ^{40}Ca and ^{48}Ca at

low excitation energy: A comparative study," *Phys. Rev. C*, vol. 59, pp. 3429–3432, Jun 1999.

[19] T. Hartmann, J. Enders, P. Mohr, K. Vogt, S. Volz, and A. Zilges, "Measurement of the Dipole and Electric Quadrupole Strength Distributions up to 10 MeV in the Doubly Magic Nuclei ^{40}Ca and ^{48}Ca," *Phys. Rev. Lett.*, vol. 85, pp. 274–277, Jul 2000.

[20] T. Hartmann, J. Enders, P. Mohr, K. Vogt, S. Volz, and A. Zilges, "Dipole and electric quadrupole excitations in ^{40,48}Ca," *Phys. Rev. C*, vol. 65, p. 034301, Feb 2002.

[21] T. Hartmann, M. Babilon, S. Kamerdzhiev, E. Litvinova, D. Savran, S. Volz, and A. Zilges, "Microscopic Nature of the Pygmy Dipole Resonance: The Stable Ca Isotopes," *Phys. Rev. Lett.*, vol. 93, p. 192501, Nov 2004.

[22] O. Wieland, A. Bracco, F. Camera, G. Benzoni, N. Blasi, S. Brambilla, F. C. L. Crespi, S. Leoni, B. Million, R. Nicolini, A. Maj, P. Bednarczyk, J. Grebosz, M. Kmiecik, W. Meczynski, J. Styczen, T. Aumann, A. Banu, T. Beck, F. Becker, L. Caceres, P. Doornenbal, H. Emling, J. Gerl, H. Geissel, M. Gorska, O. Kavatsyuk, M. Kavatsyuk, I. Kojouharov, N. Kurz, R. Lozeva, N. Saito, T. Saito, H. Schaffner, H. J. Wollersheim, J. Jolie, P. Reiter, N. Warr, G. deAngelis, A. Gadea, D. Napoli, S. Lenzi, S. Lunardi, D. Balabanski, G. LoBianco, C. Petrache, A. Saltarelli, M. Castoldi, A. Zucchiatti, J. Walker, and A. Bürger, "Search for the Pygmy Dipole Resonance in ^{68}Ni at 600 MeV/nucleon," *Phys. Rev. Lett.*, vol. 102, p. 092502, Mar 2009.

[23] O. Wieland and A. Bracco, "The pygmy dipole resonance in ^{68}Ni and the neutron skin," *Prog. Part. Nuc. Phys.*, vol. 66, no. 2, pp. 374 – 378, 2011.

[24] D. Savran, M. Fritzsche, J. Hasper, K. Lindenberg, S. Müller, V. Y. Ponomarev, K. Sonnabend, and A. Zilges, "Fine Structure of the Pygmy Dipole Resonance in ^{136}Xe," *Phys. Rev. Lett.*, vol. 100, p. 232501, Jun 2008.

[25] A. Tamii, I. Poltoratska, P. von Neumann-Cosel, Y. Fujita, T. Adachi, C. A. Bertulani, J. Carter, M. Dozono, H. Fujita, K. Fujita, K. Hatanaka, D. Ishikawa, M. Itoh, T. Kawabata, Y. Kalmykov, A. M. Krumbholz, E. Litvinova, H. Matsubara, K. Nakanishi, R. Neveling, H. Okamura, H. J. Ong, B. Özel-Tashenov, V. Y. Ponomarev, A. Richter, B. Rubio, H. Sakaguchi, Y. Sakemi, Y. Sasamoto, Y. Shimbara, Y. Shimizu, F. D. Smit, T. Suzuki, Y. Tameshige, J. Wambach, R. Yamada, M. Yosoi, and J. Zenihiro, "Complete Electric Dipole Response and the Neutron Skin in ^{208}Pb," *Phys. Rev. Lett.*, vol. 107, p. 062502, Aug 2011.

[26] R. Mohan, M. Danos, and L. C. Biedenharn, "Three-fluid hydrodynamical model of nuclei," *Phys. Rev. C*, vol. 3, pp. 1740–1749, May 1971.

[27] H. Steinwedel and J. Jensen, "Hydrodynamik von Kerndipolschwingungen," *Z. Naturforschung Teil A*, vol. 5, pp. 413–420, 1950.

[28] Y. Suzuki, K. Ikeda, and H. Sato, "New type of dipole vibration in nuclei," *Progr. Theoret. Phys.*, vol. 83, no. 2, pp. 180–184, 1990.

[29] S. Bastrukov, I. Molodtsova, D. Podgainy, S. Mişicu, and H.-K. Chang, "Elasticity of nuclear medium as a principal macrodynamical promoter of electric pygmy dipole resonance," *Phys. Lett. B*, vol. 664, no. 4–5, pp. 258 – 264, 2008.

[30] N. Tsoneva and H. Lenske, "Pygmy dipole resonances in the tin region," *Phys. Rev. C*, vol. 77, p. 024321, Feb 2008.

[31] G. Co', V. D. Donno, C. Maieron, M. Anguiano, and A. M. Lallena, "Evolution of the pygmy dipole resonance in nuclei with neutron excess," *Phys. Rev. C*, vol. 80, p. 014308, Jul 2009.

[32] K. Yoshida, "Pygmy dipole mode in deformed neutron-rich Mg isotopes close to the drip line," *Phys. Rev. C*, vol. 80, p. 044324, Oct 2009.

[33] X. Roca-Maza, G. Pozzi, M. Brenna, K. Mizuyama, and G. Colò, "Low-lying dipole response: Isospin character and collectivity in ^{68}Ni, ^{132}Sn, and ^{208}Pb," *Phys. Rev. C*, vol. 85, p. 024601, Feb 2012.

[34] J. Chambers, E. Zaremba, J. P. Adams, and B. Castel, "Pygmy dipole resonances in the calcium isotopes," *Phys. Rev. C*, vol. 50, pp. R2671–R2674, Dec 1994.

[35] D. Vretenar, N. Paar, P. Ring, and G. Lalazissis, "Collectivity of the low-lying dipole strength in relativistic random phase approximation," *Nucl. Phys. A*, vol. 692, no. 3–4, pp. 496 – 517, 2001.

[36] D. Vretenar, T. Niksic, N. Paar, and P. Ring, "Relativistic QRPA description of low-lying dipole strength in neutron-rich nuclei," *Nucl. Phys. A*, vol. 731, no. 0, pp. 281 – 288, 2004.

[37] E. Litvinova, P. Ring, and V. Tselyaev, "Relativistic quasiparticle time blocking approximation: Dipole response of open-shell nuclei," *Phys. Rev. C*, vol. 78, p. 014312, Jul 2008.

[38] D. P. Arteaga, E. Khan, and P. Ring, "Isovector dipole strength in nuclei with extreme neutron excess," *Phys. Rev. C*, vol. 79, p. 034311, Mar 2009.

[39] J. Endres, E. Litvinova, D. Savran, P. A. Butler, M. N. Harakeh, S. Harissopulos, R.-D. Herzberg, R. Krücken, A. Lagoyannis, N. Pietralla, V. Y. Ponomarev, L. Popescu, P. Ring, M. Scheck, K. Sonnabend, V. I. Stoica, H. J. Wörtche, and A. Zilges, "Isospin Character of the Pygmy Dipole Resonance in ^{124}Sn," *Phys. Rev. Lett.*, vol. 105, p. 212503, Nov 2010.

[40] D. Vretenar, Y. F. Niu, N. Paar, and J. Meng, "Low-energy isovector and isoscalar dipole response in neutron-rich nuclei," *Phys. Rev. C*, vol. 85, p. 044317, Apr 2012.

[41] V. Abrosimov and O. Davydovs'ka, "Semiclassical model of dipole pygmy-resonance in nuclei with neutron excess," *Ukr. J. Phys.*, vol. 54, pp. 1068–1072, 2009.

[42] B. Frecus, *PhD Research Report.* University of Bucharest, 2010.

[43] M. Urban, "Pygmy resonance and torus mode within Vlasov dynamics," *Phys. Rev. C*, vol. 85, p. 034322, Mar 2012.

[44] M. Baldo, P. Schuck, and X. Viñas, "Kohn–Sham density functional inspired approach to nuclear binding," *Phys. Lett. B*, vol. 663, no. 5, pp. 390 – 394, 2008.

[45] D. Brink, "Individual particle and collective aspects of the nuclear photoeffect," *Nucl. Phys.*, vol. 4, no. 0, pp. 215 – 220, 1957.

[46] M. Goldhaber and E. Teller, "On nuclear dipole vibrations," *Phys. Rev.*, vol. 74, pp. 1046–1049, Nov 1948.

[47] A. Bohr and B. R. Mottelson, *Nuclear Structure.* World Scientific, Singapore, 1998.

[48] E. Lipparini, *Modern many-body physics.* World Scientific, 2003.

[49] E. Lipparini and S. Stringari, "Sum rules and giant resonances in nuclei," *Phys. Rep.*, vol. 175, no. 3–4, pp. 103 – 261, 1989.

[50] P. Ring and P. Schuck, *The Nuclear Many-Body Problem.* Springer, 2004.

[51] V. Baran, B. Frecus, M. Colonna, and M. Di Toro, "Pygmy dipole resonance: Collective features and symmetry energy effects," *Phys. Rev. C*, vol. 85, p. 051601, May 2012.

[52] V. Baran, B. Frecus, M. Colonna, M. Di Toro, and R. Zus, "Collective dipole modes in nuclear systems," *Rom. Journ. Phys.*, vol. 57, pp. 36–48, 2012.

[53] Y. Alhassid, M. Gai, and G. F. Bertsch, "Radiative width of molecular-cluster states," *Phys. Rev. Lett.*, vol. 49, pp. 1482–1485, Nov 1982.

[54] H. Kurasawa and T. Suzuki, "A Sum-Rule Constraint on the Soft Dipole Mode," *Prog. Theor. Phys.*, vol. 94, no. 5, pp. 931–936, 1995.

[55] L.-G. Cao and Z.-Y. Ma, "Soft dipole modes in neutron-rich Ni-isotopes in QRRPA," *Mod. Phys. Lett. A*, vol. 19, no. 38, pp. 2845–2856, 2004.

[56] N. Ryezayeva, T. Hartmann, Y. Kalmykov, H. Lenske, P. von Neumann-Cosel, V. Y. Ponomarev, A. Richter, A. Shevchenko, S. Volz, and J. Wambach, "Nature of Low-Energy Dipole Strength in Nuclei: The Case of a Resonance at Particle Threshold in ^{208}Pb," *Phys. Rev. Lett.*, vol. 89, p. 272502, Dec 2002.

[57] V. Baran, C. Rizzo, M. Colonna, M. D. Toro, and D. Pierroutsakou, "Dynamical dipole mode in fusion reactions with exotic nuclear beams," *Phys. Rev. C*, vol. 79, p. 021603, Feb 2009.

[58] V. Baran, D. M. Brink, M. Colonna, and M. Di Toro, "Collective Dipole Bremsstrahlung in Fusion Reactions," *Phys. Rev. Lett.*, vol. 87, p. 182501, Oct 2001.

[59] V. Baran, M. Colonna, M. D. Toro, and A. Larionov, "Zero- to first-sound transition for the Giant Dipole propagation in hot nuclei," *Nucl. Phys. A*, vol. 649, no. 1–4, pp. 185 – 192, 1999.

[60] A. Larionov, M. Cabibbo, V. Baran, and M. D. Toro, "Zero-to-first sound transition for isovector modes in hot nuclei," *Nucl. Phys. A*, vol. 648, no. 3–4, pp. 157 – 180, 1999.

[61] P. Hohenberg and W. Kohn, "Inhomogeneous Electron Gas," *Phys. Rev.*, vol. 136, pp. B864–B871, Nov 1964.

[62] D. Lacroix, *Quantum nuclear many-body dynamics and related aspects*. Habilitation thesis, Grand Accélérateur National d'Ions Lourds, 2011.

[63] T. Skyrme, "The effective nuclear potential," *Nucl. Phys.*, vol. 9, no. 4, pp. 615 – 634, 1958–1959.

[64] K. Langanke, J. Maruhn, and S. Koonin, *Computational Nuclear Physics 2: Nuclear Reactions*. Springer-Verlag, 1993.

[65] P. Vesely, *Collective Nuclear Excitations within Skyrme Separable RPA*. Doctoral thesis, Faculty of Mathematics and Physics Charles University in Prague, 2009.

[66] V. Baran, M. Colonna, V. Greco, and M. D. Toro, "Reaction dynamics with exotic nuclei," *Phys. Rep.*, vol. 410, no. 5–6, pp. 335 – 466, 2005.

[67] G. Colò, "The compression modes in atomic nuclei and their relevance for the nuclear equation of state," *Phys. Part. Nucl.*, vol. 39, pp. 286–305, 2008.

[68] M. Colonna, M. D. Toro, and A. Larionov, "Collective modes in asymmetric nuclear matter," *Phys. Lett. B*, vol. 428, no. 1–2, pp. 1 – 7, 1998.

[69] B.-A. Li, L.-W. Chen, and C. M. Ko, "Recent progress and new challenges in isospin physics with heavy-ion reactions," *Phys. Rep.*, vol. 464, no. 4–6, pp. 113 – 281, 2008.

[70] V. Baran, M. Colonna, M. Di Toro, V. Greco, M. Zielinska-Pfabe, and H. Wolter, "Isospin effects in nuclear fragmentation," *Phys. Atom. Nucl.*, vol. 66, pp. 1460–1470, 2003.

[71] G. Bertsch and S. D. Gupta, "A guide to microscopic models for intermediate energy heavy ion collisions," *Phys. Rep.*, vol. 160, no. 4, pp. 189 – 233, 1988.

[72] D. Brink and M. D. Toro, "Dynamics of a semiclassical nuclear Hartree-Fock fluid," *Nucl. Phys. A*, vol. 372, no. 1–2, pp. 151 – 172, 1981.

[73] V. Kolomietz and S. Shlomo, "Nuclear Fermi-liquid drop model," *Phys. Rep.*, vol. 390, no. 3, pp. 133 – 233, 2004.

[74] A. Bonasera, F. Gulminelli, and J. Molitoris, "The Boltzmann equation at the borderline. A decade of Monte Carlo simulations of a quantum kinetic equation," *Phys. Rep.*, vol. 243, no. 1–2, pp. 1 – 124, 1994.

[75] C. Grégoire, B. Remaud, F. Sébille, L. Vinet, and Y. Raffray, "Semi-classical dynamics of heavy-ion reactions," *Nucl. Phys. A*, vol. 465, no. 2, pp. 317 – 338, 1987.

[76] D. C. M. Steven E. Koonin, *Computational Physics: Fortran version.* Westview Press, 1990.

[77] P. Schuck, R. Hasse, J. Jaenicke, C. Grégoire, B. Rémaud, F. Sébille, and E. Suraud, "Semiclassical and phase space approaches to dynamic and collisional problems of nuclei," *Prog. Part. Nuc. Phys.*, vol. 22, no. 0, pp. 181 – 278, 1989.

[78] S. Yoshida, H. Sagawa, and N. Takigawa, "Incompressibility and density distributions in asymmetric nuclear systems," *Phys. Rev. C*, vol. 58, pp. 2796–2806, Nov 1998.

[79] N. Paar, T. Nikšić, D. Vretenar, and P. Ring, "Isotopic dependence of the pygmy dipole resonance," *Phys. Lett. B*, vol. 606, no. 3–4, pp. 288 – 294, 2005.

[80] J. Liang, L.-G. Cao, and Z.-Y. Ma, "Pygmy and giant dipole resonances in Ni isotopes," *Phys. Rev. C*, vol. 75, p. 054320, May 2007.

[81] V. Baran, M. Colonna, M. Di Toro, and V. Greco, "Nuclear Fragmentation: Sampling the Instabilities of Binary Systems," *Phys. Rev. Lett.*, vol. 86, pp. 4492–4495, May 2001.

[82] M. Colonna, P. Chomaz, and S. Ayik, "Mechanical and Chemical Spinodal Instabilities in Finite Quantum Systems," *Phys. Rev. Lett.*, vol. 88, p. 122701, Mar 2002.

[83] A. Vitturi, E. G. Lanza, M. V. Andrés, F. Catara, and D. Gambacurta, "Giant and Pygmy Dipole Resonances in neutron-rich nuclei: their excitation via Coulomb and nuclear fields," *J. Phys. Conf. Ser.*, vol. 267, no. 1, p. 012006, 2011.

[84] E. G. Lanza, A. Vitturi, M. V. Andrés, F. Catara, and D. Gambacurta, "Excitations of pygmy dipole resonances in exotic and stable nuclei via Coulomb and nuclear fields," *Phys. Rev. C*, vol. 84, p. 064602, Dec 2011.

[85] F. Calvayrac, P. Reinhard, and E. Suraud, "Spectral Signals from Electronic Dynamics in Sodium Clusters," *Ann. Phys.*, vol. 255, no. 1, pp. 125 – 162, 1997.

[86] T. Inakura, T. Nakatsukasa, and K. Yabana, "Emergence of pygmy dipole resonances: Magic numbers and neutron skins," *Phys. Rev. C*, vol. 84, p. 021302, Aug 2011.

[87] S. W. J. Scully, E. D. Emmons, M. F. Gharaibeh, R. A. Phaneuf, A. L. D. Kilcoyne, A. S. Schlachter, S. Schippers, A. Müller, H. S. Chakraborty, M. E. Madjet, and J. M. Rost, "Photoexcitation of a Volume Plasmon in C_{60} Ions," *Phys. Rev. Lett.*, vol. 94, p. 065503, Feb 2005.

[88] D. M. Stamper-Kurn, H.-J. Miesner, S. Inouye, M. R. Andrews, and W. Ketterle, "Collisionless and Hydrodynamic Excitations of a Bose-Einstein Condensate," *Phys. Rev. Lett.*, vol. 81, pp. 500–503, Jul 1998.

List of publications

Paper I. V. Baran, B. Frecus, M. Colonna, and M. Di Toro, **Pygmy dipole resonance: Collective features and symmetry energy effects**, *Physical Review C*, **85**, 051601(2012).

Paper II. V. Baran, B. Frecus, M. Colonna, M. Di Toro, and R. Zus **Collective dipole modes in nuclear systems** , *Romanian Journal of Physics*, **57**, 36(2012).

Paper III. M. Colonna, V. Baran, M. Di Toro, B. Frecus, and Y. X. Zhang, **Reaction mechanisms in transport theories: a test of the nuclear effective interaction**, *Journal of Physics: Conference Series (JPCS)*, (2012) in press. The proceedings of the 11th International Conference on Nucleus-Nucleus Collisions (NN2012), San Antonio, Texas, USA, 2012.

Paper IV. V. Baran, B. Frecus, M. Colonna, and M. Di Toro, **On the mass dependence of Pygmy Dipole response**, Submitted to *Romanian Reports in Physics*